THE DECAY OF ARSENIC - 76, 78 and 80

by

DONALD KENNETH McMILLAN
B.A.Sc., University of British Columbia, 1963

A DISSERTATION SUBMITTED IN PARTIAL FULFILLMENT
OF THE REQUIREMENTS FOR THE DEGREE OF
DOCTOR OF PHILOSOPHY

in the Department
of
CHEMISTRY
Simon Fraser University

DECEMBER, 1970

EXAMINING COMMITTEE APPROVAL

Professor B.D. Pate
Department of Chemistry
Simon Fraser University
Research Supervisor

Professor L. Yaffe, Chairman
Department of Chemistry
McGill University
External Examiner

Professor C.H.W. Jones
Department of Chemistry
Simon Fraser University
Examining Committee

Professor D.G. Tuck
Department of Chemistry
Simon Fraser University
Examining Committee

Professor J.M. D'Auria
Department of Chemistry
Simon Fraser University
Examining Committee

Department of Chemistry
Simon Fraser University

Date February 18, 1971

ABSTRACT

The β- and γ- decay properties of the neutron-rich isotopes ^{76}As, ^{78}As and ^{80}As have been studied using high resolution Ge(Li) and Si(Li) semi-conductor detectors and a superconducting magnet beta spectrometer. Beta-γ, γ-γ and single detector measurements have allowed the assembly of decay schemes for ^{78}As and ^{80}As and the clarification of some aspects of the previously postulated decay scheme of ^{76}As. Theoretical interpretations of the proposed excited levels of these nuclei have been made in terms of the Davydov and Chaban model.

ACKNOWLEDGEMENT

It is indeed a pleasure for the author to acknowledge the help of many individuals in the Department of Chemistry at Simon Fraser University. Special thanks are extended to:

Professor B.D. Pate for patiently providing numerous helpful suggestions and encouragements during the course of this work, Dr. J.D'Auria for aid and assistance in the design of many experiments, Dr. S. Gujrathi for countless comments on nuclear models, theory and experimental techniques, Dr. D.E. Brodie and Mr. M. Billany for aid in the liquid helium experiments, Mr. P. Miller for assistance in the nuclear reactor experiments at the University of Washington, Mr. J. Gislason for expert comments on technical and other subjects, Mr. T. Bennett for skillful preparation of figures, Mrs. Ellis for accurate typing, and a host of others whose aid and counsel were appreciated. Among these were Dr. C.H.W. Jones, Dr. R. Korteling, Dr. D.G. Tuck, Dr. P. Vasudev, Mr. E. Miller, Mr. F. Wick, Mr. W. Hall, Mr. P. Hatch and members of the staff of the S.F.U. Science Workshops. Financial support of this work by the National Research Council of Canada and the Defence Research Board of Canada is gratefully acknowledged.

TABLE OF CONTENTS

Chapter			Page
1.	INTRODUCTION		1
	1.1	General Objectives	1
	1.2	Previous Work on ^{76}As, ^{78}As and ^{80}As Decay	3
		1.2.1 The Decay of ^{76}As	3
		1.2.2 The Decay of ^{78}As	4
		1.2.3 The Decay of ^{80}As	4
2.	INTRODUCTORY THEORY		6
	2.1	Nuclear Models	6
	2.2	Collective States in Even-Even Nuclei	8
	2.3	The Davydov and Chaban Model	10
3.	EXPERIMENTAL TECHNIQUES		16
	3.1	Irradiation and Source Preparation Procedures	16
		3.1.1 ^{76}As Preparation Procedure	16
		3.1.2 ^{78}As Preparation Procedure	17
		3.1.3 ^{80}As Preparation Procedure	23
		(a) Method #1	23
		(b) Method #2	31
	3.2	Radiation Measurements	33
		3.2.1 Half Life Measurements	33
		3.2.2 Gamma-Ray Counting Techniques	36
		(a) Single Detector Systems	36
		(b) Gamma-Gamma Detection Systems	37
		3.2.3 Beta-Ray Counting Techniques	39

Chapter Page

(a) Superconducting Magnet Beta Spectrometer 39
(b) Beta-Gamma Detection Systems 57

3.3 Treatment of Data 58

3.3.1 Half Life Measurements 58
3.3.2 Gamma-Ray Spectra 59

(a) Location of Peak Center Positions and Energy Calibrations 59
(b) Gamma-Ray Relative Intensity Determinations 62
(c) Gamma-Gamma Coincidence Spectra 63

3.3.3 Beta-Ray Spectra 65

(a) Superconducting Magnet Beta Spectrometer 65
(b) Beta-Gamma Coincidence Spectra 66

4. EXPERIMENTAL RESULTS 68

4.1 Decay of ^{76}As 68

4.1.1 Half Life and Gamma-Ray Spectra 68
4.1.2 Gamma-Gamma Coincidence Spectra 75
4.1.3 Beta-Gamma Coincidence Spectra 81
4.1.4 Discussion of Results and Decay Scheme 84

4.2 Decay of ^{78}As 92

4.2.1 Half Life and Gamma-Ray Spectra 92
4.2.2 Gamma-Gamma Coincidence Spectra 101
4.2.3 Beta-Ray and Beta-Gamma Coincidence Spectra 102
4.2.4 Discussion of Results and Decay Scheme 115

Chapter Page

4.3 Decay of ^{80}As 125

4.3.1 Half Life Measurements 125
4.3.2 Gamma-Ray Spectra 125
4.3.3 Gamma-Gamma Coincidence Spectra 135
4.3.4 Discussion of Results and Decay Scheme 136

5. SUMMARY AND CONCLUSIONS 143

5.1 Comparison of Results with Other Even-Even Nuclei and Theory 143

5.2 Conclusions 151

REFERENCES 156

APPENDIX - GRAYPLOT Fortran Computer Program 164

LIST OF TABLES

Table		Page
1	Energy and Relative Intensity Values for Gamma-Rays Following the Decay of ^{76}As . . .	70
2	Comparisons of Energy and Relative Intensity Values for Gamma-Rays Following the Decay of ^{76}As	76
3	Gamma-Gamma Coincidences in ^{76}As	83
4	Energy and Relative Intensity Values for Gamma-Rays Following the Decay of ^{78}As . . .	100
5	Gamma-Gamma Coincidences in ^{78}As	102
6	Level Energies and Spin Assignments of ^{78}Se	124
7	Short-Lived γ-Radiations Resulting from the 14-MeV Neutron Bombardment of Natural Selenium Metal	133-134
8	Gamma-Rays Appearing in γ-γ Spectra in Coincidence with the 665.8 keV γ-Ray	137
9	Level Energies and Spin Assignments of ^{80}Se	141

LIST OF FIGURES

Figure		Page
1	First 2^+ energy and ratio of second 2^+ energy to first 2^+ energy as a function of neutron number. Isotopic lines marked with proton numbers	7
2	Simplified models showing β- and γ-vibrations	12
3	Comparisons of experimentally measured energy levels of even-even nuclei with the Davydov and Chaban model	15
4	Arsine generating apparatus	19
5	Filter tube details	22
6	^{80}As electrolytic cell-process flow diagram	25
7	^{80}As electrolytic cell-front view	27
8	^{80}As electrolytic cell-side view	28
9	$^{76}AsH_3$ activity from the electrolytic cell as a function of time	30
10	^{80}As half life measurement-circuit diagram	34
11	Electronic apparatus used in γ-γ coincidence experiments	40
12	Si(Li) superconducting magnet beta spectrometer system (diagrammatic) showing detector and source positions	41
13	Si(Li) superconducting magnet beta spectrometer system (diagrammatic) showing on the right, enlarged details of detector holder	42

Figure		Page
14	Electronic apparatus used with the superconducting magnet beta spectrometer	45
15	Electron paths described by electrons in a homogeneous field parallel to the z-axis	46
16	Maximum electron radii for β-particles emitted perpendicular to magnetic field B	49
17	Operating characteristics of the superconducting magnet beta spectrometer	50
18	Increase in counting-rate of Si(Li) detectors as a function of magnetic field strength . .	52
19	^{207}Bi conversion electron spectrum with no magnetic field, detector outputs summed . . .	53
20	^{207}Bi conversion electron spectrum with 30 kG magnetic field, detector outputs summed	54
21	^{32}P β-spectrum with 30 kG magnetic field, detector outputs summed	55
22	Fermi-Kurie plot of ^{32}P	56
23	Decay curve of ^{76}As and ^{78}As	69
24	The ^{76}As γ-ray spectrum showing the 740-1130 keV energy region obtained with a single 23.8 cm^3 Ge(Li) detector	72
25	Portions of the ^{76}As γ-ray spectrum obtained with a single 0.155 cm^3 Ge(Li) detector . .	73
26	Comparison of the FWHM values of the 559.6 keV ^{76}As γ-ray peak and the 569.6 keV ^{207}Bi γ-ray peak	74
27	Ge(Li) γ-spectrum from ^{76}As decay in coincidence with the 559.6 keV γ-ray	77
28	Ge(Li) γ-spectrum from ^{76}As decay in coincidence with the 657.4 keV γ-ray	78

Figure		Page
29	Ge(Li) γ-spectrum from ^{76}As decay in coincidence with γ-ray events of about 1200 keV	79
30	Ge(Li) γ-spectrum from ^{76}As decay in coincidence with γ-ray events of about 1226 keV	80
31	Low energy Ge(Li) γ-spectra from ^{76}As decay obtained (a) in coincidence with the 559.6 keV γ-ray and (b) with a single detector	82
32	^{76}As Fermi-Kurie plot for β-rays in coincidence with the 559.6 keV γ-ray	85
33	^{76}As Fermi-Kurie plot for β-rays in coincidence with the 657.4 keV γ-ray	86
34	^{76}As Ge(Li) γ-spectrum in coincidence with β-rays	87
35	Proposed decay scheme of ^{76}As. All energies in MeV; numbers at arrow heads are intensities relative to the 559.6 keV transition = 100	90
36	Top half: Single detector Ge(Li) γ-ray spectrum from ^{76}As and ^{78}As decay measured shortly after the end of bombardment. Bottom half: Single detector Ge(Li) γ-ray spectrum from ^{76}As decay measured one day after the end of bombardment. All energies in MeV	94
37	Single detector NaI(Tl) γ-ray spectrum from ^{76}As and ^{78}As decay measured shortly after the end of bombardment	95
38	Double escape peak data for a 8 cm^3 Ge(Li) detector versus γ-ray energy	97
39	Full width at half maximum height (FWHM) of ^{78}As γ-peaks versus γ-ray energy	98
40	Graphical resolutions of 686.7 and 694.7 keV γ-rays in ^{78}As γ-spectrum obtained with a 8 cm^3 Ge(Li) detector	99

Figure		Page
41	Ge(Li) γ-spectrum from ^{78}As decay in coincidence with 613.5 keV γ-ray	103
42	Ge(Li) γ-spectrum from ^{78}As decay in coincidence with 694.7 keV γ-ray	104
43	Ge(Li) γ-spectrum from ^{78}As decay in coincidence with 827.8 keV γ-ray	105
44	Ge(Li) γ-spectrum from ^{78}As decay in coincidence with 1239.9 keV γ-ray	106
45	Ge(Li) γ-spectrum from ^{78}As decay in coincidence with 1308.3 keV γ-ray	107
46	NaI(Tl) γ-spectrum from ^{78}As decay in coincidence with 613.5 keV γ-ray	108
47	NaI(Tl) γ-spectrum from ^{78}As decay in coincidence with 694.7 keV γ-ray. The weak 1308.3 keV peak is believed to be coincident with the 686.7 keV peak and not the 694.7 keV peak	109
48	NaI(Tl) γ-spectrum from ^{78}As decay in coincidence with 827.8 keV γ-ray	110
49	NaI(Tl) γ-spectrum from ^{78}As decay in coincidence with 1239.9 keV γ-ray	111
50	NaI(Tl) γ-spectrum from ^{78}As decay in coincidence with 1713.4 keV γ-ray	112
51	^{78}As β-spectrum obtained using the superconducting magnet beta spectrometer; magnetic field--30 kilogauss; Si(Li) detector outputs summed	113
52	^{78}As Fermi-Kurie plot of high-energy portion of β-spectrum	114
53	^{78}As Fermi-Kurie plot for β-rays in coincidence with 694.7 keV γ-ray	116
54	^{78}As Fermi-Kurie plot for β-rays in coincidence with 827.8 keV γ-ray	117

Figure		Page
55	^{78}As Fermi-Kurie plot for β-rays in coincidence with 1308.3 keV γ-ray	118
56	Proposed decay scheme of ^{78}As. All energies in MeV; numbers at arrow heads are intensities relative to the 613.5 keV transition = 100.	123
57	Ge(Li) γ-ray spectra of 14-MeV neutron bombarded natural selenium beginning (a) 3 seconds and (b) 3 minutes after the end of bombardment; 610-700 keV energy region . . .	127
58	Ge(Li) γ-ray spectra of 14-MeV neutron bombarded natural selenium beginning (a) 3 seconds and (b) 3 minutes after the end of bombardment; 760-950 keV energy region . . .	128
59	Ge(Li) γ-ray spectra of 14-MeV neutron bombarded natural selenium beginning (a) 3 seconds and (b) 3 minutes after the end of bombardment; 1200-1350 keV energy region . .	129
60	Ge(Li) γ-ray spectra of 14-MeV neutron bombarded natural selenium beginning (a) 3 seconds and (b) 3 minutes after the end of bombardment; 1400-1740 keV energy region . .	130
61	Ge(Li) γ-ray spectra of 14-MeV neutron bombarded natural selenium beginning (a) 3 seconds and (b) 3 minutes after the end of bombardment; top and bottom parts show 1820-1900 keV and 1940-2370 keV energy regions respectively	131
62	Ge(Li) γ-ray spectra of 14-MeV neutron bombarded natural selenium beginning (a) 3 seconds and (b) 3 minutes after the end of bombardment; top and bottom parts show 2500-2780 keV and 2800-3070 keV energy regions respectively	132
63	Proposed decay scheme of ^{80}As. All energies in MeV; numbers at arrow heads are intensities relative to the 665.8 keV transition = 100	142

Figure		Page
64	Level schemes of even-even selenium isotopes with mass numbers 72 to 82	144
65	Level schemes of ^{76}Se and neighbouring nuclei	146
66	Level schemes of ^{78}Se and neighbouring nuclei	147
67	Level schemes of ^{80}Se and neighbouring nuclei	148
68	Comparison of experimental levels and the theoretical predictions of the Davydov and Chaban model for ^{76}Se	152
69	Comparison of experimental levels and the theoretical predictions of the Davydov and Chaban model for ^{78}Se	153
70	Comparison of experimental levels and the theoretical predictions of the Davydov and Chaban model for ^{80}Se	154

CONTRIBUTION TO KNOWLEDGE

The decay scheme studies performed in this work have provided new and additional information on the β- and γ-decay properties of ^{76}As, ^{78}As and ^{80}As. In the case of ^{78}As and ^{80}As, the results represent substantial improvements over previous investigations.

Two previously unobserved ^{76}As γ-transitions at 563.5 and 981.2 keV energy are proposed as resulting from decay of known ^{76}Se levels at 1123.1 and 2671.5 keV respectively. In addition, the positions in the ^{76}As decay scheme of the 740.0, 772.5, 883.0, 1130.5, 1568.0, 1613.0 and 1870.5 keV γ-transitions have been confirmed by γ-γ coincidence studies performed for the first time in this study with NaI(Tl) and Ge(Li) detectors.

Energies and intensities for 32 γ-rays following the β-decay of ^{78}As have been measured, most of these for the first time. Coupled with β-γ, γ-γ and β-ray measurements, these data have allowed construction of a new ^{78}As decay scheme consisting of 18 excited levels in ^{78}Se with energies of 613.5, 1308.2, 1496.5, 1502.1, 1693.0, 1853.4, 1995.6, 2326.9, 2452.6, 2536.0, 2681.2, 2838.0, 3144.0, 3192.4, 3223.5, 3294.0, 3410.5 and 3495.0 keV. A total decay energy of 4.27 ± 0.1 MeV

and a half life of 90.7 ± 0.2 min for ^{78}As decay have also been deduced from experimental data obtained in this study.

Energies and intensities for 23 γ-rays following the β-decay of ^{80}As are reported, most of these also for the first time. Along with γ-γ coincidence measurements, these data have allowed construction of a new ^{80}As decay scheme consisting of 15 excited levels at 665.8, 1448.8, 1477.1, 1731.0, 1872.6, 1960.1, 2310.9, 2514.0, 2562.0, 2774.2, 2836.2, 3024.0, 3422.7, 3606.1 and 3726.6 keV. A half life for ^{80}As decay of 16.5 ± 0.3 sec was also determined from the decay of 665.8 keV γ-ray events.

CHAPTER 1

INTRODUCTION

1.1 General Objectives

During the past several years, the detection and precise energy measurement of nuclear radiations have been greatly facilitated by the development of lithium-drifted silicon and germanium detectors. The advantages of these detectors include excellent energy resolution, fast response, compact size, simple power supply requirements and reasonable cost. These have resulted in their extensive use in nuclear reaction studies[1,2] and β- and γ-decay scheme studies,[3] carried out previously by means of other types of detectors of lower resolution made from scintillating plastic, anthracene and NaI(Tl) crystals.

The high energy resolution of Ge(Li) detectors, now in the 0.1-0.2% range for 1 MeV γ-rays (almost two orders of magnitude better than that of NaI(Tl) scintillation detectors), have permitted accurate analyses of complex γ-spectra and more precise measurements of the properties of low-lying nuclear energy levels. The low γ-detection efficiency of Ge(Li) detectors, resulting from their

relatively small size compared to NaI(Tl) detectors, has been their main drawback. However, continued progress in lithium ion drift techniques and fabricated detector size indicates this disadvantage may be overcome.

Si(Li) detectors have been increasingly applied to the study of β-spectra, β-γ coincidences and internal conversion processes. In comparison with conventional magnetic spectrometers, Si(Li) detectors show comparable resolutions with higher transmissions and can be readily used as multichannel rather than single-channel devices.[76] In addition, β-ray spectral distortions caused by electron backscattering effects and γ-ray interactions have been largely eliminated by locating assemblies of these detectors in strong magnetic fields such as those produced by superconducting solenoids.[28,68,70]

It is the intent of this dissertation to present nuclear decay scheme studies of the neutron-rich isotopes ^{76}As, ^{78}As, ^{80}As performed using high resolution Ge(Li) and Si(Li) detectors and a superconducting magnet beta spectrometer. Comparisons are made with previous studies performed with other detection systems and the theoretical predictions of the Davydov and Chaban vibrational model.

1.2 Previous Work on ^{76}As, ^{78}As and ^{80}As Decay

1.2.1 The Decay of ^{76}As

The β- and γ- decay properties of ^{76}As have been extensively investigated in the past by many authors through use of bent-crystal,[17] double-focusing,[20] magnetic,[5,14,25-27] and NaI(Tl)[4-6] spectrometers. Use of Ge(Li) and Si(Li) detectors has also been reported recently by Aten et al.,[16] Murray et al[15] and McMillan and Pate[28] (the latter being publication of some preliminary data from the present study). While all these studies have resulted in considerable information on the decay scheme of ^{76}As, uncertainties still persist regarding the energies and positions in the decay scheme of some of the γ-rays. For example, several previous investigators[4,15,16] have predicted the existence of (but have not been able to resolve completely) pairs of ^{76}As γ-rays found at energies of about 0.559, 1.215, 1.613 and 1.957 MeV. In addition, some weak intensity γ-rays found by Aten et al.[16] and Vitman et al.[14] are not included in the most recently published decay schemes of ^{76}As by Murray et al.[15] and Nagarajan et al.,[25] presumably due to their assignment to ^{76}As being in doubt. Accordingly, the present ^{76}As decay scheme work was undertaken to search for as yet unobserved γ-lines and to perform β-γ and γ-γ coincidence measurements using higher resolution Ge(Li) and Si(Li) detectors than had been previously employed.

1.2.2 The Decay of ^{78}As

Information concerning the level structure of ^{78}Se prior to the present work on ^{78}As decay, resulted primarily from (p,p'), (d,d') and (d,p) reactions,[23,24] Coulomb excitation experiments,[33] and ^{78}As γ-spectrum measurements (using NaI(Tl) detectors) by Maddison,[30] Nemilov et al.[31] and Van Lieshout.[32] These previous studies did not resolve numerous uncertainties regarding ^{78}Se level energies. Therefore, the present study was undertaken with a view to obtaining more accurate data on the energies and relative intensities of the γ-rays accompanying the β-decay of ^{78}As. In addition, β-γ and γ-γ coincidence measurements were made to permit the identification of γ-γ cascades and the establishment of a more complete ^{78}As decay scheme. Following publication of the present work on ^{78}As decay,[28] similar results were reported by Paradellis and Hontzeas.[29]

1.2.3 The Decay of ^{80}As

The β- and γ- spectra of ^{80}Se following the β-decay of ^{80}As were first investigated by Meads et al.[42] with NaI(Tl) and anthracene detectors. Other information on ^{80}Se energy levels have resulted from (p,p') and (d,d') reaction studies,[24,93] Coulomb excitation experiments[33,111] and β^+, E.C. - decay scheme studies[88] of ^{80}Br. Uncertainties in the spins, parities and energies of most of these levels

remain due to the generally poor resolution of the detectors employed in these previous studies. The present work involved application of a large volume, high resolution Ge(Li) detector plus γ-γ coincidence techniques to further study of this problem.

CHAPTER 2

INTRODUCTORY THEORY

2.1 Nuclear Models

Decay scheme studies performed over the past few decades have provided important data for the development of nuclear structure theories. These studies have revealed significant differences between the spectra of odd A and even-even nuclei, the latter exhibiting a striking absence of low-lying intrinsic excitations.

It has been possible to interpret many observed nuclear properties such as energies, spins, parities and magnetic moments by considering the independent motion of individual nucleons in a spherically symmetric potential.[50] The classification of data on isomeric transitions and the explanation of "magic numbers" (neutron and proton numbers which form particularly stable nuclear configurations), gave further support to the independent-particle or shell model. For example, Figure 1 shows the first 2^+ state energies of even-even nuclei versus their neutron number and reveals some experimental evidence for shell structure in these nuclei at the magic numbers 28, 50 and 82.

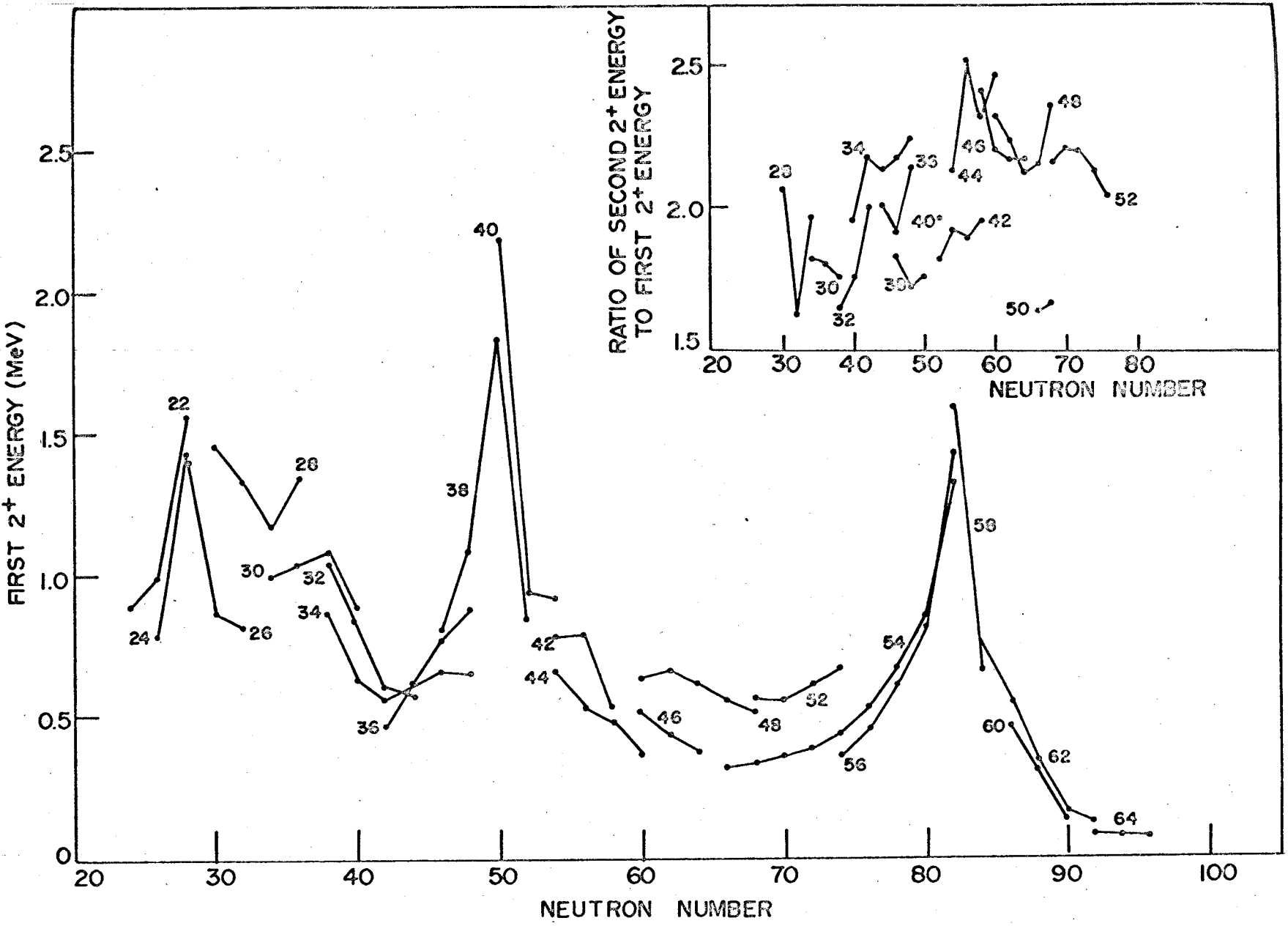

Figure 1 First 2^+ energy and ratio of second 2^+ energy to first 2^+ energy as a function of neutron number. Isotopic lines marked with proton numbers

On the other hand, considerable data on large quadrupole moments, strong E2 transition rates and the discovery of rotational bands in a large class of nuclear spectra have implied the occurrence of collective phenomena in nuclei.[49,50] Collective and individual particle effects have been combined in the "unified model"[83] but a truly comprehensive unified model which would explain all nuclear spectroscopic observations has not yet been formulated.

2.2 Collective States in Even-Even Nuclei

Experimental evidence of quadrupole moments and enhanced E2 transition rates has been interpreted in terms of spheroidal rather than spherical nuclear charge distributions. Current concepts of nuclear structure suggest closed-shell nuclei possess spherical shapes which can be deformed by the addition of nucleons.[49] An even-even nucleus, spheroidally deformed by the polarizing effect of many nucleons beyond closed-shell configurations, may have angular-momenta that reflect the coherent motion of the nucleus as a whole rather than the motion of a few nucleons moving independently in shell model states. The quantization of this coherent motion forms the basis for various collective models.

Such models make interesting predictions for low-lying excited states of highly deformed even-even nuclei,

which are found in the mass regions A≃24, 150<A<190, and A>220. Nuclei in the above regions exhibit rotational spectra with energies having the same sequence as those of a rigid rotating symmetric top, given by the following.[49]

$$E_{rot}(I) = \frac{\hbar^2}{2\mathcal{I}} I(I+1) \qquad (2\text{-}1)$$

$$I = 0, 2, 4, 6 \ldots \text{ even parity.}$$

For even-even nuclei in the medium weight region ($50 < A < 150$) close to closed-shell configurations, simplified nuclear vibrational models[80] (based on concepts derived initially from classical theories of the modes of motion of incompressible, liquid drops), predict excited states with energies $N\hbar w_\lambda$, classified by phonon quantum numbers N of multiple order 2^λ. Each phonon of type $\lambda\mu$ carries an angular momentum quantum number λ, with Z-component μ, and parity $(-1)^\lambda$. The first collective excitations in the low energy spectral region of even-even nuclei usually involve quadrupole ($\lambda=2$) and sometimes octupole ($\lambda=3$) oscillations.

For the first phonon (N=1), quadrupole excited state, the predicted spin and parity is 2^+; for N=2, the state is a degenerate triplet with I^π of 0^+, 2^+, and 4^+; for N=3, the state is five fold degenerate with I^π of 0^+, 2^+, 3^+, 4^+ and 6^+. The degeneracy of these levels is removed in

real nuclei by perturbations not considered here.[53]

Similarly, octupole oscillations have a one phonon level with spin and parity 3^- and a two phonon degenerate state with I^π of 0^+, 2^+, 4^+ and 6^+. In real nuclei, coupling of low-lying (N=1) quadrupole and octupole states can result in intermediate states of odd parity (1^-, 2^-, . . . etc.).

Comprehensive surveys of the properties of even-even nuclei by Eichler[53] and Scharff-Goldhaber[54] show many of these nuclei possess low lying first excited states with spin and parity 2^+ (except for ^{90}Zr and ^{72}Ge which have 0^+ first excited states) and second-excited states (with I^π of 0^+, 2^+ or 4^+) at energies varying between 2 and 2.5 times that of the first excited state. See Figure 1. Although these data agree surprisingly well with the general aspects of nuclear vibrational models with quadrupole oscillations, better agreement is obtained with nuclear collective models, such as the following, which describe the excited states of axially asymmetric nuclei.

2.3 The Davydov and Chaban Model

Vibrational states due to "γ*-vibrations" in spheroidally deformed nuclei about the condition of axial symmetry

---

*The γ-parameter determines the deviation of the shape of the nucleus from axial symmetry - see Figure 2.

were first investigated in models proposed by Bohr and Mottelson.[94,95] The consequences of dropping the assumption of axial symmetry was investigated in a series of papers by Davydov et al.[58-61]

Initially, Davydov and Filippov[58] considered the rotational excited states (and the electromagnetic transitions between them) of a nucleus with an ellipsoidal shape under the adiabatic approximation that rotation of the nucleus takes place without a change in its state of intrinsic excitation. However, a more general asymmetric rotor model was proposed by Davydov and Chaban[61] who took into account "β^*-vibrations" perturbed by the coupling between rotational and vibrational motions due to centrifugal forces.

The energies of collective nuclear excitations predicted by Davydov and Chaban's model are given by:

$$\frac{E_{K\nu_\ell}(J)}{\hbar w_o} = (\nu_\ell + 1/2)\sqrt{1 + 3/2\left(\frac{\mu}{p}\right)^4 \varepsilon_K(J)} + 1/4\left(\frac{\mu}{p}\right)^2 \varepsilon_K(J) + \frac{(p-1)^2}{2\mu^2} \quad \ldots \quad (2\text{-}2)$$

where

μ = the "nonadiabaticity" parameter, $(0<\mu<1)$;

$\varepsilon_K(J)$ = the energy of the K^{th} spin-J level of a hydrodynamical asymmetric rotor,[58] a function of the "nonaxiality" parameter γ;

---

*The β-parameter is a measure of the total deformation of a nucleus from a spherical shape - see Figure 2.

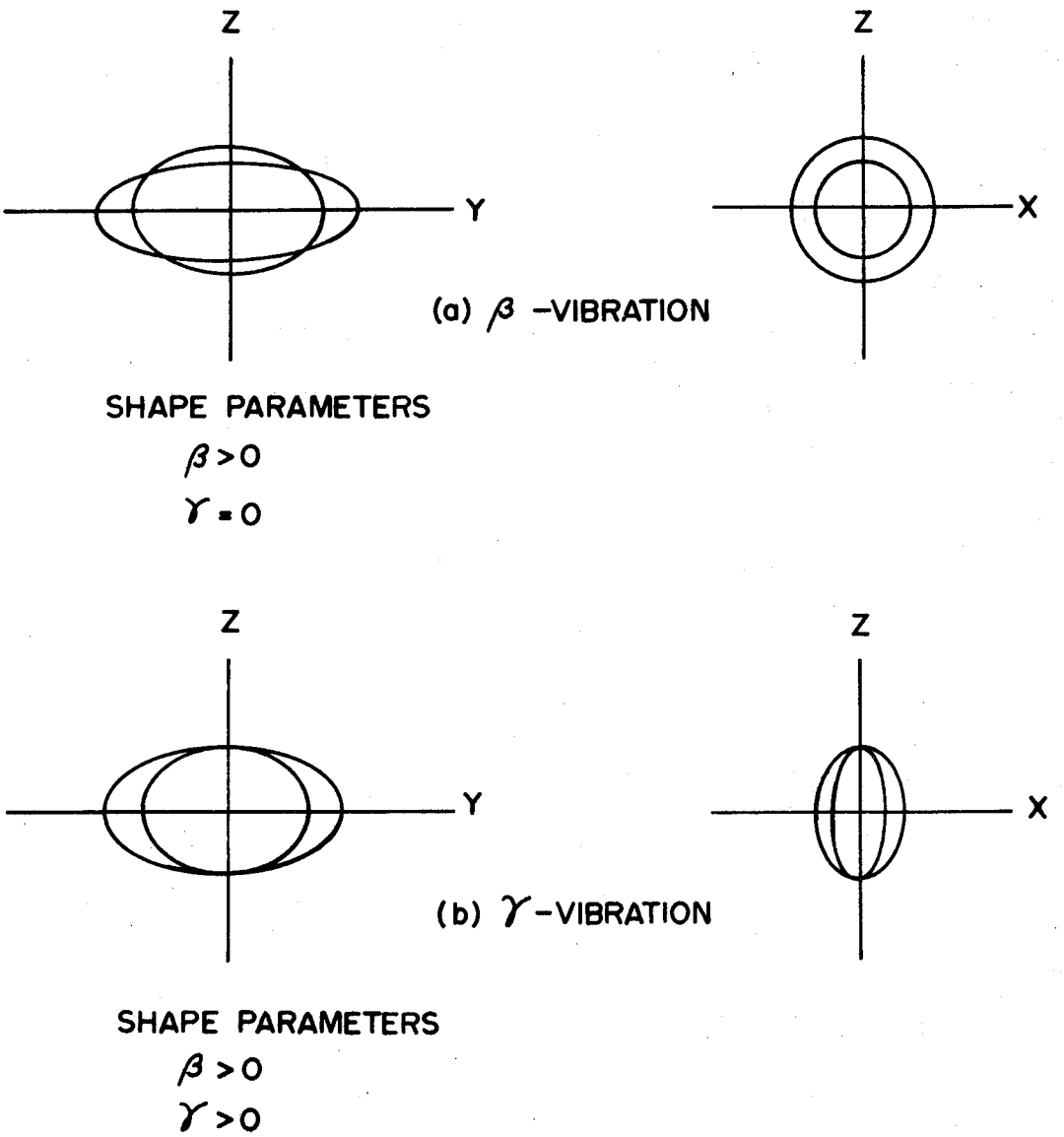

Figure 2 Simplified models showing β- and γ- vibrations

p = a parameter related to μ and $\varepsilon_K(J)$;

ν_ℓ = a quantum number defined in reference 61.

Computer calculations of the predicted level energies have been performed by Day et al.[57] for ease of comparison with experimental results.

In the general case collective excitation corresponding to a definite value of the total angular momentum J is a complicated combination of vibrational and rotational motions. The "nonadiabaticity" parameter μ, serves as a guide to the extent that the rotational and vibrational modes are coupled. For example, values of $\mu < 0.3$ are predicted for heavy nuclei far away from closed shells (such as ^{160}Dy, ^{186}Os, ^{188}Os, and ^{168}Er) in which rotational excitations are comparatively distinct while values of $\mu > 0.5$ are found for lighter nuclei (such as ^{56}Fe, ^{110}Cd and ^{114}Cd). Comparison of Davydov and Chaban's model with experimental data by Klema et al.[63] and Davydov et al.[61] indicated it was reasonably successful for a rather wide range of even-even nuclei although the correlation between theory and experiment was not always within experimental error.

The two phenomenological parameters μ and γ, are often determined for each nucleus by comparisons of experimental and theoretical data for three low-lying levels, such as the first two $I=2^+$ and $I=4^+$ levels. Figure 3 compares experimental excited level energies for several nuclei with

theoretical predictions using the Davydov and Chaban model for the case $\mu=0.3$. The energy of levels shown in this figure for various spins J is expressed in terms of the following ratio:

$$R_{K\ell}(J) = \frac{E_{K\nu_\ell}(J) - E_{1\nu_1}(0)}{\Delta} \qquad (2\text{-}3)$$

where $\Delta = E_{1\nu_1}(2) - E_{1\nu_1}(0)$ is the energy of the first excited 2^+ level.

Comparisons of this theory with experimental data accumulated on the levels of ^{76}Se, ^{78}Se and ^{80}Se in the present studies are included in a following section.

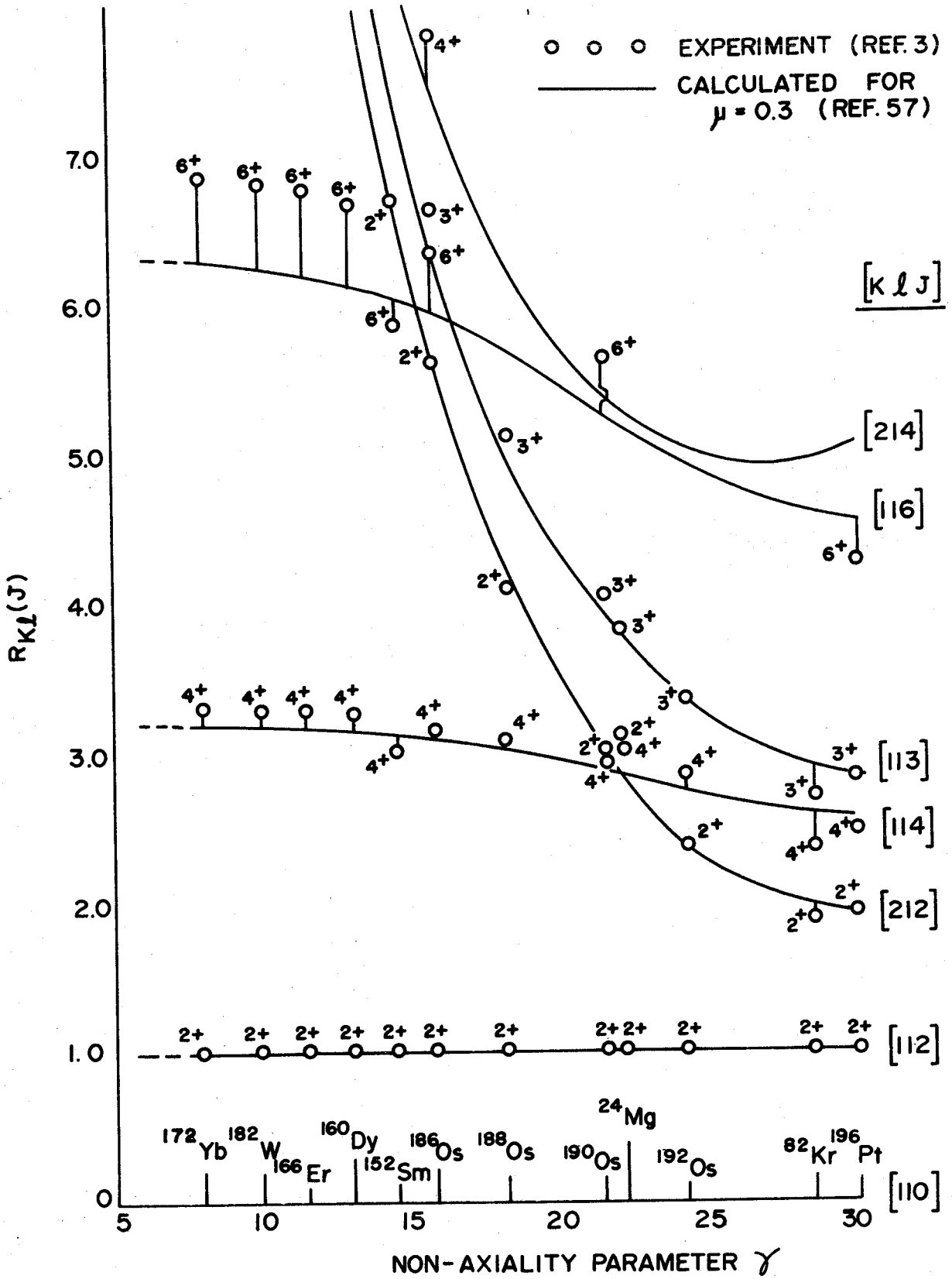

Figure 3 Comparisons of experimentally measured energy levels of even-even nuclei with the Davydov and Chaban model

CHAPTER 3

EXPERIMENTAL TECHNIQUES

3.1 Irradiation and Source Preparation Procedures

3.1.1 ^{76}As Preparation Procedure

Radioactive ^{76}As samples used in the following experiments were prepared from the $^{75}As(n,\gamma)$ reaction by bombarding solid As_2O_3* in the 100 kW nuclear reactor at the University of Washington in Seattle. Initial ^{76}As activities of approximately 10 mci were produced by 4-5 hour irradiations of 100 mg samples of As_2O_3, heat sealed inside polyethylene capsules, at a thermal neutron flux of about 10^{12} neutrons/sec-cm^2.

Experience showed that the polyethylene capsules used in the reactor irradiations became contaminated with activities from the reactor rabbit system and the neutron activation of trace impurities in the polyethylene. It was therefore imperative that this source of extraneous activity be eliminated by transferring the irradiated As_2O_3 to fresh,

---

*Obtained from Fisher Scientific Company, primary standard ACS.

polyethylene capsules before γ-radiation measurements began. One day after the irradiations, a single decay component with a 26.4 ± 0.1 h half-life was found in good agreement with the literature value[3] and demonstrated the absence of any significant foreign activities greater than about 1 part in 10^3. No further chemical separations were performed on these samples.

To prepare thin uniform samples of ^{76}As for β-measurements, aliquots of a solution (prepared by dissolving the irradiated As_2O_3 in 6NHCl) were pipetted on to 6.3 μm thick Al foil, previously treated with zinc insulin to promote deposit uniformity.[56] The solution was evaporated under IR and gave 0.2 - 0.5 cm diameter sources, of a superficial density judged adequately thin for measurements on the 2.97-MeV β-rays of ^{76}As.

3.1.2 ^{78}As Preparation Procedure

Samples of 91-min ^{78}As were prepared from the $^{81}Br(n,\alpha)$ reaction by bombarding 300 g samples of granular sodium bromide* in polyethylene bags with 14-MeV neutrons from the Texas Nuclear Corporation model 9900 neutron generator of the Nuclear Chemistry laboratories at Simon Fraser University. Bombardments of 1/2 hour duration at an average flux of 10^9

---

*Obtained from Fisher Scientific Company.

neutrons/sec-cm^2 were sufficient to yield initial activities of about 10^5 d/s in which ^{78}As accounted for 85-90% of the total arsenic activity with the remaining 10-15% due to ^{76}As.

The arsenic activity was chemically separated from other reaction products by volatilization as AsH_3 gas. Figure 4 shows the arrangement of the apparatus used. Measurements of the γ-ray spectrum of ^{78}As ordinarily began 10-15 minutes after the end of bombardment although times as short as 2-3 minutes were accomplished when required without serious loss of yield and activity.

The precise chemical details of the techniques involved in the chemical separation of ^{78}As are as follows:

A few minutes after the end of bombardment, a mixture of 10 g of granular zinc metal (20 mesh) and the irradiated sodium bromide was prepared and poured into a distilling flask pre-heated to boiling water temperature by an electrical-heating mantle. Immediately following this step, 1 ml of 10 mg As^{+3}/ml and 2 mls of 10 mg Se^{+4}/ml carrier solutions were added to the distilling flask. The water aspirator was turned on to maintain an air stream through the apparatus. A volume of 400 to 500 mls of a sulphuric acid solution was then added to the zinc and sodium bromide mixture over a time period of about 1-2 minutes and typically contained the following components:

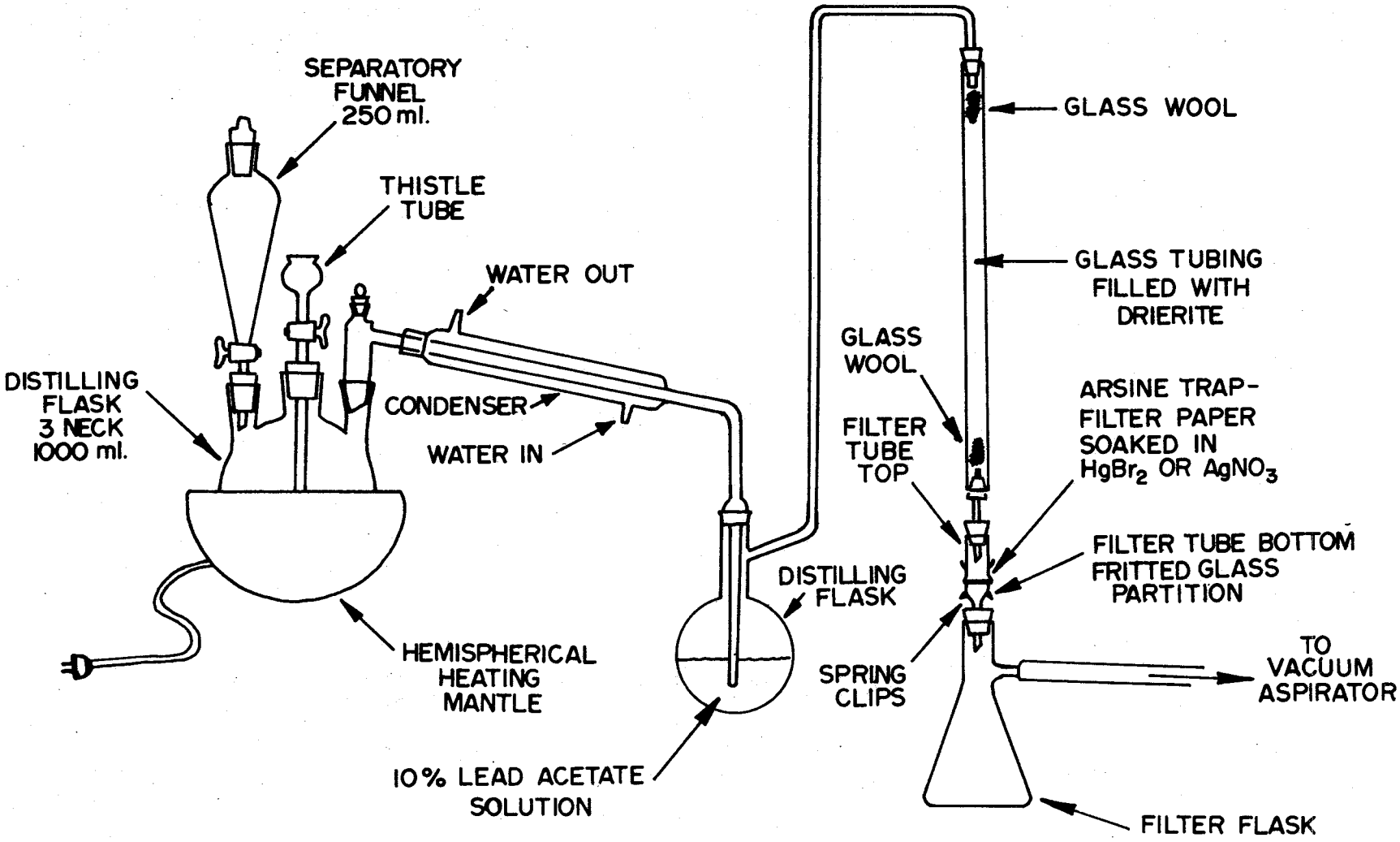

Figure 4 Arsine generating apparatus

400-500 mls boiling, distilled water

30 mls conc. H_2SO_4

2 mls of 10 mg I^-/ml

2 mls of 1 mg Sn^{++}/ml

2 mls of 1 mg Fe^{++}/ml

The generation of AsH_3 gas resulted from the zinc reduction of arsenites and arsenates in the sulphuric acid solution by means, for example, of the following reaction.

$$AsO_3^{-3} + 3Zn(s) + 9H^+ \rightarrow 3Zn^{+2} + 3H_2O + AsH_3 \uparrow$$

The reducing agents I^-, Sn^{++} and Fe^{++} (derived from NaI, $SnCl_2$ and $FeCl_2$ respectively) improved the rapid generation of AsH_3 gas. The liberated AsH_3 gas, after passing through a 10% lead acetate solution and a column of granular anhydrous calcium sulphate (Drierite) to remove contaminant bromide and selenium activities, was trapped on Whatman No. 1 filter papers previously impregnated with either aqueous $AgNO_3$ or alcoholic $HgBr_2$. See Figure 5(a). Both the $AgNO_3$ and $HgBr_2$ filter papers proved effective in trapping most of the AsH_3 gas passing through them by the following reactions.[120]

(i) $AgNO_3$ Filter Paper

$$AsH_3 + 6\ AgNO_3 \longrightarrow 3HNO_3 + (AsAg_3 \cdot 3AgNO_3)\downarrow$$

$$(AsAg_3 \cdot 3AgNO_3) + 3H_2O \longrightarrow H_3AsO_3 + 3HNO_3 + 6Ag\downarrow$$

(ii) $HgBr_2$ Filter Paper

$$AsH_3 + 3HgBr_2 \longrightarrow 3HBr + As(HgBr)_3\downarrow$$

$$2As(HgBr)_3 + AsH_3 \longrightarrow 3AsH(HgBr)_2$$

$$As(HgBr)_3 + AsH_3 \longrightarrow 3HBr + As_2Hg_3$$

The formation of bright yellow precipitates on the surface of the filter papers a few seconds after the addition of the acid solution and the detection of radioactivity in the filter tube assembly by a portable Geiger-Müller counter signaled the deposition of ^{78}As. After 10-15 minutes, the filter papers were removed from the spring-loaded filter tube, mounted for γ-radiation assay purposes on 3" x 3" square aluminum cards and covered with Scotch tape.

For the β-counting experiments, samples of ^{78}As were prepared by allowing the AsH_3 gas to impinge on 6.3 μm thick Al foil in the center of which $AgNO_3$ had been previously deposited. The Al foil was prepared in the same manner as

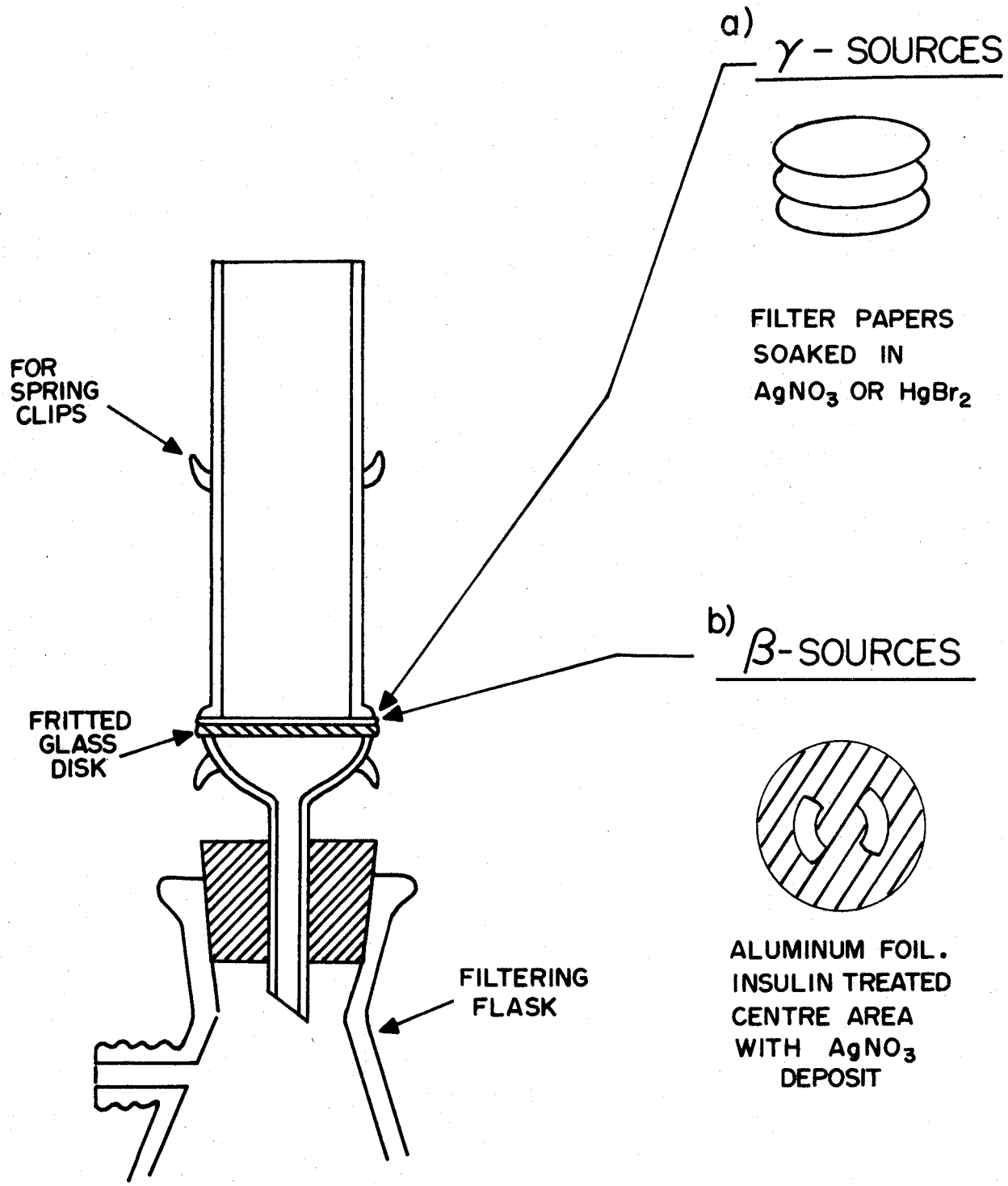

Figure 5 Filter tube details

described in sub-section 3.1.1 except that a dilute solution of $AgNO_3$ was substituted for the acidic As_2O_3 solution. Hydrogen gas liberated in the distillation procedure flowed through two holes cut in the aluminum as shown in insert (b) of Figure 5.

3.1.3 ^{80}As Preparation Procedure

Attempts to produce ^{80}As activities from the ^{80}Se (n,p) reaction induced by 14-MeV neutrons, adequate for γ-ray spectrum measurements, were made by two different methods. Details of the techniques involved in these two methods, only the second of which was successful, are as follows.

(a) Method # 1. ^{80}As Electrolytic Cell Process

This method involved the continuous production of $^{80}AsH_3$ gas by the electrolytic reduction of a selenous acid solution bombarded with 14-MeV neutrons. The solution was prepared by dissolving 2-4 g of selenous acid* and about 1 mg of As_2O_3 carrier in 300 mls of 6-7 N sulphuric acid. The process flow diagram of the ^{80}As electrolytic cell is shown in Figure 6. A Manostat varistaltic liquid pump constantly circulated the selenous acid electrolyte to

*Obtained from Fisher Scientific Company.

successively the constant level reservoir, the cathode compartment, and the selenium metal settling vessel through 1/4" diameter tygon tubing. The settling vessel attached to the exit opening of the cathode compartment was designed to trap and hold selenium metal formed during the electrolysis. The D.C. power supply used in this experiment was capable of delivering a maximum current of 100 amperes at 24 volts from a 208 volt, 3 phase A.C. input. However, the resistance of the cell, typically about 1 ohm, allowed a maximum current of only 25 amperes.

The 16.5-sec half life of ^{80}As required that this isotope be separated from other reaction products, transported to the detector position and its radiations measured, in a few seconds after its formation. Although experimental data on the decay properties of ^{80}As were not obtained by this method, the results obtained with it suggested that the process could have been used if higher neutron fluxes were available. In addition, the process can be applied in a general way, with appropriate physical changes, to the study of short-lived isotopes produced in such reactions as ^{235}U (n,f) or ^{238}U (n,f) whenever they can be reduced to a gaseous form by electrolysis.[78,79]

Arsine gas, produced in the cathode compartment of the electrolytic cell shown approximately full size in Figures 7 and 8 (front and side views respectively), was

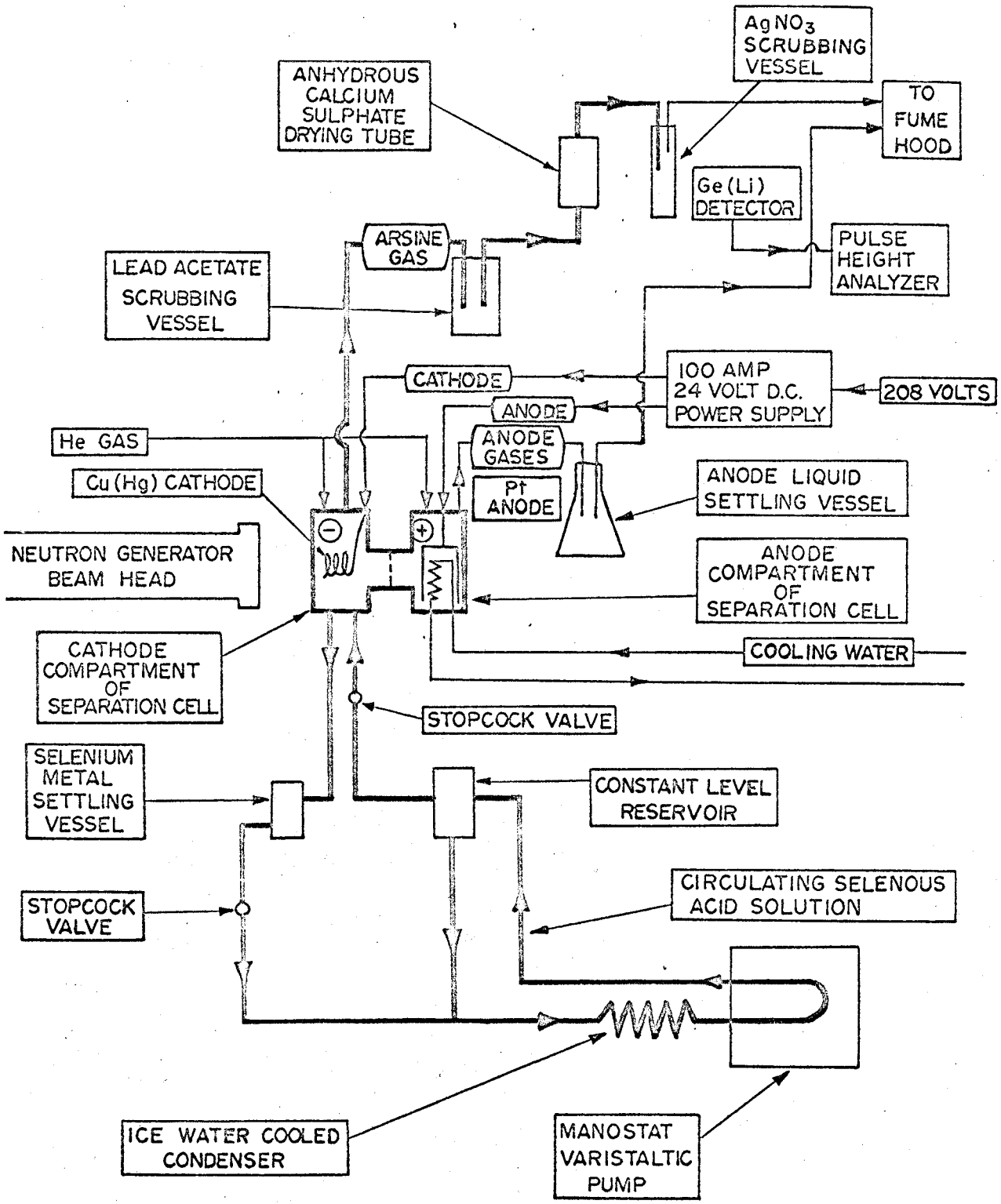

Figure 6 ^{80}As electrolytic cell - process flow diagram

passed through a 10% lead acetate solution and a column of granular anhydrous calcium sulphate (Drierite) to remove entrained liquids carried over from the cell and contaminant gaseous selenium activities in the form of H_2Se. Carried by the helium gas, the arsine was transported 35 feet through 1/8" diameter tygon tubing to a lead shielded detector position and then bubbled through and trapped in a saturated solution of $AgNO_3$. Hydrogen and helium gases were then allowed to flow to a fume hood through another 5 feet of 3/8" diameter tygon tubing attached to the outlet of the $AgNO_3$ scrubbing vessel.

Anode gases produced in the anode compartment of the electrolytic cell were first passed through a liquid settling vessel to catch entrained liquids and then through 35 feet of tygon tubing to a fume hood. The use of helium gas and the relatively long length of tygon tubing helped establish a pressure balance between the two compartments of the cell. The 1 1/4" diameter coiled cathode, made from 3/16" diameter mercury-coated copper wire, extended to the outside of the cell through a small rubber stopper and was attached to a cable from the negative terminal of the D.C. power supply. The anode, made from a perforated 1" diameter, 2" high cylinder of platinum, was connected to a cable from the positive terminal of the D.C. power supply by two tungsten wires.

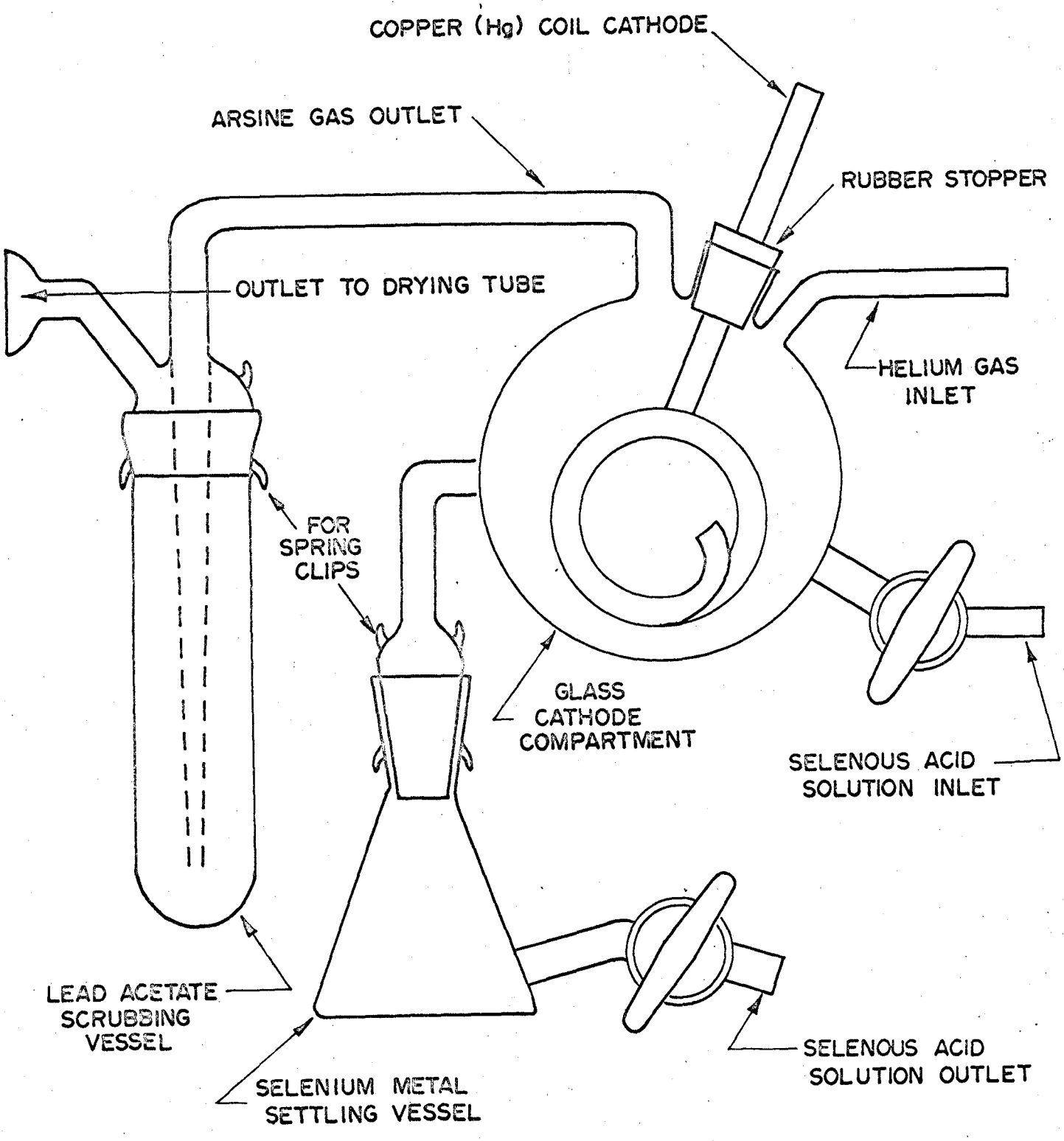

Figure 7 ^{80}As electrolytic cell-front view

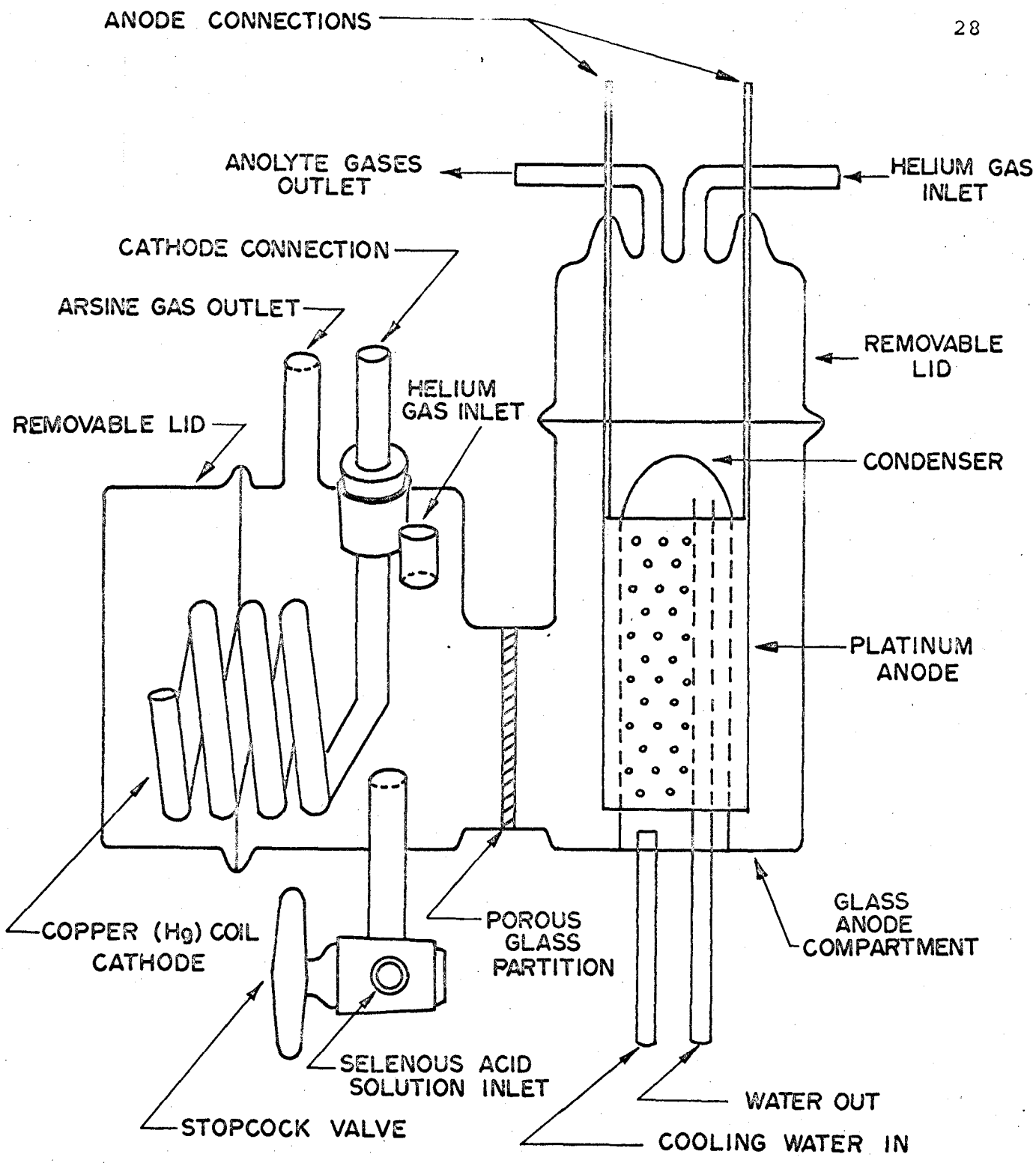

Figure 8 ^{80}As electrolytic cell-side view

Heat generated in the electrolytic cell was removed by three methods. They involved (a) circulating water through a 3/4" diameter by 2 3/4" high cooling chamber located inside the platinum cylinder anode, (b) passing spent electrolyte through a glass coil cooled by an ice water bath, and (c) directing a stream of compressed air onto the cell at the porous glass partition site. All three methods were required to control adequately the heat generated during the electrolysis.

The condition of the electrolysis cell was continuously monitored during each run with a closed-circuit T.V. camera.

A few trials using about 1 mci of 26.4-h ^{76}As carrier dissolved in the electrolyte were made to determine cell efficiency. All other parameters of the cell were maintained the same as before except that the neutron generator was not turned on. A 23.8 cm^3 Ge(Li) co-axial detector was mounted in front of the $AgNO_3$ scrubbing vessel and connected to a conventional amplifier-scaler counting apparatus. Figure 9 shows the scaler output of the Ge(Li) detector system counting radioactive $^{76}AsH_3$ gas trapped in the $AgNO_3$ as a function of time after the electrolysis current was turned on. As can be seen, the scaler count rate increased by a factor of about 25 above the background rate after 5 1/2 minutes of current flow. These data were interpreted to mean that the basic chemical principles of the electrolytic method of separating AsH_3 gas were working properly.

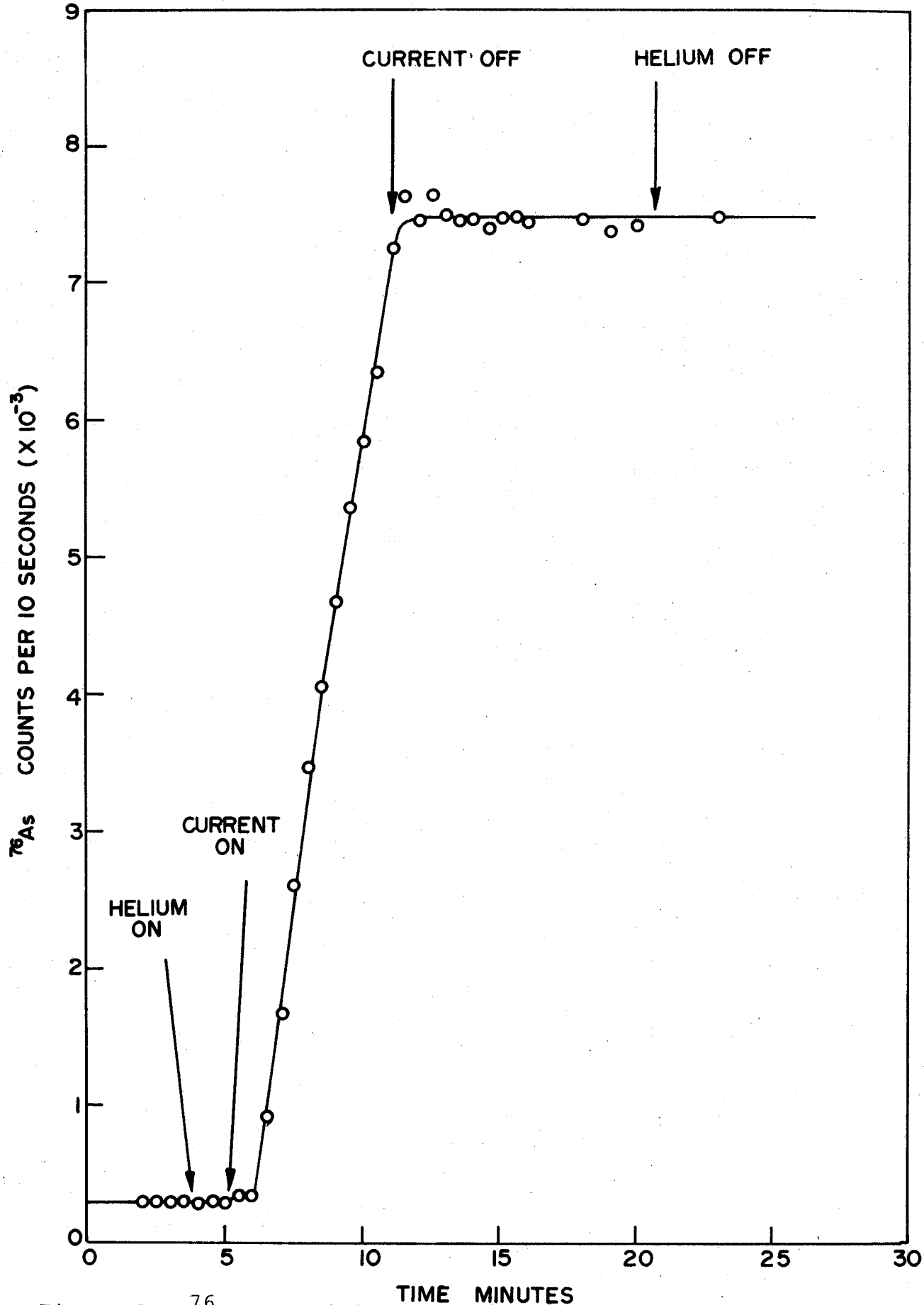

Figure 9 $^{76}AsH_3$ activity from the electrolytic cell as a function of time

The cell efficiency was very low, however, as reflected by the fact that only about 0.025% of the 1 mci of 26.4 h-^{76}As activity placed initially in the cell was transported to the detector position per second of current flow. In the study of short-lived isotopes, the counting rate at the detector position would be decreased further by the amount of decay occurring in the approximately 15 second transit time. In the case of 16.5-sec ^{80}As, this would involve a decay factor of about 50%

Experiments in which the neutron generator was used to generate ^{80}As in the electrolyte failed to produce significant increases in detector counting rates above background. The failure to accumulate appreciable ^{80}As γ-activity at the detector position was accorded, amongst other possible reasons, to too low a neutron flux from the neutron generator for the given ^{80}Se(n,p) ^{80}As reaction cross-section and too low a chemical yield from the electrolytic cell. Therefore, since it appeared that both these factors would have to be improved by a considerable amount in order to make the process useful, further development was discontinued.

(b) Method #2. ^{80}As Batch Process

Samples of ^{80}As of useful strength were successfully prepared from the ^{80}Se(n,p) reaction by the 14-MeV neutron bombardment of polyethylene capsules containing 25 g of

natural selenium metal powder.* Due to the relatively short half-life of this isotope, a timer-controlled pneumatic rabbit transport system was used to carry the samples rapidly back and forth between the neutron generator and the Ge(Li) detector position. Typical irradiation cycles in these experiments involved an 18-sec irradiation time followed by a 36-sec count time with transit times in both directions of about 3 sec. This cycle was repeated continuously for several hours with γ-ray spectrum data from successive irradiations automatically added to accumulate sufficient statistics for adequate analysis. By exchanging the irradiated selenium samples with fresh samples several times during each run and by keeping the irradiation time period short at 18 sec, background radiations due to long-lived activities were kept to a minimum. However, they were not entirely eliminated due to the absence of a chemical separation of the ^{80}As and the use of natural Se (49.82% ^{80}Se) rather than Se enriched in ^{80}Se for reasons of cost.

Corrections for these radiations involved (a) repeating the same measurements as above, but incorporating a 100 sec delay between the end of irradiation and the beginning of radiation measurements, and (b) recording the γ-spectrum (containing lines due to ^{28}Al from the ^{28}Si(n,p) reaction) of the irradiated empty polyethylene capsules.

---

* 99% Se; obtained from Fisher Scientific Company.

A third background measurement of weaker background radiations involved a 2 hour count of the irradiated selenium metal capsules beginning 3 minutes after the end of the last irradiation cycle. An analysis of the γ-lines appearing in these three latter spectra constituted the basis for eliminating them from further consideration as arising from decay of 16.5-sec ^{80}As or 14-sec ^{82}As.

3.2 Radiation Measurements

3.2.1 Half Life Measurements

Half life measurements for ^{76}As, ^{78}As and ^{80}As were accomplished by two methods. The first method, applied to ^{76}As and ^{78}As, involved following β- and γ- activity (without energy analysis) as a function of time using gas flow proportional counters and NaI(Tl) detectors. The second method, applied to ^{80}As, involved following the decay of individual γ-rays.

The electronic apparatus used in the determination of the half life of ^{80}As is shown in Figure 10. Samples of natural selenium metal were bombarded for 18 sec periods and rapidly transported to the Ge(Li) detector position by the same rabbit system as was used in the γ-ray spectrum measurements. (See sub-section 3.1.3(b)). A single channel analyzer and a linear gate were used to place a narrow

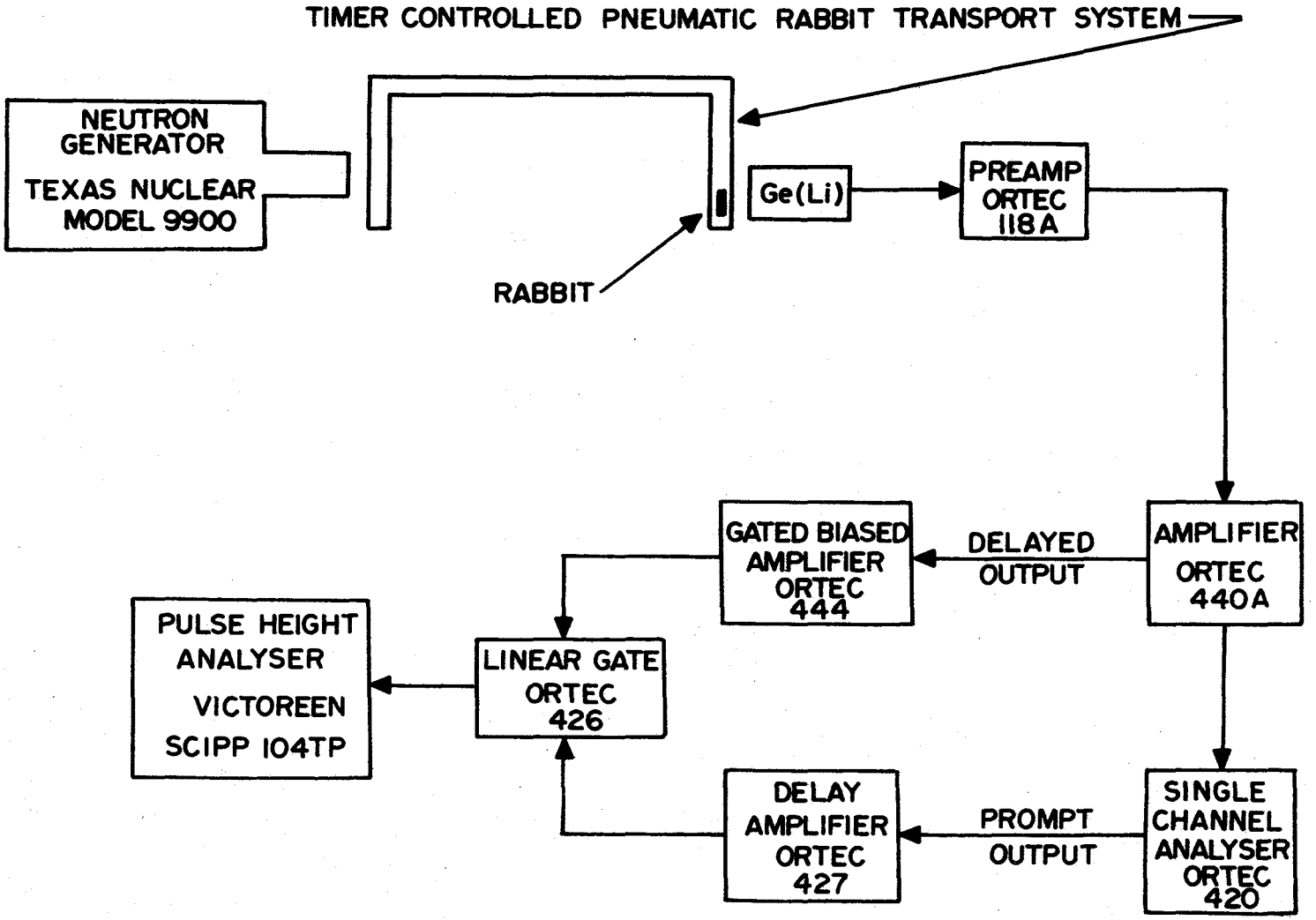

Figure 10 ^{80}As half-life measurement-circuit diagram

window on the intense 665.8 keV γ-ray known from previous work[42] to follow the decay of ^{80}As. Electronic pulses from the amplifier, in coincidence with pulses in this gated window, were recorded by a Victoreen Scipp 104TP pulse height analyzer operating in a multiscaling mode with an internal time base of about 1 sec per channel. Counting of this γ-ray continued for approximately 200 seconds. The selenium sample was then automatically returned to the neutron generator vault and the above process repeated 10-20 times with counts from each run added in order to accumulate data with a higher degree of statistical significance.

The high resolution of the Ge(Li) detector allowed a narrow window to be placed on the γ-ray of interest, thereby excluding significant contributions from other nearby (in energy) γ-rays from other activities. For example, in this experiment, the 14-MeV neutron bombardment of natural selenium produces some ^{82}As as well as ^{80}As activity. Since the most intense ^{82}As γ-ray at 654.7 keV[91,92] is only about 11 keV less in energy than that of the most intense ^{80}As γ-ray at 665.8 keV,[42] a Ge(Li) detector has to be used to resolve them completely. The above method of determining half lives was tested by following the decay of the ^{23}Ne-440 keV γ-ray and the ^{77m}Se-161 keV γ-ray. Half lives obtained for these two nuclides were in close agreement with previously accepted values.[3]

3.2.2 Gamma-Ray Counting Techniques

(a) Single Detector Systems

The theoretical principles and operating characteristics of the Ge(Li) semi-conductor detectors used in the present measurements have been extensively reviewed by A.H. Sher.[65] Single detector γ-ray spectra of ^{78}As were obtained using an 8 cm^3 Ge(Li) planar detector (FWHM of 3.8 keV at 613.5 keV energy) fabricated in the Nuclear Chemistry laboratories at Simon Fraser University. The single detector γ-ray spectra of ^{76}As and ^{80}As were observed using a 23.8 cm^3 Ge(Li) co-axial detector* (FWHM of 3.5 keV at 1332.5 keV energy) and a 0.155 cm^3 Ge(Li) X-ray detector* (FWHM of 1.1 keV at 569.6 keV energy). The exceptionally high resolution of the 0.155 cm^3 Ge(Li) detector was advantageously applied in the case of observations of the γ-ray spectra of ^{76}As where previously unresolved high energy pairs of γ-rays were found.

A 7.6 cm by 7.6 cm NaI(Tl) detector was used as one detector in γ-γ studies (see sub-section 3.2.2(b)). The single detector γ-ray spectrum of ^{78}As (see Figure 37) obtained with this detector does not however, resolve the many γ-lines present and illustrates the impact on this field of the availability of Ge(Li) detectors. All single detector γ-ray spectra used in this study of ^{76}As, ^{78}As and ^{80}As were

*From ORTEC (Oak Ridge Technical Enterprises Corporation), Oak Ridge, Tennessee.

in fact obtained using the Ge(Li) detectors listed above.

Pulses from the Ge(Li) detectors were amplified by ORTEC model 118A preamplifiers and ORTEC model 440A selectable active filter amplifiers before being fed into either a Nuclear Data 160 1024-channel or a Victoreen Scipp 104TP 3200-channel pulse height analyzer. When it was desired to examine certain areas of the γ-ray spectra at higher gain, this was achieved through use of ORTEC model 444 gated biased amplifiers.

(b) Gamma-Gamma Detection Systems

In γ-γ coincidence spectrum measurements, a γ-ray spectrum is recorded of events detected in one γ-detector which are coincident within a resolving time 2τ with events detected by a second γ-detector. When a "single parameter" experiment is performed, events in the second detector of the energy of interest are selected by a single channel pulse height analyzer, the output of which is used to "gate" on the multichannel pulse height analyzer by which the spectrum from the first detector is measured. When a "two-parameter" experiment is performed, events from the two detectors which are found to be coincident in time are then both analysed and the pulse heights measured for the time-correlated event-pairs stored as a two-dimensional spectrum.

In a single parameter measurement, a "window" of the single channel pulse height analyzer is set around only

one of the γ-rays of the spectrum of interest at a time. The disadvantage of the single parameter experiment compared with a two-parameter one is that the former does not allow the simultaneous measurement and determination of effects in coincident spectra due to Compton events from higher energy γ-rays which are conveniently permitted by the two-parameter mode.

Gamma-gamma coincidence measurements in this work normally involved a 7.6 cm by 7.6 cm NaI(Tl) detector together with one of the larger Ge(Li) detectors listed in the preceding section. For certain studies of weak intensity γ-γ cascades in ^{78}As, two 7.6 cm by 7.6 cm NaI(Tl) detectors were employed. In a few of the γ-γ coincidence measurements of ^{76}As, however, the 23.8 cm^3-Ge(Li) and the 0.155 cm^3-Ge(Li) ORTEC detectors were used to take advantage of their very high resolution capabilities.

Coincidence measurements on ^{76}As and ^{78}As were usually made with the center lines of the two detectors at 180° and passing through the centre of the source. The source was typically 3 or 4 cm from each detector and placed between 0.5-1 cm thick plates of plexiglass to absorb β-rays.

For single parameter measurements, the electronic apparatus shown in the block diagram of Figure 11 was used with the detection of coincident events and the selection of event energies accomplished with a Cosmic Radiation model

801 coincidence unit utilizing a fast coincidence resolving time 2τ of 30-180 nanoseconds. A Nuclear Data 160 1024-channel pulse height analyzer was used to record the Ge(Li) γ-spectrum.

For the two parameter γ-γ spectra, the Nuclear Data 160 and Victoreen Scipp 104TP analyzers were used in 256 by 16 channel and 100 by 100 channel configurations respectively.

3.2.3 Beta-Ray Counting Techniques

(a) Superconducting Magnet Beta Spectrometer

All the β-ray spectra shown in the following data sections were measured using Si(Li) detectors. The β-ray spectrum of ^{78}As was measured using a liquid helium cooled superconducting solenoidal magnet* to steer the electrons onto two identical Si(Li) detectors in the arrangement shown in Figures 12 and 13. Both detectors (supplied by Simtec Limited, Montreal, Quebec), had an active area of 200 mm^2, a depletion depth of 3 mm, and an energy resolution of 10-15 keV at 1 MeV electron energy. The detectors and source were in vacuum at temperatures near or below that of liquid nitrogen. This instrument, capable of a 30 kG maximum field strength, is essentially identical to the

---

*Manufactured by Westinghouse Electric Corporation, New Products Division, 7800 Susquehanna Street, Pittsburgh, Pa., U.S.A.

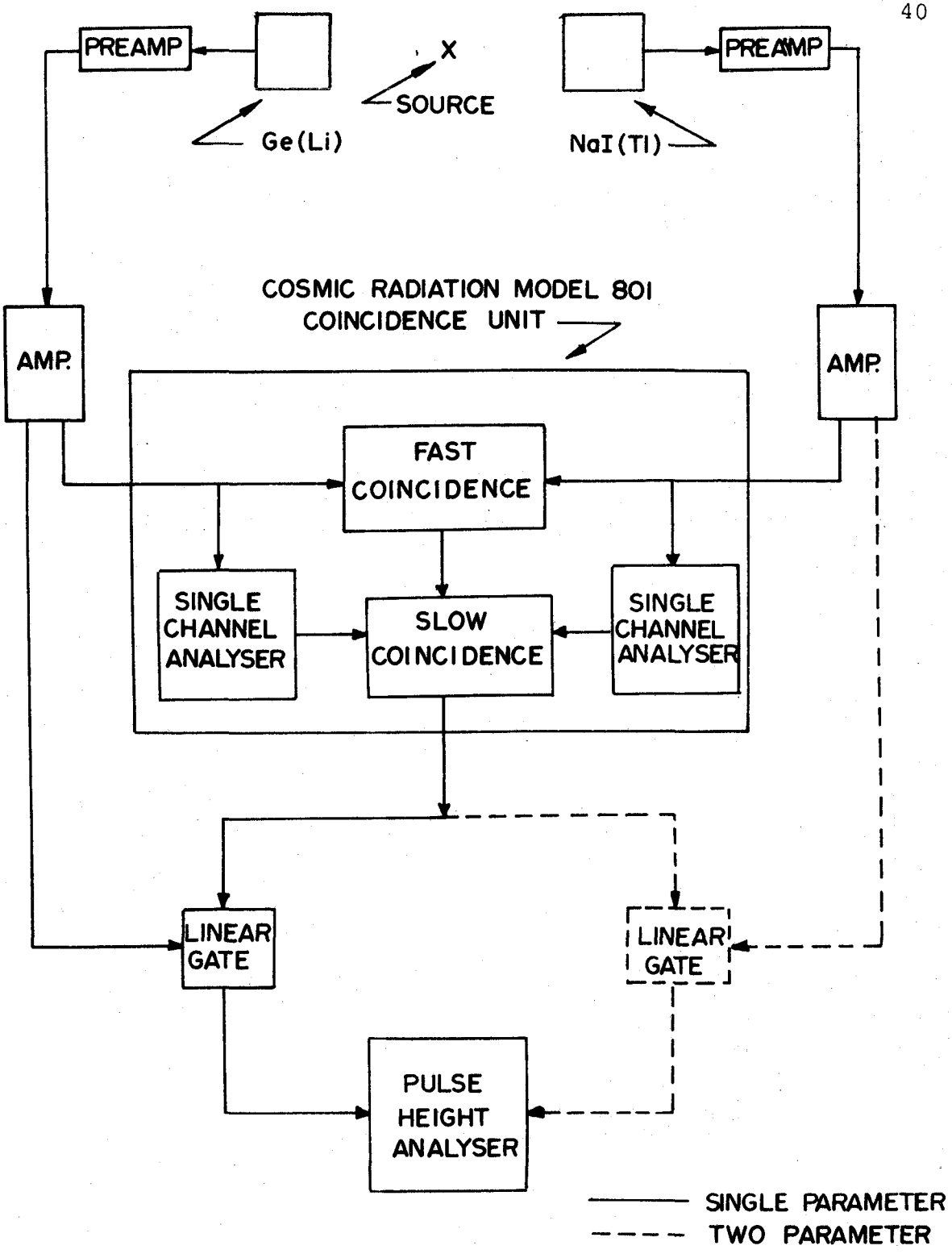

Figure 11 Electronic apparatus used in γ-γ coincidence experiments

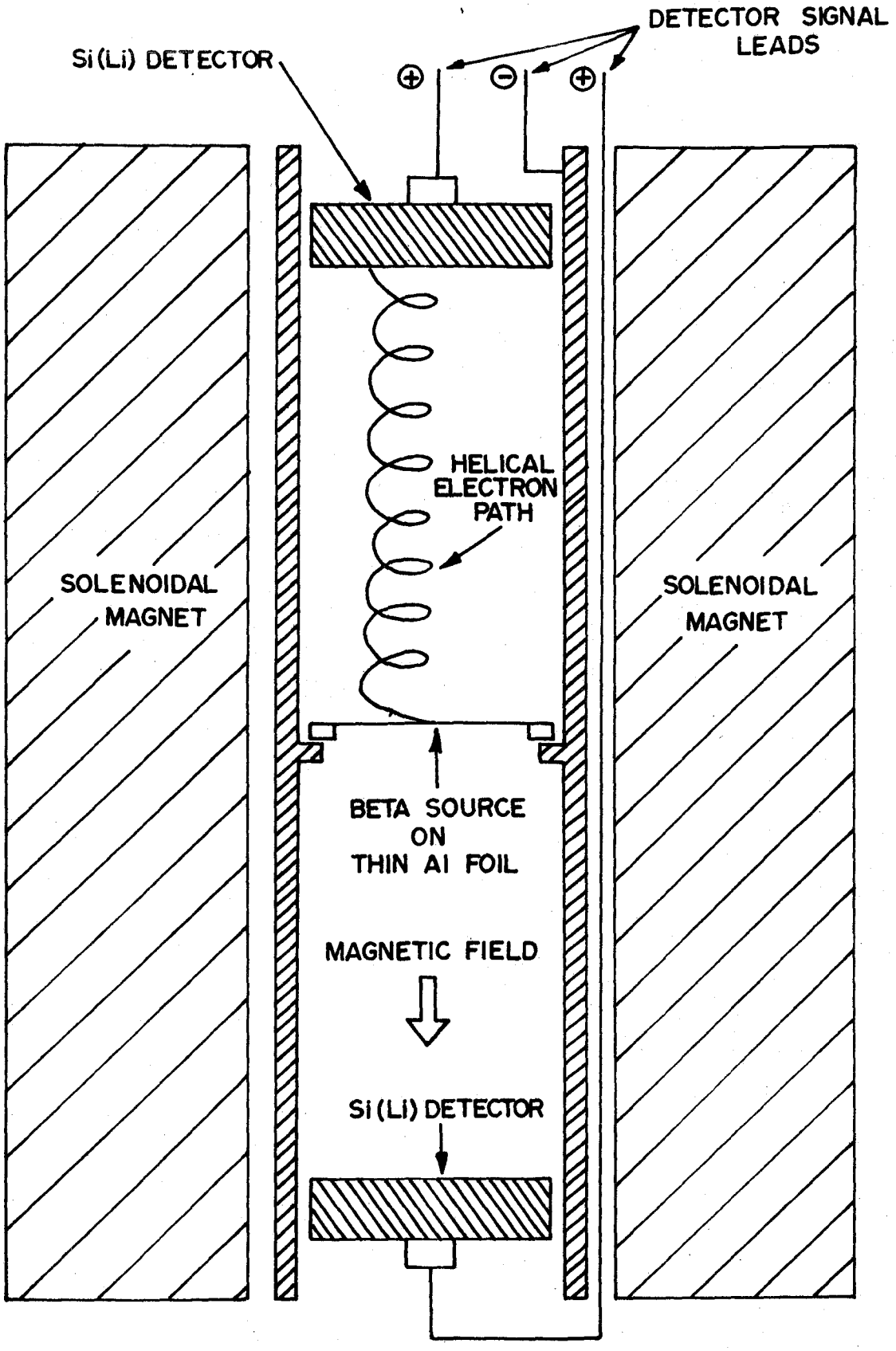

Figure 12 Si(Li) superconducting magnet beta spectrometer system (diagrammatic) showing detector and source positions

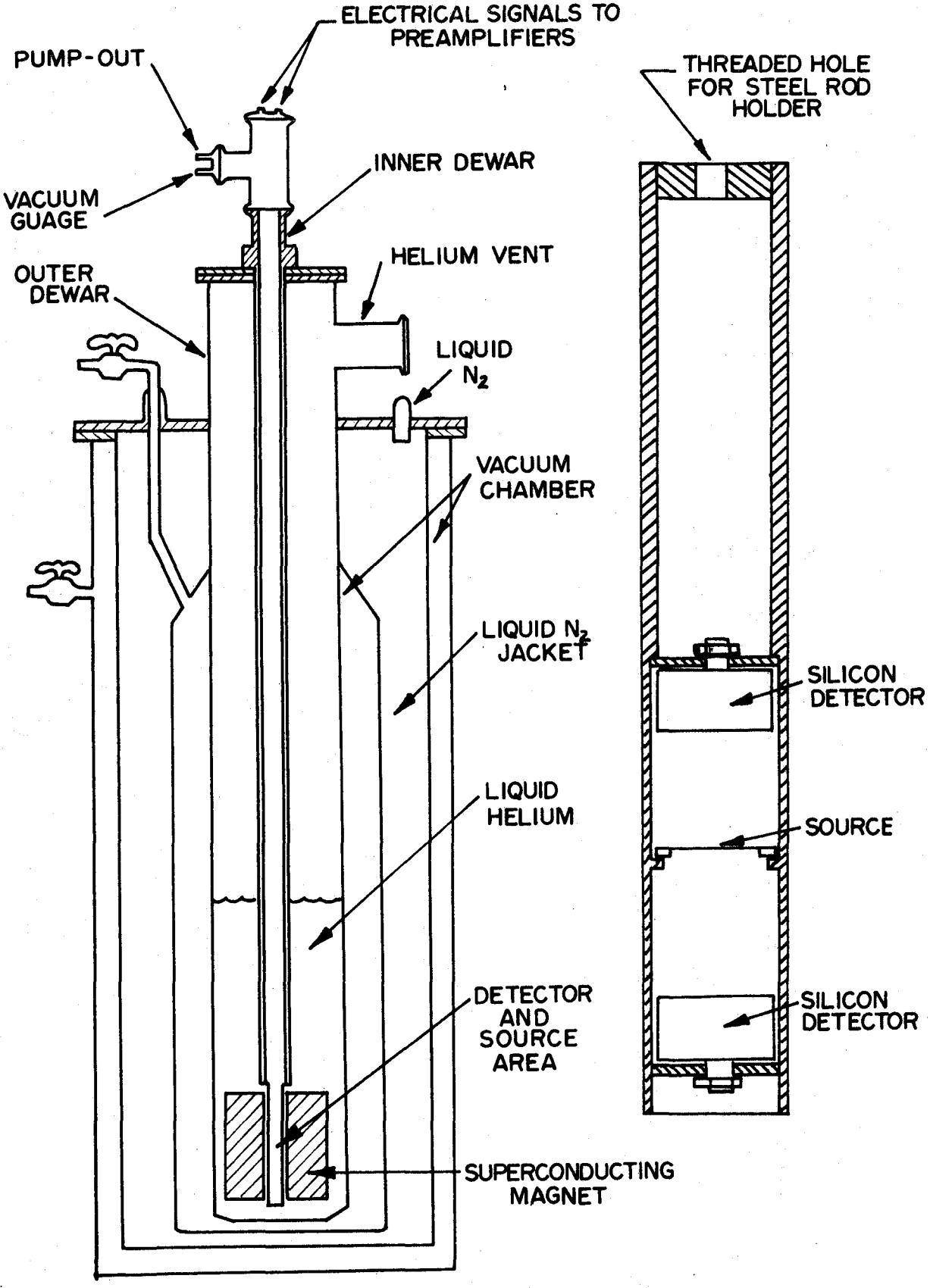

Figure 13 Si(Li) superconducting magnet beta spectrometer system (diagrammatic) showing on the right, enlarged details of detector holder

$4\pi\beta$-spectrometers described by Shera et al.[68] and Andersen et al.[70,71] Radioactive sources emitting electrons were mounted midway between the two Si(Li) detectors on the axis of the solenoidal magnet. Since the magnetic field is directed parallel to this axis, all electrons with energies below a maximum determined by the apparatus dimensions will spiral about this axis in helical orbits towards the detectors. If an electron backscatters from one of the detectors, it travels back down a similar trajectory and is incident on the other detector (provided it is not absorbed in the source mounting foil). If the two detector outputs are added in a circuit with a time resolution of about 1 μsec as shown in Figure 14, the pulses arising from the initial and backscattering events are added to yield a pulse height proportional to the total energy of the emitted electron. The advantages of this design are:

1. a 4π efficiency for the detection of electrons up to the maximum energy referred to above, (calculated in our apparatus to be about 3.1 MeV);
2. a reduction in the amount of scattering due to the use of thinner and weaker sources permitted by the complete collection of emitted particles;
3. a smaller contribution to the β-spectra from γ-rays due to the small solid angle subtended by the detectors at the source position; and

4. most important, a substantial reduction of spectrum components (continua) due to escape of backscattered electrons carrying off a sizeable fraction of their initial energy.

As was noted above, electrons emitted by radioactive sources follow helical paths in the magnetic field. For a point source (mounted on the solenoidal axis), the axis of the helix is displaced from the axis of the solenoid by the radius of the helix. In order to calculate these electron orbits, consider Figure 15 which shows a cylindrical coordinate system with the z-direction along the solenoidal axis. The equation of motion of the electrons is given by:[112]

$$\frac{d(m\bar{v})}{dt} = - e \cdot \bar{v} \times \bar{B} \qquad (3\text{-}1)$$

where

m = the mass of the electron,

$\bar{v}$ = the velocity of the electron,

$\bar{B}$ = the magnetic field strength,

e = the charge of the electron.

In a homogeneous field, this differential equation can be solved to yield the following solutions.[112]

$$r = D \sin\alpha \sin\psi \qquad (3\text{-}2)$$

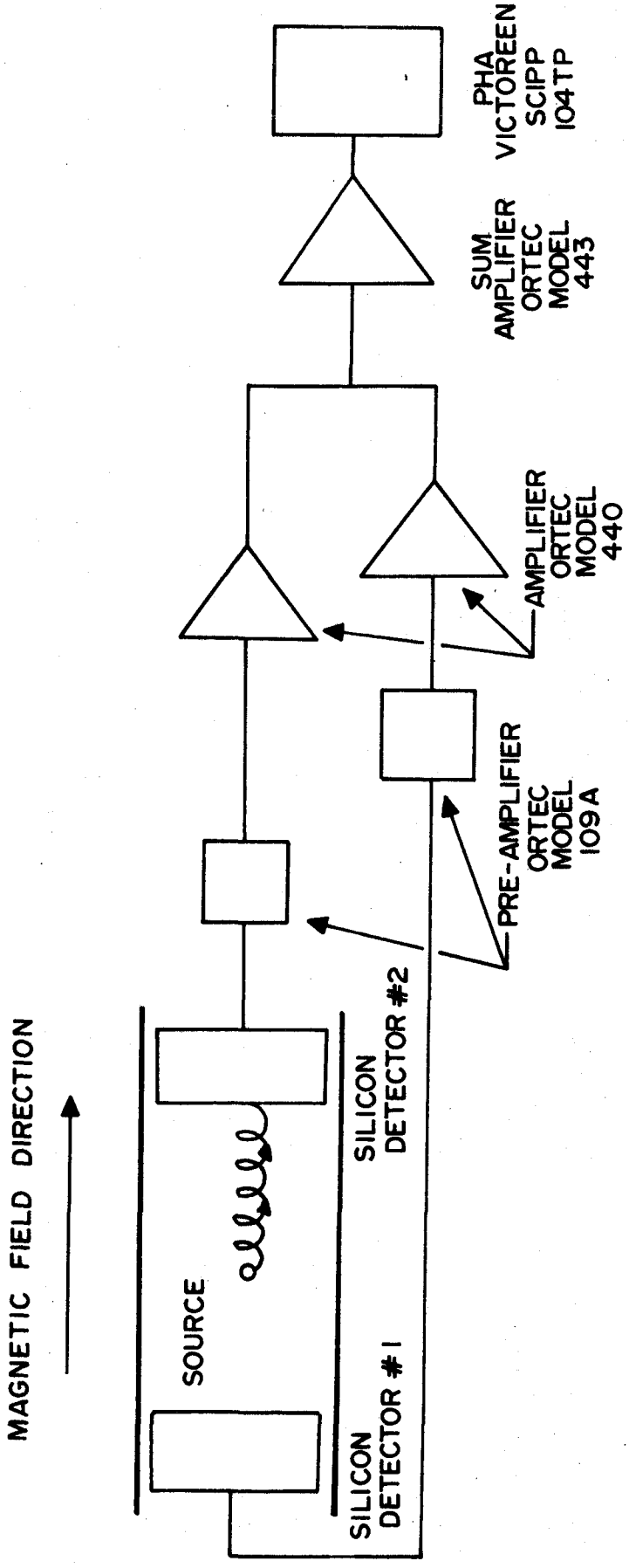

Figure 14 Electronic apparatus used with the superconducting magnet beta spectrometer

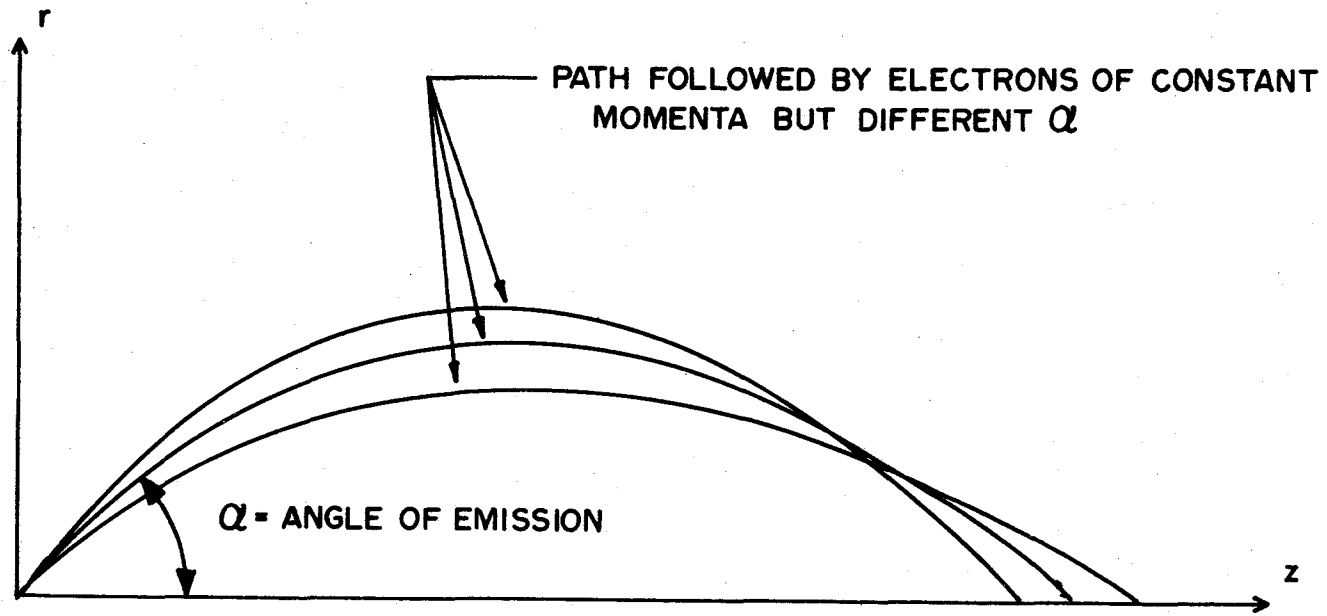

Figure 15 Electron paths described by electrons in a homogeneous field parallel to the z-axis

$$\psi = z/D \sin\alpha \quad (3\text{-}3)$$

$$D = 2mv/eB = 2(B\rho)/B \quad (3\text{-}4)$$

where

α = the angle of emission of the electron,

D = the diameter of a circle corresponding to an electron with momentum mv emitted at $\alpha = 90°$,

ψ = the angle the electron makes with a reference axis located in a plane perpendicular to the direction of the magnetic field,

r = the actual locus of the path traced out by the electron.

The maximum radius for an electron of kinetic energy T is given by the following expression:

$$\rho = \frac{3.33564\ (T^2+1.022T)^{1/2}}{B} \quad (3\text{-}5)$$

where

ρ = the maximum electron radius (mm),

B = the magnetic field strength (gauss x 10^{-4}),

T = the kinetic energy of the electron (MeV).

For an electron to be registered by the spectrometer detection system, ρ must be no greater than 1/2 the radius of the active circular area of the solid state detectors being used. Any electron orbit larger than this maximum will be intercepted by the inside walls of the solenoid. Figure 16

shows the maximum radius calculated from the above formula plotted for several values of the magnetic field B. Theoretically, the spectrometer assembled at Simon Fraser University with a maximum field of 30 kG coupled with the maximum allowable electron radius of 4 mm (one half of the radius of the 200 mm^2 active surface area of the Si(Li) detectors), should detect all electrons with kinetic energies up to about 3.1 MeV. This latter figure assumes a homogeneous magnetic field of 30 kG between the two detectors, a detector depletion depth greater than the range of a 3.1 MeV electron in silicon, and a small diameter, thin source located on the axis of the solenoid. Unfortunately none of these assumptions is completely valid and consequently the detection system was calibrated with emitters of β-rays and conversion electrons of known energies and intensities such as ^{32}P, ^{144}Ce and ^{207}Bi. Electrons with energies greater than 3.1 MeV will be detected only when the angle of emission α is less than the value α_m which results in a maximum orbit radius of 4 mm. Figure 17 shows graphically this maximum angle of emission, α_m, permitted in a field of 30 kG as a function of the electron energy. The maximum geometrical solid angle subtended by the half angle α_m, (and hence the percentage of the total number of emitted electrons contained in this solid angle), rapidly decreases as the energy of the electron increases beyond 3.1 MeV.

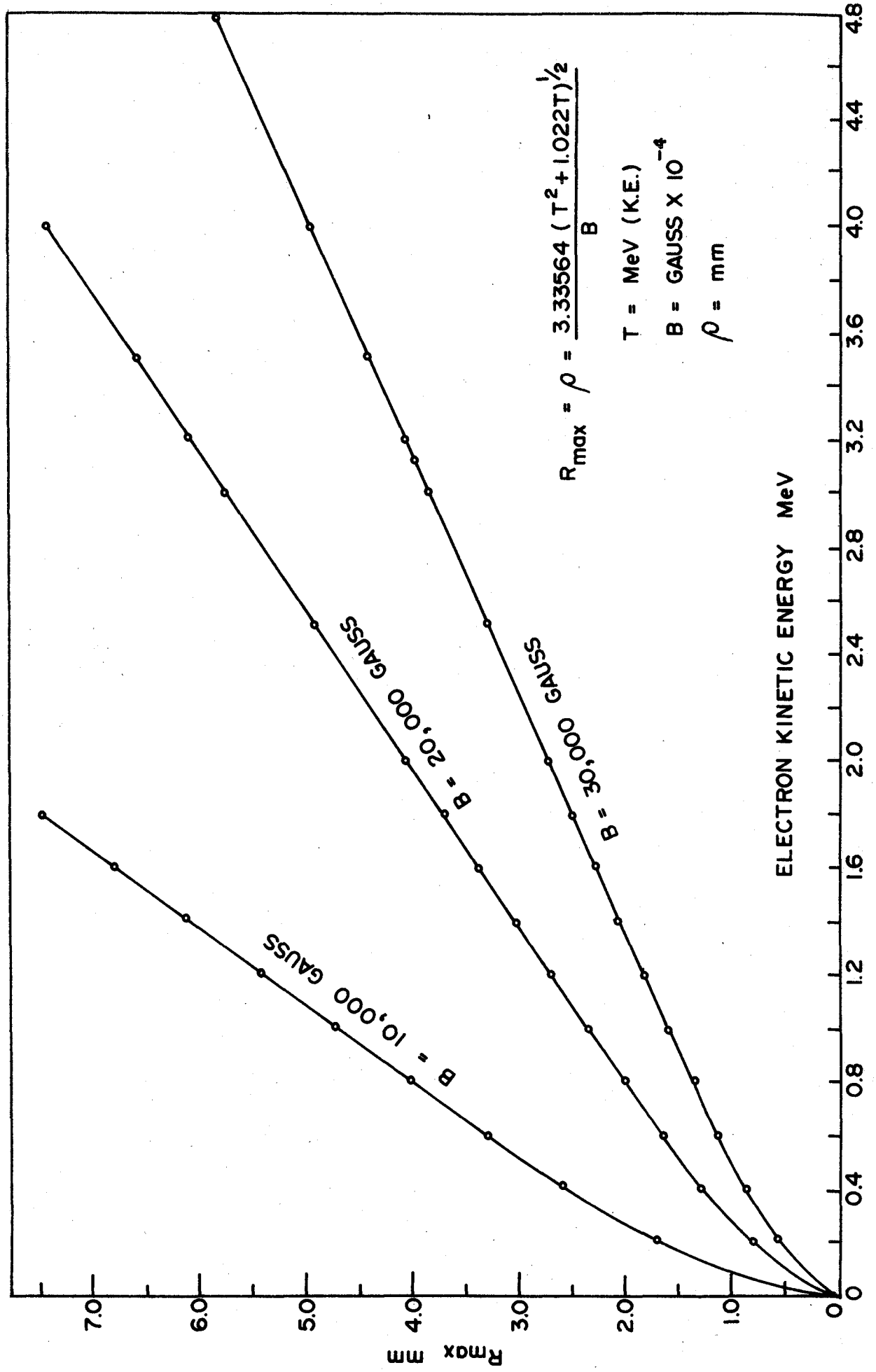

Figure 16 Maximum electron radii for β-particles emitted perpendicular to magnetic field B

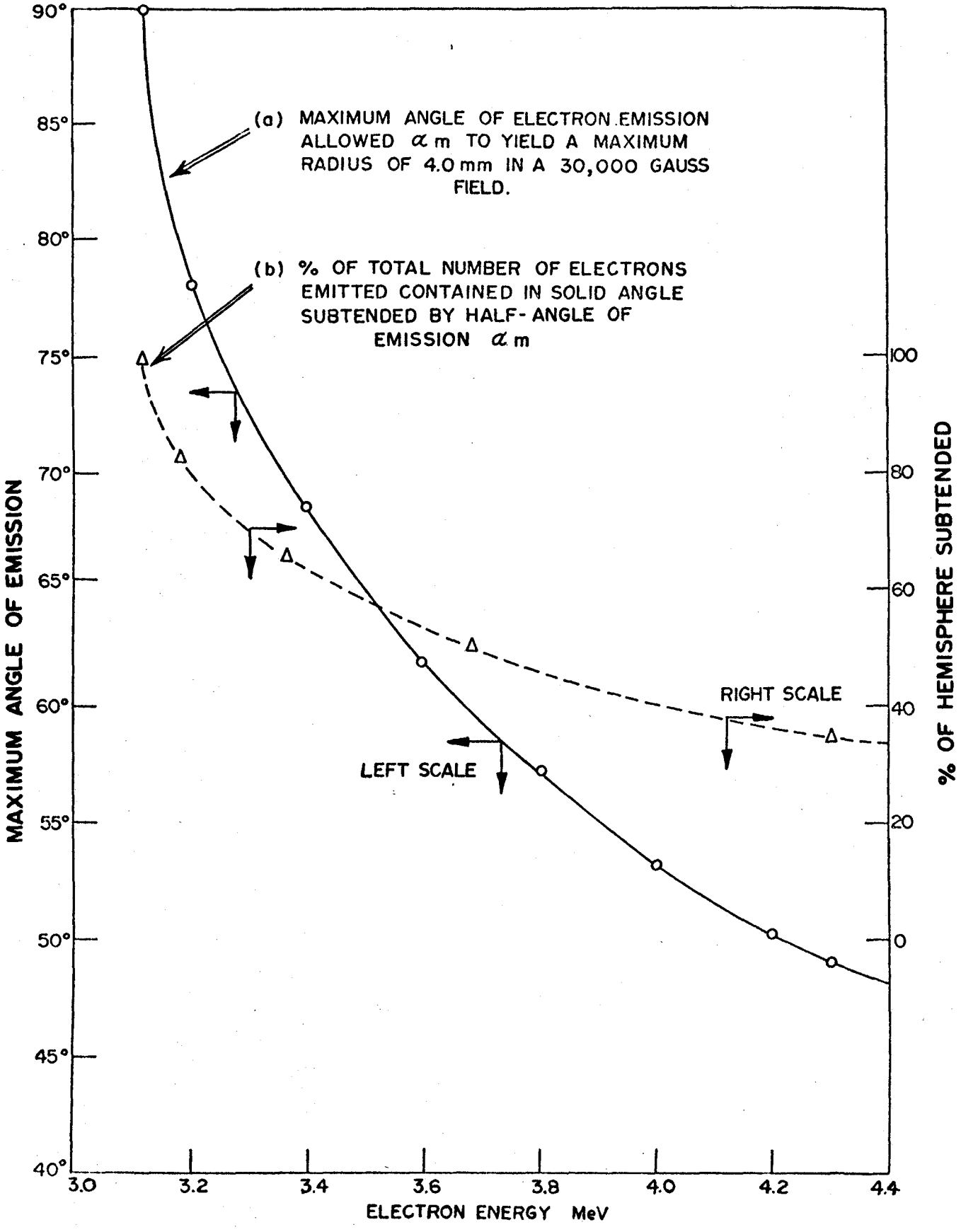

Figure 17 Operating characteristics of the superconducting magnet beta spectrometer

The effect of the magnetic field on the β-ray counting efficiency of the two Si(Li) detectors arranged in the configuration illustrated in Figure 12 is shown in Figure 18. In this latter figure, the summed and independent outputs of both detectors registering β-ray events from a ^{32}P reference source (E_{max}= 1.71 MeV)[3] as a function of the magnetic field strength, is shown. For magnetic field strengths greater than about 19 kG no further increase in count-rate is observed indicating that all the β-rays emitted by this source at various initial angles are being recorded. This information agrees well with the calculated data of Figure 16. Further data on the performance of the spectrometer is shown in Figures 19 and 20 which show the conversion electron spectrum of ^{207}Bi with and without a 30 kG magnetic field respectively. Figure 20 also shows sum peaks resulting from the coincident summing of the intense K line of the 1063.4 keV conversion electron transition with that of the K and L lines of the 569.6 KeV conversion electron transition.[3,114] The β-ray spectrum of ^{32}P (taken with a 30 kG field and with both detectors outputs summed) is shown in Figure 21 with the resulting Fermi-Kurie plot in Figure 22. The straight line plot in this latter figure with an indicated maximum end-point energy for ^{32}P of 1.68 MeV, close to the accepted value of 1.71 MeV,[3] confirms the reduction of spectral distortions by this instrument. The low intensity,

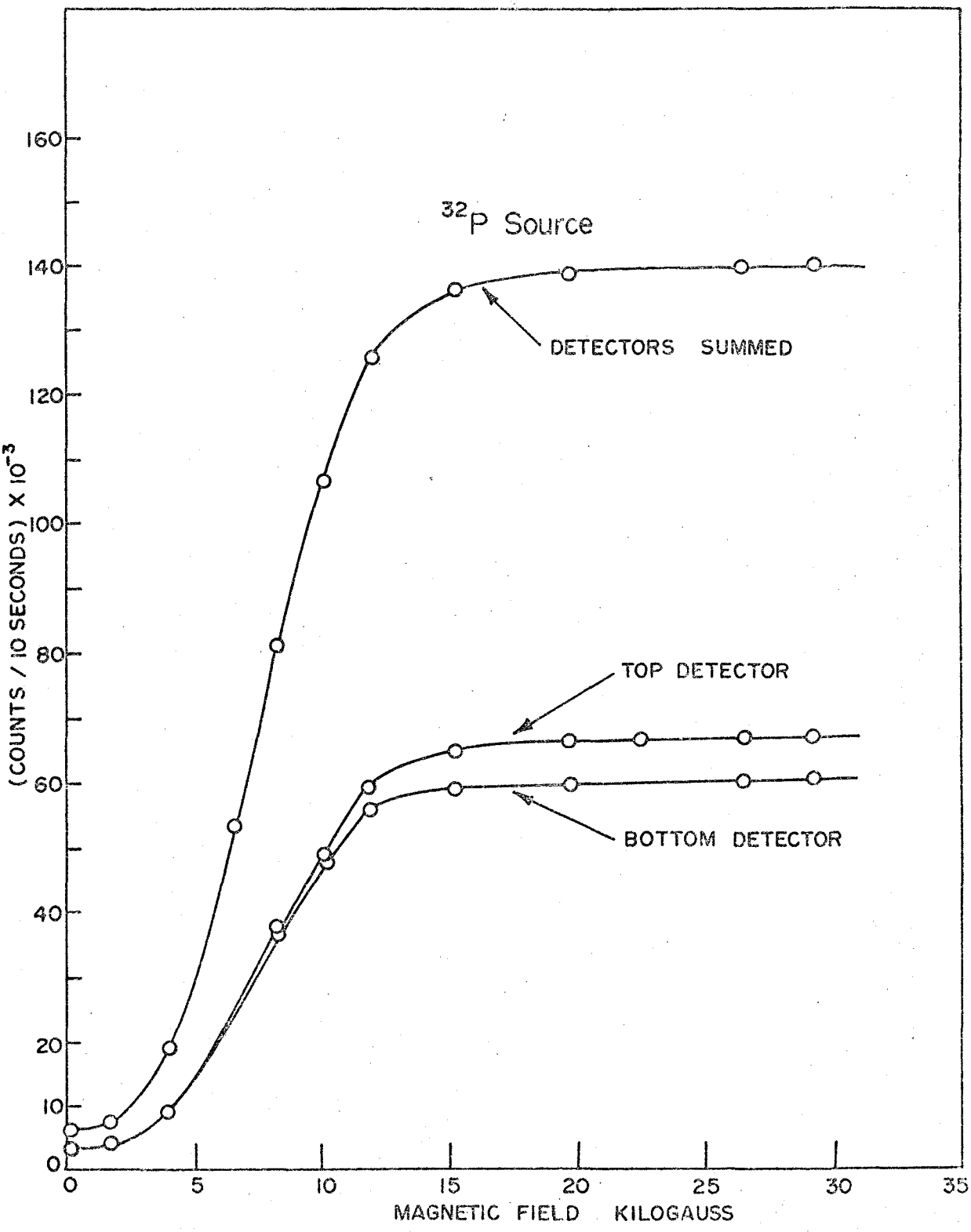

Figure 18 Increase in counting-rate of Si(Li) detectors as a function of magnetic field strength

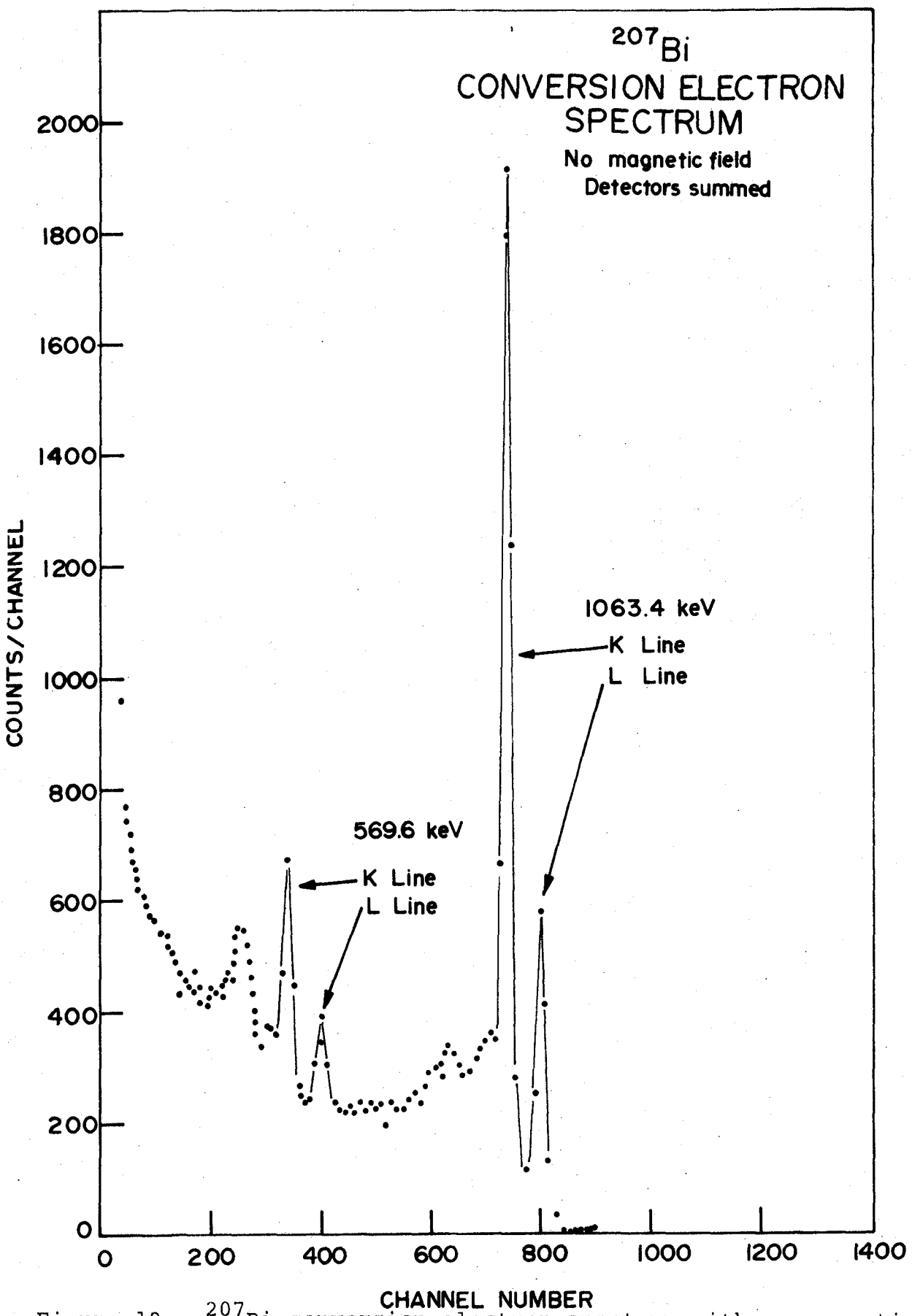

Figure 19 ^{207}Bi conversion electron spectrum with no magnetic field, detector outputs summed

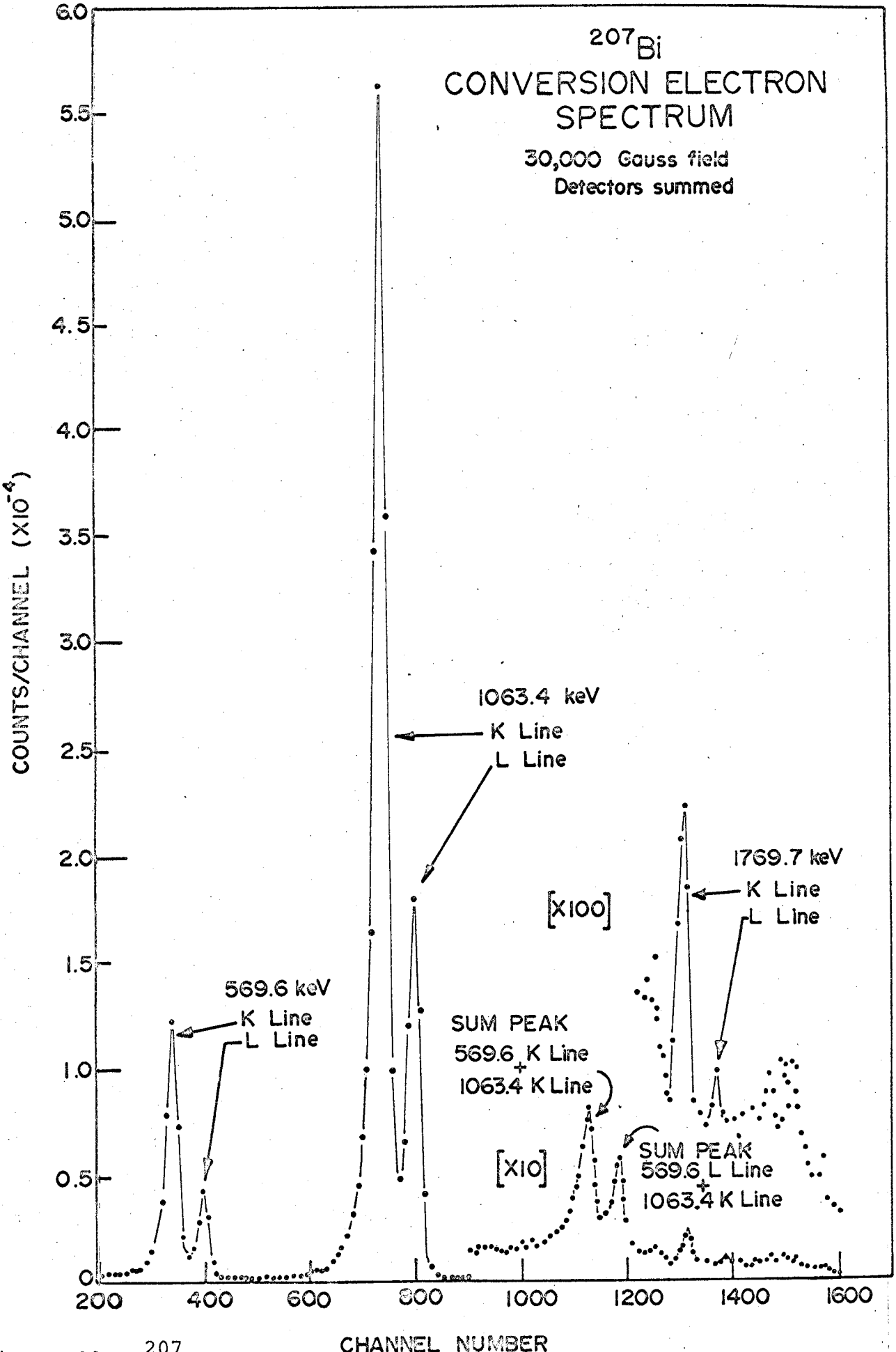

Figure 20 ^{207}Bi conversion electron spectrum with 30 kG magnetic field, detector outputs summed

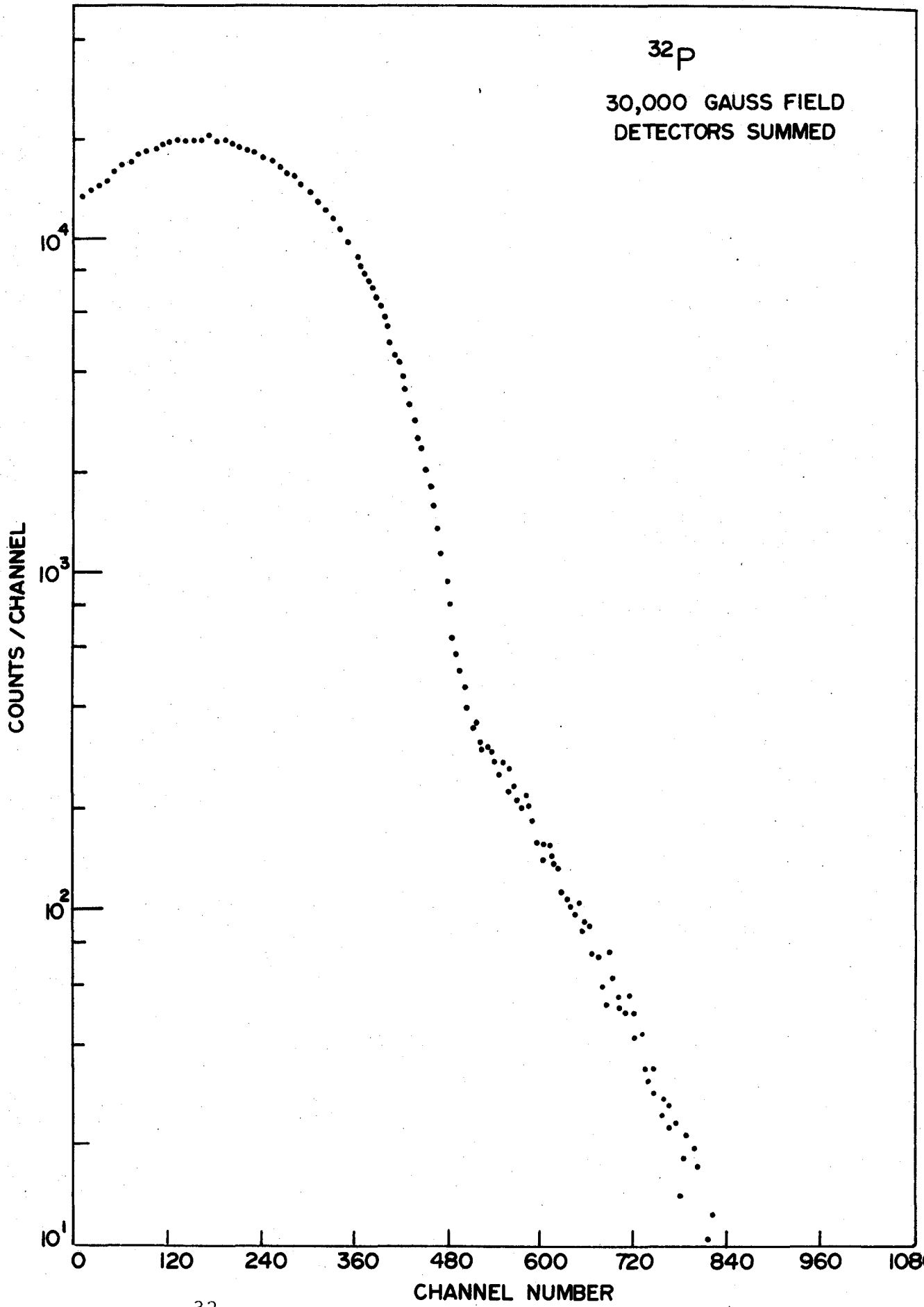

Figure 21 ^{32}P β-spectrum with 30 kG magnetic field, detector outputs summed

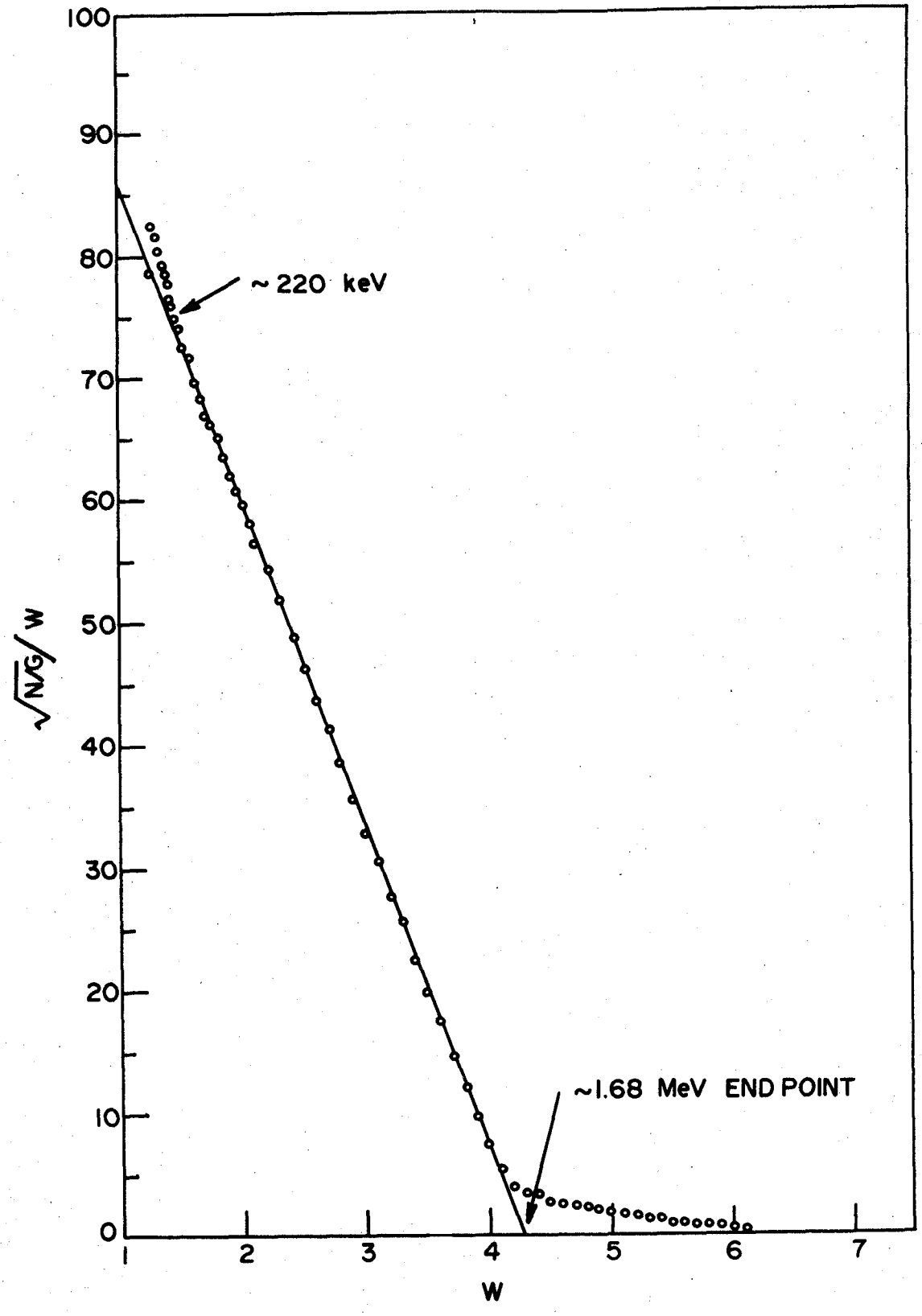

Figure 22 Fermi-Kurie plot of ^{32}P

high energy tail on this spectrum is due to the chance summing of electrons from different decay events;[113] the relative intensity being a function of source strength.

(b) Beta-Gamma Detection Systems

Since γ-detectors sufficiently small to be placed inside the solenoidal magnet were not available, the superconducting magnet beta spectrometer was not used for the following β-γ measurements. Most of the β-γ coincidence studies on ^{76}As and ^{78}As were performed in air using a 80 mm^2 x 2 mm Si(Li) detector (10 keV resolution at 975 keV, ^{207}Bi conversion line) and a 7.6 cm by 7.6 cm NaI(Tl) detector. In the case of ^{76}As, a few β-γ studies were also performed using a 5 cm by 5 cm Harshaw anthracene detector and a 0.155 cm^3-Ge(Li) ORTEC detector. No β-γ coincidence studies on ^{80}As were made due to intensity and source preparation problems.

Self absorption and source mount backscattering effects were minimized by mounting the arsenic activity on 6.3 μm Al foil by methods described earlier. (See sub-section 3.1.2). Air absorption of electrons was investigated by noting the shift in apparent energy of the conversion electrons from ^{207}Bi as a function of distance from the Si(Li) detector. This effect was evidently negligible for distances less than 1 cm and for electrons with energies greater than about 250 keV.

The β-γ coincidence measurements on ^{76}As and ^{78}As were usually made with the center lines of the two detectors at 180° and passing through the center of the source. A 0.5 cm thick plexiglass electron absorber was placed between the γ-detector and the source. The output pulses from the two detectors were fed to the Nuclear Data 160 analyzer set-up in a "two parameter" mode of operation and gated by a Cosmic Radiation Model 801 coincidence unit. (See Figure 11) This experimental arrangement permitted the simultaneous measurement of β-spectra coincident with several γ-rays of interest. After recording β-γ coincidence results due to ^{78}As decay for one or two hours, the same experimental apparatus and source were used one day later to obtain β-γ coincidence results from ^{76}As decay. These latter results provided internal energy calibration data confirming the calibration data from separate experiments using γ- and β-ray reference sources of ^{22}Na, ^{137}Cs, ^{207}Bi, ^{32}P and ^{144}Ce.

3.3 Treatment of Data

3.3.1 Half-Life Measurements

Half lives determined by following β- and γ- activity as a function of time can lead, in some cases, to considerable errors if many longer lived activities are present or if the half lives of the several activities present are relatively close to one another. These uncertainties result from

cumulative errors involved in the subtraction procedures of the decay curve analysis method.[66] However, the decay curve analysis of the ^{76}As plus ^{78}As samples produced in these experiments did not suffer unduly from these errors due to purification from contaminants and by the fact that the half lives of these two isotopes are widely different from one another.

Half life data for all the isotopes under investigation were reduced by both graphical analysis methods and computer techniques. The Brookhaven decay curve analysis program CLSQ, due to J.B. Cumming,[38] which carries out the analysis of multicomponent decay curves by a least-squares procedure, was extensively used for these computer determinations.

3.3.2 Gamma-Ray Spectra

(a) Location of Peak Center Positions and Energy Calibrations

Most of the procedures for extracting energies and relative intensities of γ-rays from the Ge(Li) γ-ray spectra of ^{76}As, ^{78}As and ^{80}As obtained in this work are similar to those described by A.H. Sher.[65]

In the present work, all the pulse height γ-ray spectra were analyzed by an appropriate combination of manual plotting and computer programming techniques. A computer

program, called GRAYPLOT, coded in Fortran IV and run on the IBM-360/40 computer at Simon Fraser University, was developed during the early stages of this work and was extensively used to help analyse the many γ-ray spectra observed in the decay of ^{76}As, ^{78}As and ^{80}As. Paper tape output from the analyzers containing counts versus channel number data for each γ-ray spectrum was converted to computer cards for subsequent computer analysis by an IBM tape to card converter. These tapes were also used to print numbers for visual inspection, manual plotting and analysis techniques.

The GRAYPLOT computer code for γ-ray analysis was programmed to locate peak centers of γ-lines by a method of weighted averages of the form:

$$\bar{x} = \frac{\Sigma g_i x_i}{\Sigma g_i} \qquad (3\text{-}6)$$

where $\bar{x}$ is the peak center of the γ-line expressed in channel numbers, and g_i are weight factors equal to the number of counts in channel x_i after background counts had been subtracted. Background counts under each γ-line, due primarily to Compton events from higher energy γ-lines, were normally obtained by straight-line interpolation between the "valleys" on either side of the peak studied. Errors in locating peak centers by this method were estimated to be less than ±0.5 channels whenever the conversion gain of the analyzer, in

keV per channel, was such that each γ-line extended over 10 or more channels. This condition was easily achieved by using the Scipp 104TP Victoreen analyzer at conversion gains of less than 1 keV per channel over the available range of 3200 channels.

Having obtained the peak centers of the various γ-lines with known energies (from ^{22}Na, ^{56}Co, ^{60}Co, ^{137}Cs and ^{207}Bi decay) using the above procedure, the resulting energy versus channel number relationships were fitted by a least squares computer program, called MFIT,[65] to a polynomial of the following form:

$$E = A + Bx + Cx^2 + Dx^3 \qquad (3\text{-}7)$$

where x is the peak center in channel numbers of the γ-line with energy E and A, B, C, and D are the parameters to be fitted. In most cases, the non-linearity of the pulse height versus energy response of the system was small as reflected by very low values for the parameters C and D.

In certain situations where pairs of γ-rays were too close in energy to be completely resolved by the Ge(Li) detectors, a graphical resolution technique was developed. This procedure involved first subtracting the background common to both γ-lines and then graphically resolving the resulting distribution assuming each peak in the doublet

possessed the same general Gaussian shape as nearby, completely resolved γ-lines of the same spectrum. A typical graphical resolution of one of the line doublets observed in the decay of ^{78}As is shown in Figure 40.

(b) Gamma-Ray Relative Intensity Determinations

Relative intensity values for the γ-rays observed in the single detector spectra were obtained from the calculated peak areas and the Ge(Li) detector efficiencies, established as a function of energy via reference sources[65] such as ^{56}Co. The following formula was used:

$$I_i = (A_i/\eta_i) \qquad (3\text{-}8)$$

where I_i, A_i and η_i are the intensity, peak-area and full-energy peak efficiency of the i^{th} γ-ray respectively. The calculated relative intensity I_i values for different γ-rays belonging to each isotopic decay were normalized by equating the intensity of the most intense γ-ray photon to 100.

Relative intensity values reported in this work for ^{76}As and ^{78}As γ-rays were determined from the arithmetic mean values, $\bar{x}_i$, obtained from a minimum of six independent measurements. The standard deviations (σ_i) of these mean values were estimated by means of the expression:[115]

$$\sigma_i = \left[\frac{1}{N_o - 1} \sum_{j=1}^{No} (x_j - \bar{x}_i)^2 \right]^{1/2} \qquad (3\text{-}9)$$

where N_o is the total number of different determinations of the relative intensity of the i^{th} γ-ray, and x_j is the relative intensity of the j^{th} determination. The above formula was found useful for determinations of the standard deviations of the mean relative intensity values only in cases where several independent measurements had been made. However, in the ^{80}As case, where only one γ-ray spectrum was obtained, the standard deviation (σ_i) associated with the relative intensity (I_i) of the i^{th} γ-ray was estimated from the following expression:[116]

$$\sigma_i = I_i \left[\sum_j (\Delta x_j / x_j)^2 \right]^{1/2} \qquad (3\text{-}10)$$

where the $\Delta x_j / x_j$ values were the estimated relative errors in the peak-areas and the full energy peak efficiencies associated with the i^{th} γ-ray and the reference γ-ray used for normalization purposes.

(c) Gamma-Gamma Coincidence Spectra

Most of the γ-γ coincidence spectra observed in the decay studies of ^{76}As and ^{78}As were collected in a "two

parameter" format, typically with pulses from the Ge(Li) detector stored in 256 channels in coincidence with pulses from the NaI(Tl) detector stored in 16 channels. Some of the γ-γ coincidence spectra displayed in the following data sections were obtained by a subtraction procedure, i.e., Ge(Li) spectra in coincidence events of a given energy in a NaI(Tl) detector were subtracted from Ge(Li) spectra in coincidence with NaI(Tl) events of a somewhat higher energy. Proper intensity normalization and energy choices were expected then to lead to correction for the effects of Compton escape events from higher energy γ-rays and of background.

Accidental or random coincidences due to the finite resolving time, τ, of the coincidence units were usually negligible in these experiments because of low counting rates from the relatively weak sources. The relation,[115] $N_r = N_1 N_2 2\tau$, where N_1 and N_2 are input pulse rates for two γ-rays, can be used to calculate the chance coincidence rate N_r. The ratio of accidental to true coincidences, R, was checked by introducing a large time delay (relative to the resolving time τ), on one side of the coincidence circuit. In all cases, source to detector distances and τ were adjusted so that R was less than about 1.0%.

3.3.3 Beta-Ray Spectra

(a) Superconducting Magnet Beta Spectrometer

Beta-spectra obtained in this work using the Si(Li) superconducting magnet spectrometer were analyzed by Fermi-Kurie procedures.[52] The calculations of the Fermi function $[N(W)/G]^{1/2}/W$ were performed by an IBM-360 computer using Fermi functions tabulated by Rose.[52] In cases where more than one group of β-rays was present, the number of counts per unit energy interval, $N_1(W)$, corresponding to the highest energy β-group and its extrapolation to low energy, was determined and a new Fermi plot made from the difference $N(W) - N_1(W)$.

Comparison of β-ray decay probabilities were made according to their log ft values given by the following expression:[3,117]

$$\log ft = \log f_o t + \log C + \Delta \log ft,$$

where $\log f_o t$, log C and Δ log ft are the comparative half life, Coulomb correction, and branching factor terms respectively. Procedures for the rapid determination of log ft values were carried out according to methods described by Moszkowski.[118]

(b) Beta-Gamma Coincidence Spectra

The Si(Li) β- spectra obtained in the present β-γ coincidence experiments were analyzed by methods described by Charoenkwan.[76] Basically, these methods involve correcting the Si(Li) β-spectra using a standard reference β- source to eliminate spectral distortions caused by electrons penetrating through the detector and by backscattering effects.

According to Charoenkwan,[76] these corrections can be accounted for by considering the Fermi-Kurie equation:

$$\sqrt{N(W)/G}\Big/ W = K(W_o - W) \qquad (3\text{-}11)$$

where

W_o = the end-point energy,

K = a proportionality constant,

G = the modified Fermi function,[52] and

N(W) = the number of particles per unit energy interval at energy W.

If M(W) is the number of events per unit energy interval at energy W recorded from the Si(Li) detector (which is usually greater than N(W) due to backscattering effects), the relation between N(W) and M(W) can be expressed by the factor a(W) as a function of energy.

$$N(W) = a(W)M(W) \qquad (3\text{-}12)$$

Solving for a(W) using equation (3-11) yields the result:

$$a(W) = K'(W_{o_s} - W)^2 W^2 G_s / M_s(W) \qquad (3\text{-}13)$$

where the subscript s stands for the chosen standard source.

Substitution of equations (3-12) and (3-13) into equation (3-11) gives:

$$(W_{o_s} - W)\sqrt{\frac{G_s M(W)}{G\, M_s(W)}} = K(W_o - W) \qquad (3\text{-}14)$$

Fermi-Kurie plots of ^{76}As and ^{78}As β-spectra obtained in the β-γ coincidence experiments (using the above equation and a standard reference source of ^{144}Pr) usually resulted in straight lines allowing end-point energies to be obtained. These end-point energy values were then used to determine total decay energies for the isotopes studied and to assist the assembly of their decay achemes.

CHAPTER 4

EXPERIMENTAL RESULTS

4.1 Decay of ^{76}As

4.1.1 Half Life and Gamma-Ray Spectra

The decay of the gross β-activity of ^{76}As samples, separated chemically from neutron bombarded sodium bromide, was analyzed by the CLSQ computer program.[38] As shown in Figure 23, a single component with a half life of 26.4 ± 0.1 h was obtained after the decay of the shorter-lived ^{78}As and demonstrated the absence of any significant foreign activities greater than about 1 part in 10^3.

The γ-spectrum from ^{76}As decay was recorded several times using Ge(Li) detectors of different active volumes. Although initial γ-studies were made with an 8 cm^3 planar detector (see bottom half of Figure 36), most of the investigations of the weak intensity γ-rays were carried out using a large volume 23.8 cm^3 co-axial detector. The 730-1150 keV energy region of the ^{76}As γ-spectrum obtained with this latter detector is shown in Figure 24. Finally, to resolve more completely the pairs of high-energy lines recorded by these two large detectors, a small volume

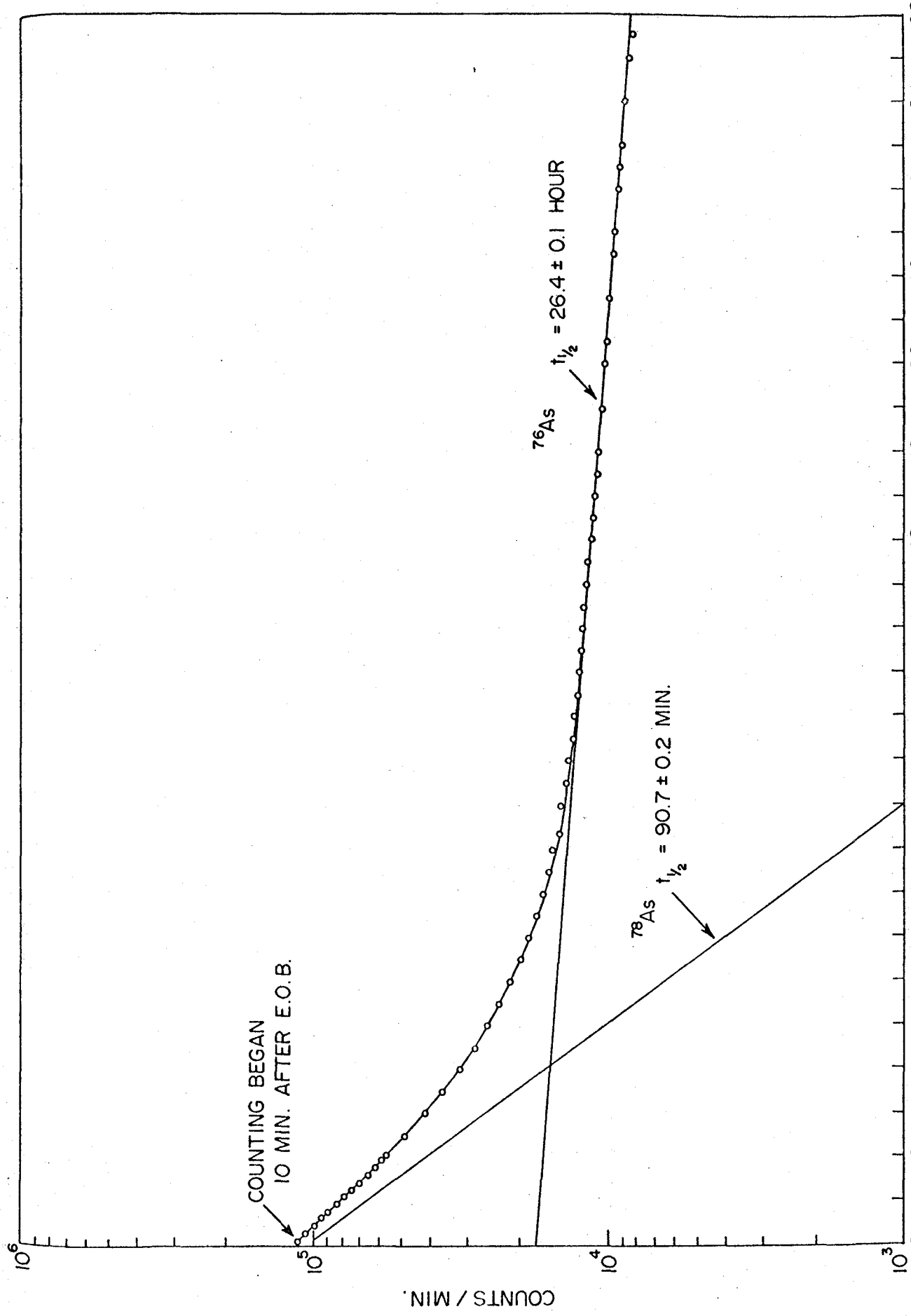

Figure 23 Decay curve of ^{76}As and ^{78}As

TABLE 1

ENERGY AND RELATIVE INTENSITY VALUES FOR γ-RAYS FOLLOWING THE DECAY OF ^{76}As

(a)		(b)	
Energy (KeV)	Intensity	Energy (KeV)	Intensity
559.6	100	1228.9	2.9 ± 0.4
563.5	2.1 ± 0.5	1440.0	0.7 ± 0.1
571.7	0.3 ± 0.1	1454.5	0.3 ± 0.05
657.4	13.5 ± 1.2	1534.7	0.08 ± 0.03
666.0	1.0 ± 0.2	1568.0 ± 1	0.01 ± 0.01
740.0	0.26 ± 0.08	1613.0 ± 1	0.01 ± 0.01
772.5	0.28 ± 0.07	1788.4	0.70 ± 0.1
868.6	0.28 ± 0.06	1870.5	0.13 ± 0.02
883.0	0.16 ± 0.06	2097.4	1.5 ± 0.2
981.2 ± 1	0.07 ± 0.03	2111.9	0.8 ± 0.2
1130.5	0.27 ± 0.05	2430.0	0.08 ± 0.03
1213.5	3.8 ± 0.5	2657.0	0.09 ± 0.02
1217.0	8.4 ± 0.7		

Notes

(a) Energy uncertainties ± 0.5 keV unless otherwise specified. (See sub-section 3.3.2) Intensity uncertainties obtained from six independent spectrum measurements.

(b) Weak intensity γ-lines, found at about 576, 727, 807, 1177, 1550, 1585, 1743, 1957 and 2306 keV, could not be reliably placed in the decay scheme due to large energy and relative intensity uncertainties. Some of these transitions were shown dotted, however, in possible positions in the ^{76}As decay scheme of Figure 35.

0.155 cm^3 detector was employed. For example, use of this latter detector resulted in the clear resolution for the first time of the 559.6-563.5 keV pair and the 1213.5-1217.0 keV pair as shown in Figure 25. In order to demonstrate the absence of further structure in the 559.6 keV γ-line, this detector was used again to count simultaneously the 559.6 keV ^{76}As γ-ray and the 569.6 keV ^{207}Bi γ-ray. Identical FWHM values of 1.08 keV for these two peaks as shown in Figure 26 provided strong evidence the 559.6 keV ^{76}As peak was due to only one γ-ray and was not further resolvable.

Energies and relative intensity values for 25 γ-rays assigned to ^{76}As decay are presented in Table 1. Indications of weak intensity γ-lines, not assignable to background radiations but all with energy and intensity uncertainties too large to allow their definite placement in the proposed ^{76}As decay scheme of Figure 35, were found at 576, 727, 807, 1177, 1550, 1585, 1743, 1957 and 2306 keV energy. The possibility that these γ-lines may be due to ^{76}As decay is included in the discussion of the ^{76}As decay scheme in subsection 4.1.4. Table 2 compares the energies and relative intensities of the ^{76}As γ-rays found in this work with those due to other workers.

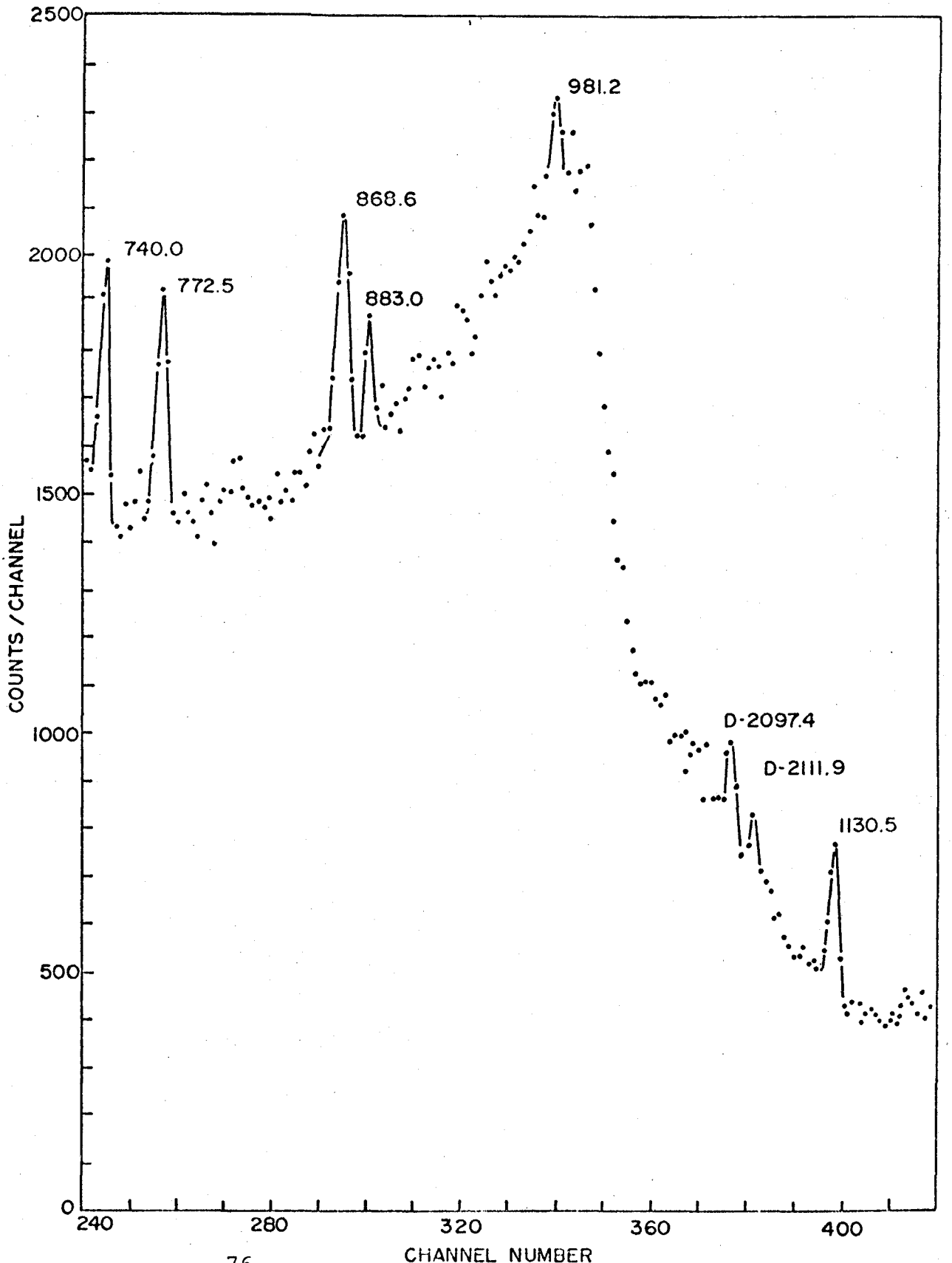

Figure 24 The ^{76}As γ-ray spectrum showing the 740-1130 keV energy region obtained with a single 23.8 cm^3 Ge(Li) detector

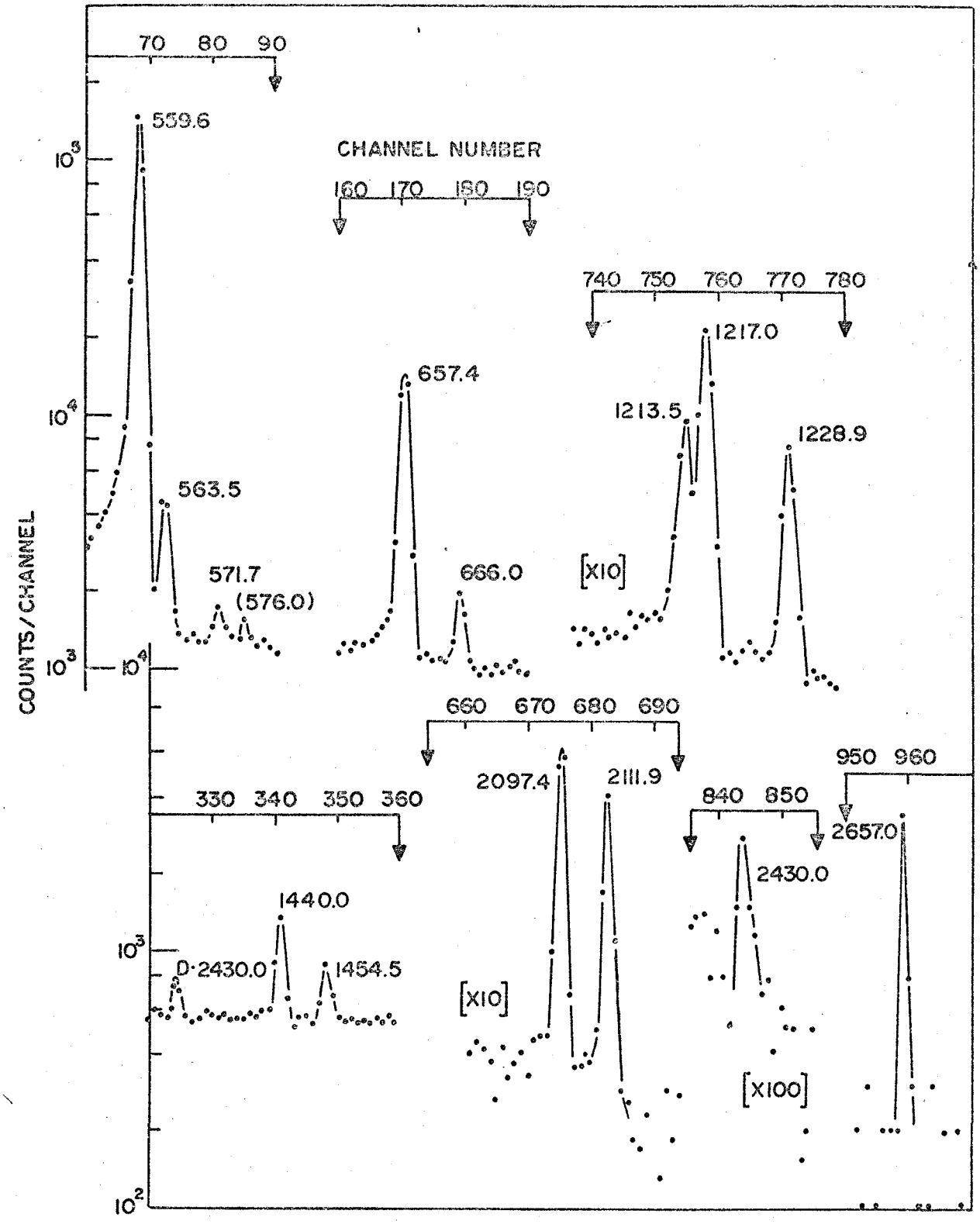

Figure 25 Portions of the ^{76}As γ-ray spectrum obtained with a single 0.155 cm^3-Ge(Li) detector

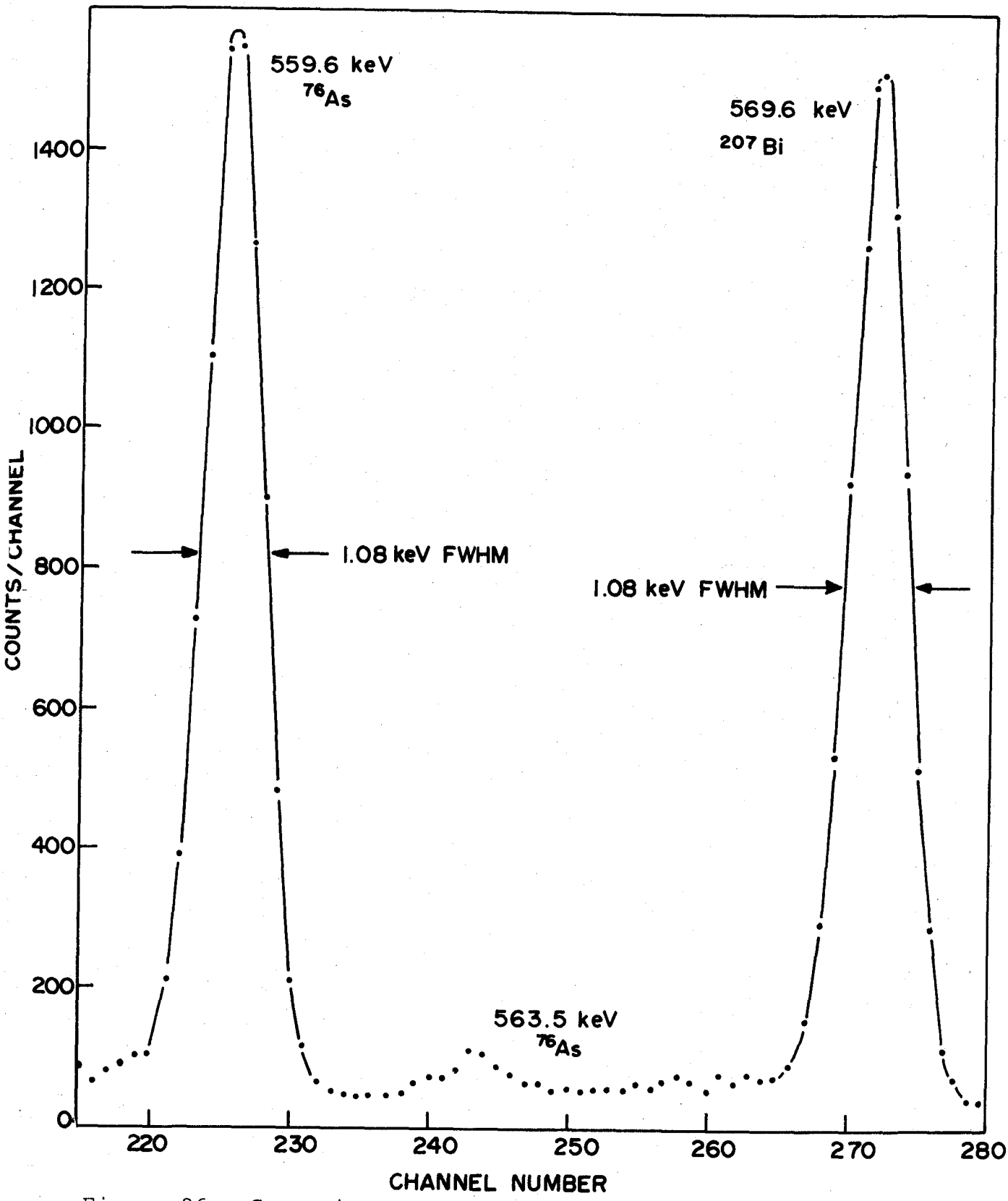

Figure 26 Comparison of the FWHM values of the 559.6 keV ^{76}As γ-ray peak and the 569.6 keV ^{207}Bi γ-ray peak

4.1.2 Gamma-Gamma Coincidence Spectra

Several coincidence experiments on γ-γ cascades due to ^{76}As decay were carried out. In the first experiment, sixteen -256 channel Ge(Li) spectra showing the 0-2600 keV energy region of the ^{76}As γ-spectrum were recorded with a 23.8 cm^3-Ge(Li) detector in coincidence with the 559.6 keV and 657.4 keV γ-rays recorded with a 7.6 cm by 7.6 cm NaI(Tl) detector.

Figure 27 shows one of these Ge(Li) spectra, corrected for the effects (at the selected energy in the NaI(Tl) detector) of Compton escape events from higher energy γ-rays, coincident with NaI(Tl) events of about 559.6 keV energy. Similarly, Figure 28 shows a Ge(Li) spectrum coincident with NaI(Tl) events of about 657.4 keV energy.

In the second experiment, the 16 channels used to record the NaI(Tl) spectrum were adjusted in pulse height to include events primarily from the 1213.5, 1217.0 and 1228.9 keV γ-rays. Although the NaI(Tl) detector was incapable of resolving completely these three γ-rays, certain of the sixteen Ge(Li) spectra were expected to contain mostly events coincident with the first two γ-rays (e.g. the spectrum in Figure 29) and others, mostly events coincident with the last two (e.g. the spectrum in Figure 30). All of these Ge(Li) spectra, however, contained some contributions

Table 2 COMPARISONS OF ENERGY AND RELATIVE INTENSITY VALUES FOR GAMMA-RAYS FOLLOWING THE DECAY OF ^{76}As

THIS WORK		MURRAY ET AL.[15]		J. ATEN ET AL.[16]		VITMAN ET AL.[14]		BACKSTROM ET AL.[20]	
E(keV)	Int.	E(keV)	Int.	E(keV)	Int.	E(keV)	Int.	E(keV)	Int.
								510	0.5
559.6	100	559.3	100	559.8	100	561	100	559.28	100
563.5	2.1	-		-		-		-	
571.7	0.3	572.1	0.5	571.6	0.20	624	1.0	(572)	2.1
657.4	13.5	657.4	13.8	657.6	11.6	657.5	14.8	657.36	14.1
666.0	1.0	666.1	0.7	666.1	0.92	-		-	
-		-		-		708	0.35	-	
740.0	0.26	-		740.8	0.30	740	0.48	-	
772.5	0.28	773.0	0.4	773.4	0.19	775	0.36	767.9	0.17
-		-		-		820	0.3	-	
-		-		-		858	0.28	-	
868.6	0.28	869.0	0.4	867.7	0.25	870	0.25	-	
883.0	0.16	-		-		882	0.15	-	
981.2	0.07	-		-		972	0.13	-	
1130.5	0.27	-		1130.7	0.23	1131	0.31	-	
1213.5	3.8	1213.0	6.4	-		-		-	
1217.0	8.4	1216.3	10.8	1215.6	7.5	1215	10.55	1216.0	9.7
1228.9	2.9	1228.6	4.3	1228.7	2.10	1228	2.75	1228.7	2.3
1440.0	0.7	1440.0	1.2	1440.2	0.43	1441	0.67	1438.3	1.2
1454.5	0.3	1453.7	0.5	1454.9	0.18	1458	0.21	1453.5	0.54
1534.7	0.08	-		1534.6	0.030	1537	0.056	-	
1568.0	0.01	-		1569.9	0.013	-		(1553)	0.2
-		-		1583.2	0.007	-		-	
1613.0	0.01	-		1613.1	0.014	1610	0.02	-	
1788.4	0.70	1788.4	1.6	1788.8	0.50	1790	0.62	1788.6	0.71
1870.5	0.13	1883.0	0.2	1871.0	0.10	1873	0.116	(1875)	0.2
-		-		1956.8	0.025	-		-	
2097.4	1.5	2096.2	2.6	2096.3	1.15	2099	1.17	2097.2	1.32
2111.9	0.8	2111.0	1.6	2110.8	0.70	2114	0.54	2111.8	0.73
2430.0	0.08	2430.1	0.2	2430.0	0.08	2426	0.061	2433.6	0.05
2657.0	0.09	2655.2	0.2	2656.9	0.12	2654	0.088	2656.1	0.077

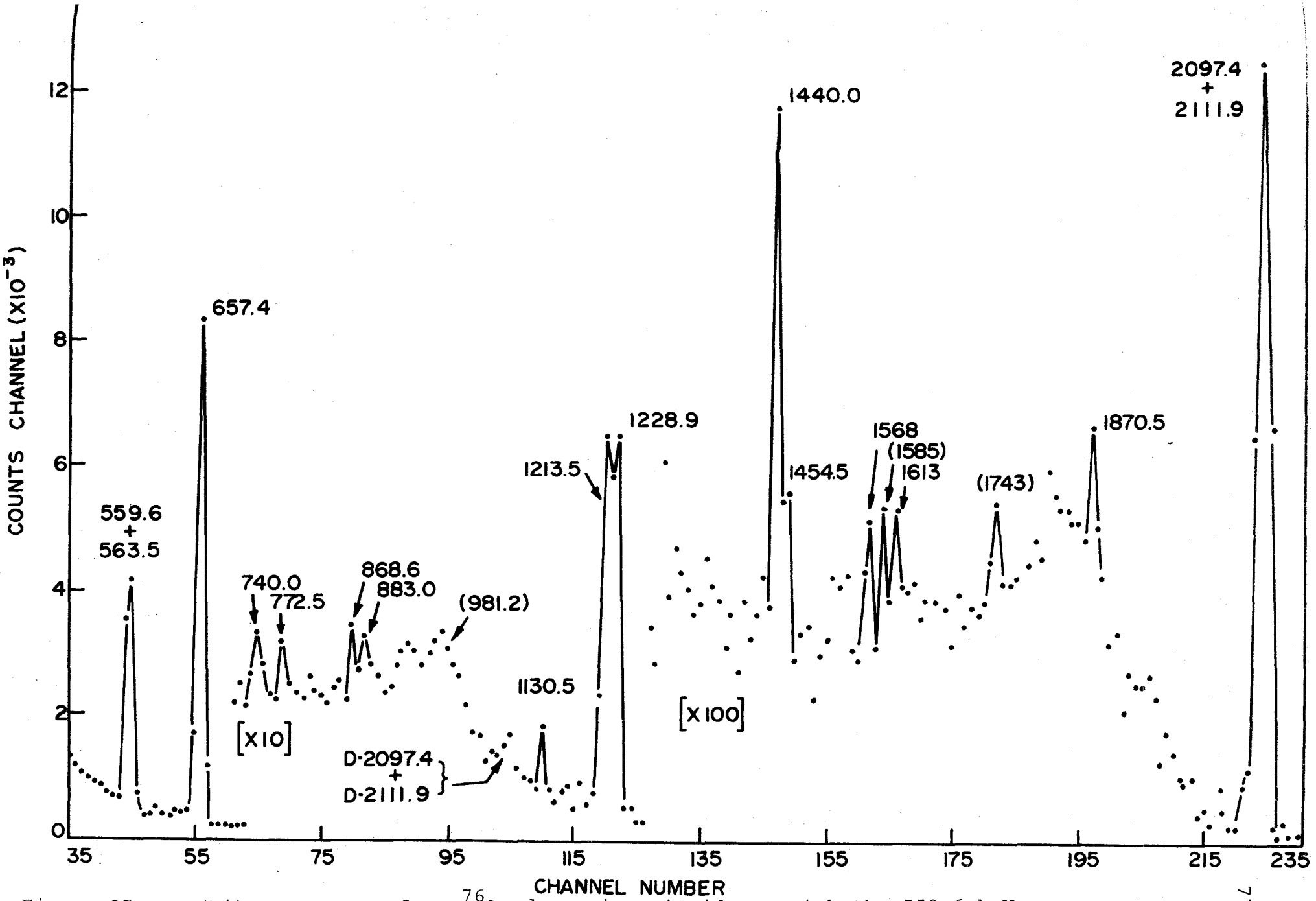

Figure 27 Ge(Li) γ-spectrum from ^{76}As decay in coincidence with the 559.6 keV γ-ray

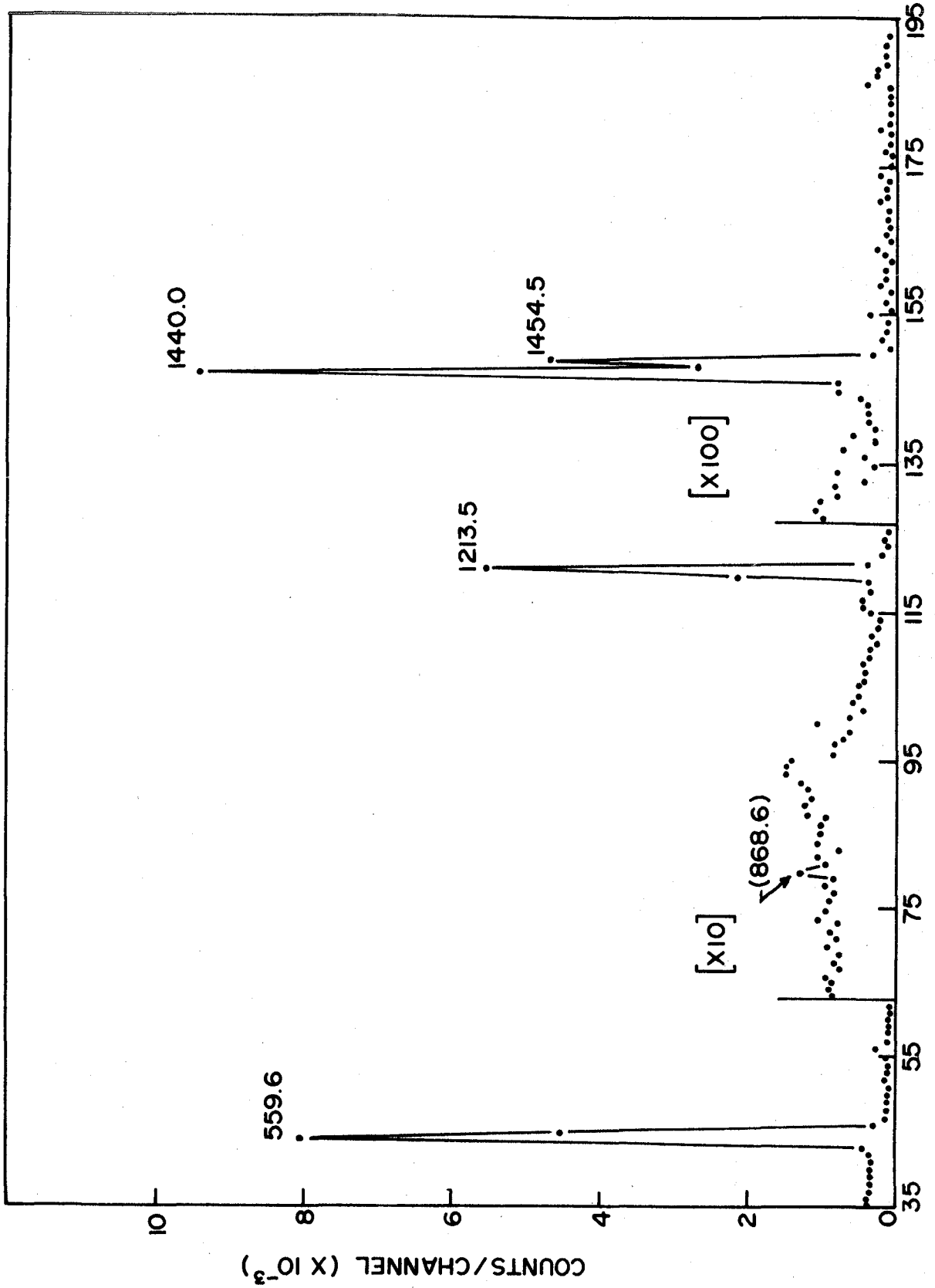

Figure 28 Ge(Li) γ-spectrum from ^{76}As decay in coincidence with the 657.4 keV γ-ray

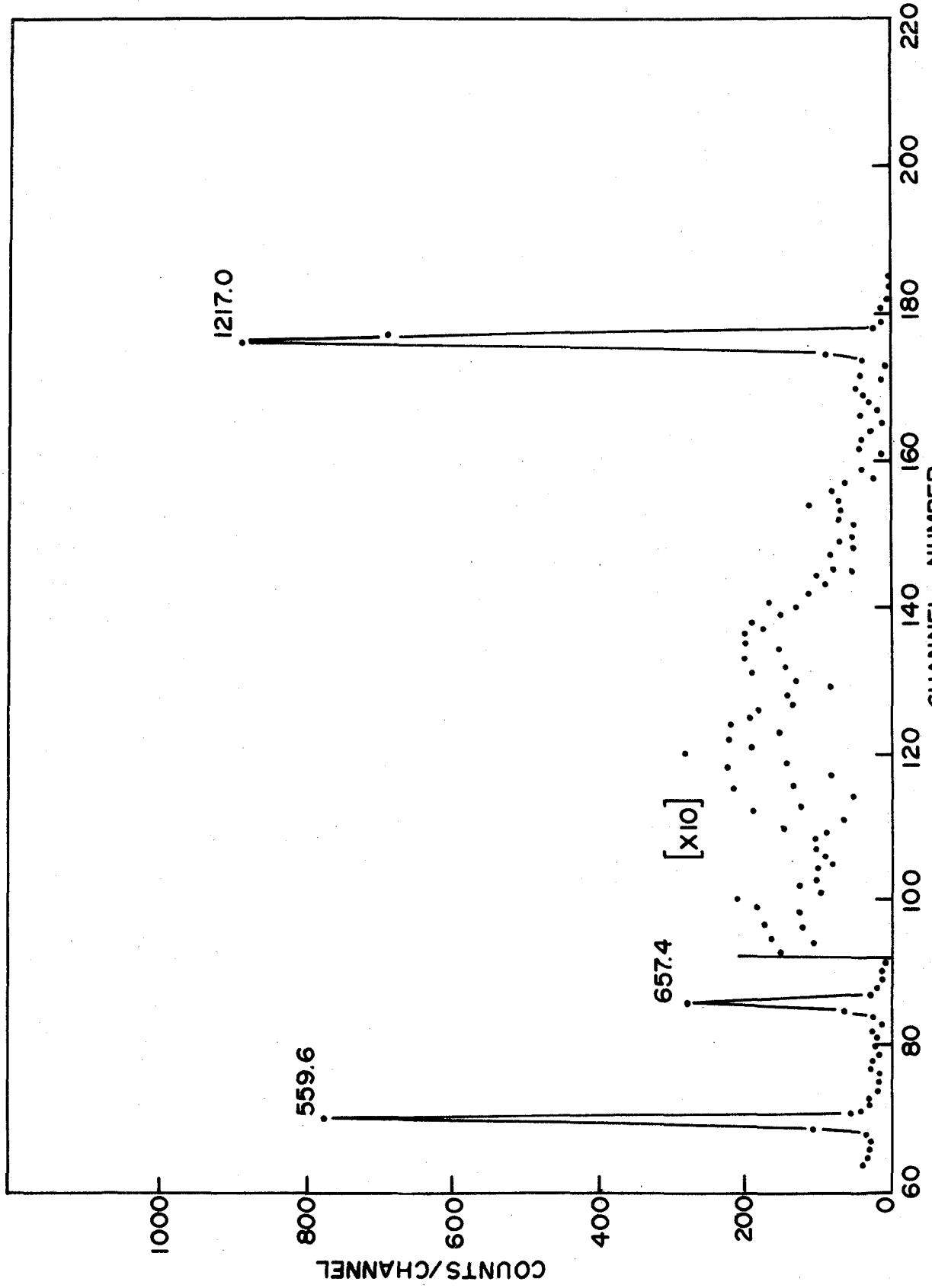

Figure 29 Ge(Li) γ-spectrum from ^{76}As decay in coincidence with γ-ray events of about 1200 keV

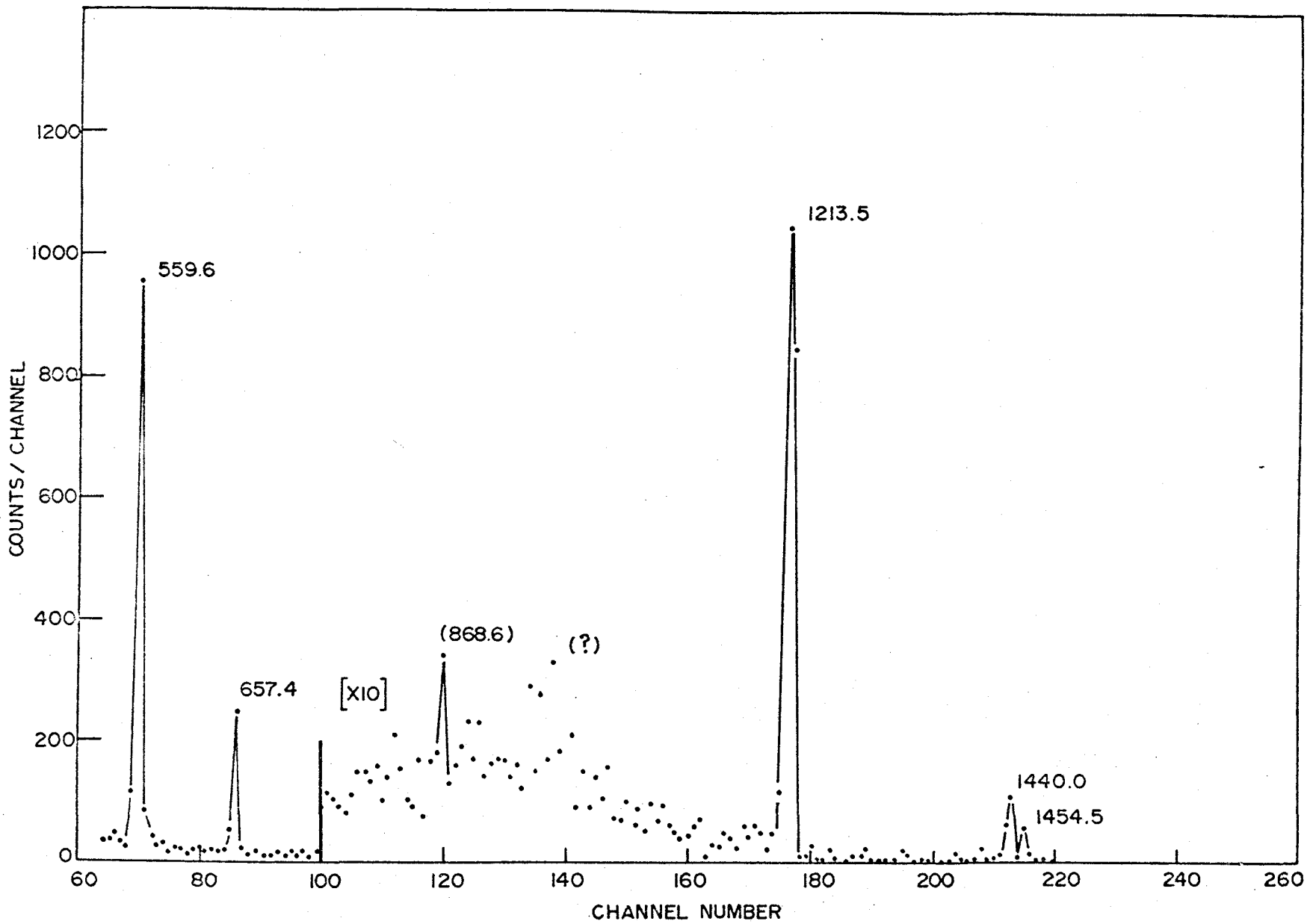

Figure 30 Ge(Li) γ-spectrum from ^{76}As decay in coincidence with γ-ray events of about 1226 keV

from events coincident with all three of these γ-rays.

In a third experiment, a Ge(Li) ^{76}As γ-spectrum covering the 540-700 keV energy region was recorded using a high resolution 0.155 cm^3 X-ray detector in coincidence with events in a narrow energy window set around the 559.6 keV γ-peak using a 23.8 cm^3-Ge(Li) detector. The coincident spectrum shown in Figure 31(a) was then compared with the single detector spectrum (measured without the coincidence requirement), shown in Figure 31(b). Strong enhancement of the 563.5, 657.4 and 666.0 keV γ-rays suggests they are coincident with the 559.6 keV γ-ray (which is also observed in the coincident spectrum due to Compton escape events from higher-energy γ-rays falling in the window selected). Table 3 summarizes the ^{76}As γ-γ coincidence data obtained in this study.

4.1.3 Beta-Gamma Coincidence Spectra

Fermi-Kurie plots of ^{76}As β-spectra (measured with a 2 mm x 80 mm^2 Si(Li) detector), in coincidence with the 559.6 and 657.4 keV γ-rays (detected by a 7.6 cm x 7.6 cm NaI(Tl) detector), are shown in Figures 32 and 33 respectively. The ^{76}As β-spectra, corrected for distortion effects by methods described in sub-section 3.3.3, were recorded by a ND-160 pulse height analyzer operated in a (64 channel by 64 channel) "two parameter" mode.

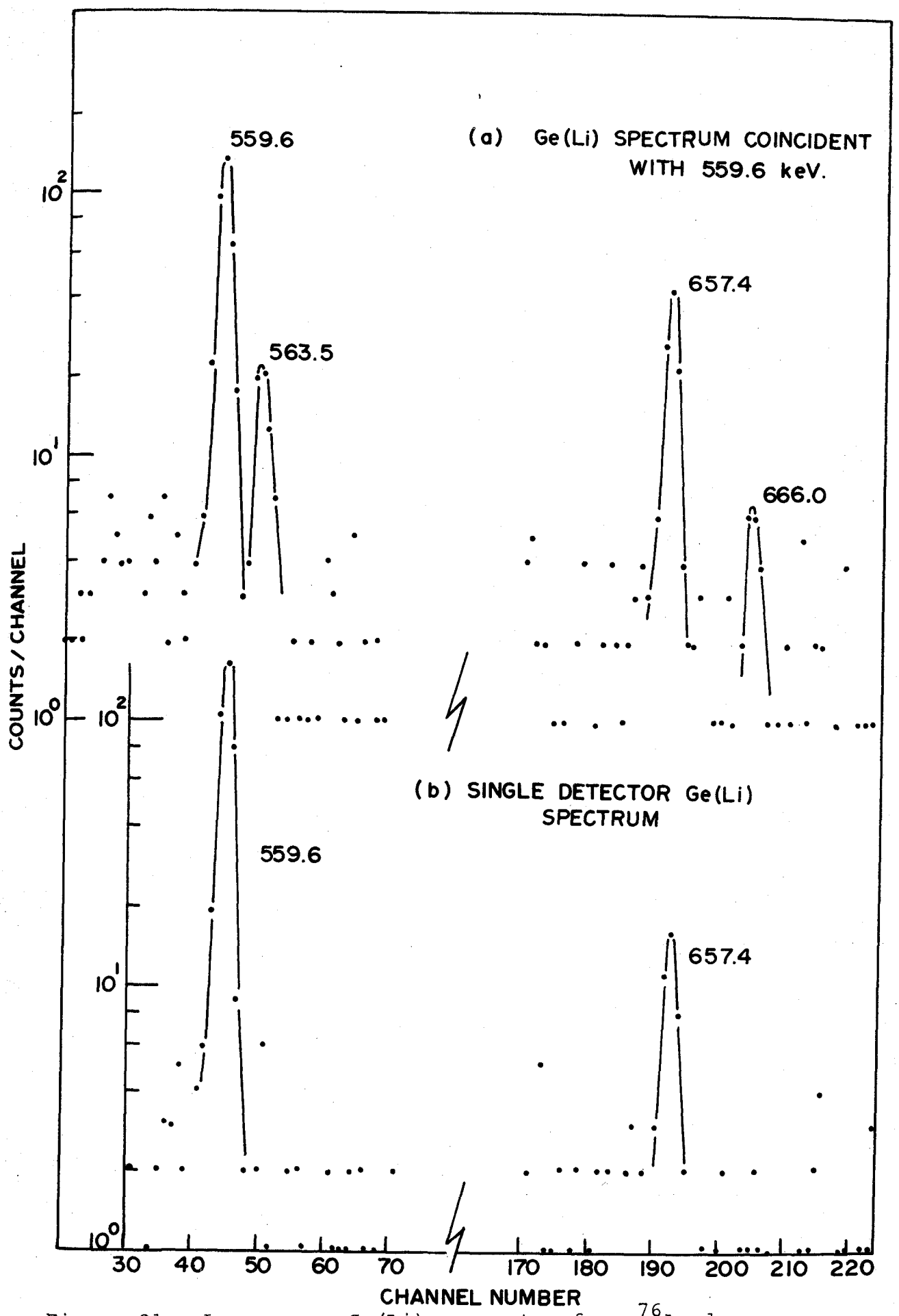

Figure 31 Low energy Ge(Li) γ-spectra from ^{76}As decay

TABLE 3

GAMMA-GAMMA COINCIDENCES[a] IN ^{76}As

Gamma-Ray keV	560[e]	657	1200[b]	1226
559.6	-	S	S	S[c]
563.5	S	-	-	-
657.4	S	-	S	W[b]
740.0	M	-	-	-
772.5	M	-	-	-
868.6	M	M	-	M[c]
883.0	M	W	-	W[c]
1130.5	S	-	-	-
1213.5	S	S	-	S[d]
1217.0	-	-	S	-
1228.9	S	-	-	-
1440.0	S	S	-	S[d]
1454.5	S	S	-	S[d]
1534.7	W	-	-	-
1568.0	M	-	-	-
1613.0	M	-	-	-
1870.5	S	-	-	-
2097.4	S	-	-	-
2111.9	S	-	-	-

Notes

(a) S = strong coincidence.
M = moderately strong coincidence.
W = weak coincidence.
Dashes (-) indicate no coincidence or no information.

(b) Coincidences presumed due mostly to 1213.5 keV peak, see text and Figure 29.

(c) Coincidences due mostly to 1228.9 keV peak, see Figure 30.

(d) Coincidences presumed due mostly to 1217.0 keV peak.

(e) Very weak intensity γ-lines at about 1585 keV and 1743 keV, found to be coincident with the 559.6 keV γ-ray, were not listed in this table due to poor statistics.

To investigate the possibility[12,13] that the 563.5 keV γ-ray may have resulted from ^{76}As electron-capture decay to the first excited state of ^{76}Ge rather than β-decay to an excited level in ^{76}Se and to confirm the γ-γ coincidence data of Figure 31(a), a "single parameter" β-γ coincidence experiment was performed using a 5 cm by 5 cm anthracene detector and a 0.155 cm^3 Ge(Li) detector. The Ge(Li) γ-spectrum in Figure 34 shows events coincident with β-rays measured with no pulse height discrimination by the anthracene detector. The appearance of both the 559.6 and the 563.5 keV γ-rays, with about the same relative intensities as were obtained in the single detector spectrum of Figure 25, confirmed the assignment of the 563.5 keV γ-ray to de-excitation of ^{76}Se.

4.1.4 Discussion of Results and Decay Scheme

Excited levels of ^{76}Se have been previously studied by many investigators via the β-decay[4,15,20] of 26.4-h ^{76}As, the β^+- and E.C.-decay[18,22] of 16.1-h ^{76}Br and via (p,p'), (d,d') and (d,t) nuclear reactions.[23,24,93] The present work has re-examined the β-decay of ^{76}As, has confirmed the existence of ^{76}Se levels at 1123.1, 1690.1, 2127.6, 2172.6 keV energy and has clarified several other features of previously postulated ^{76}As decay schemes.[15,20]

The weak intensity 563.5 keV transition (shown resolved from the strong 559.6 keV transition in Figure 25),

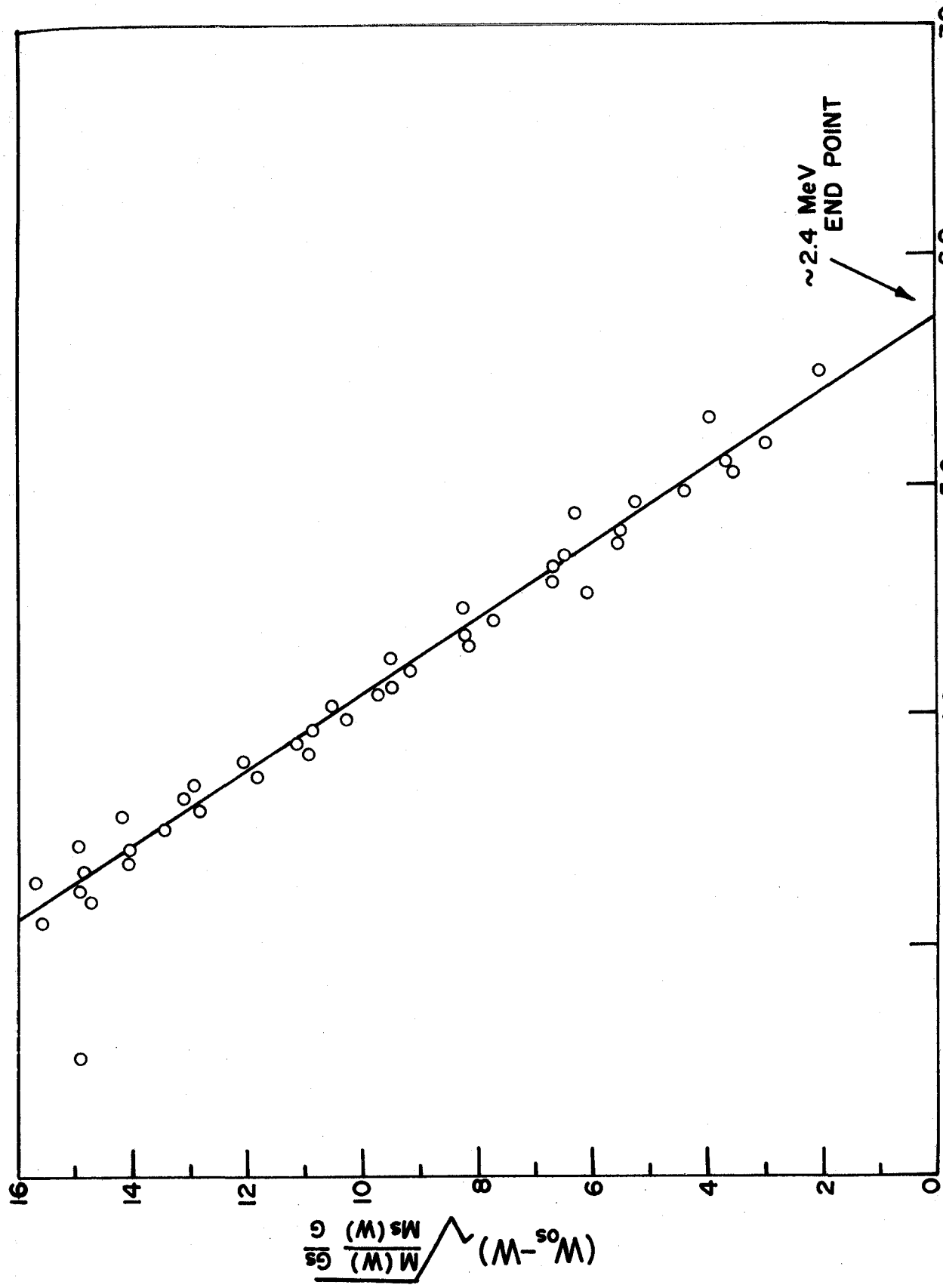

Figure 32 ^{76}As Fermi-Kurie plot for β-rays in coincidence with the 559.6 keV γ-ray

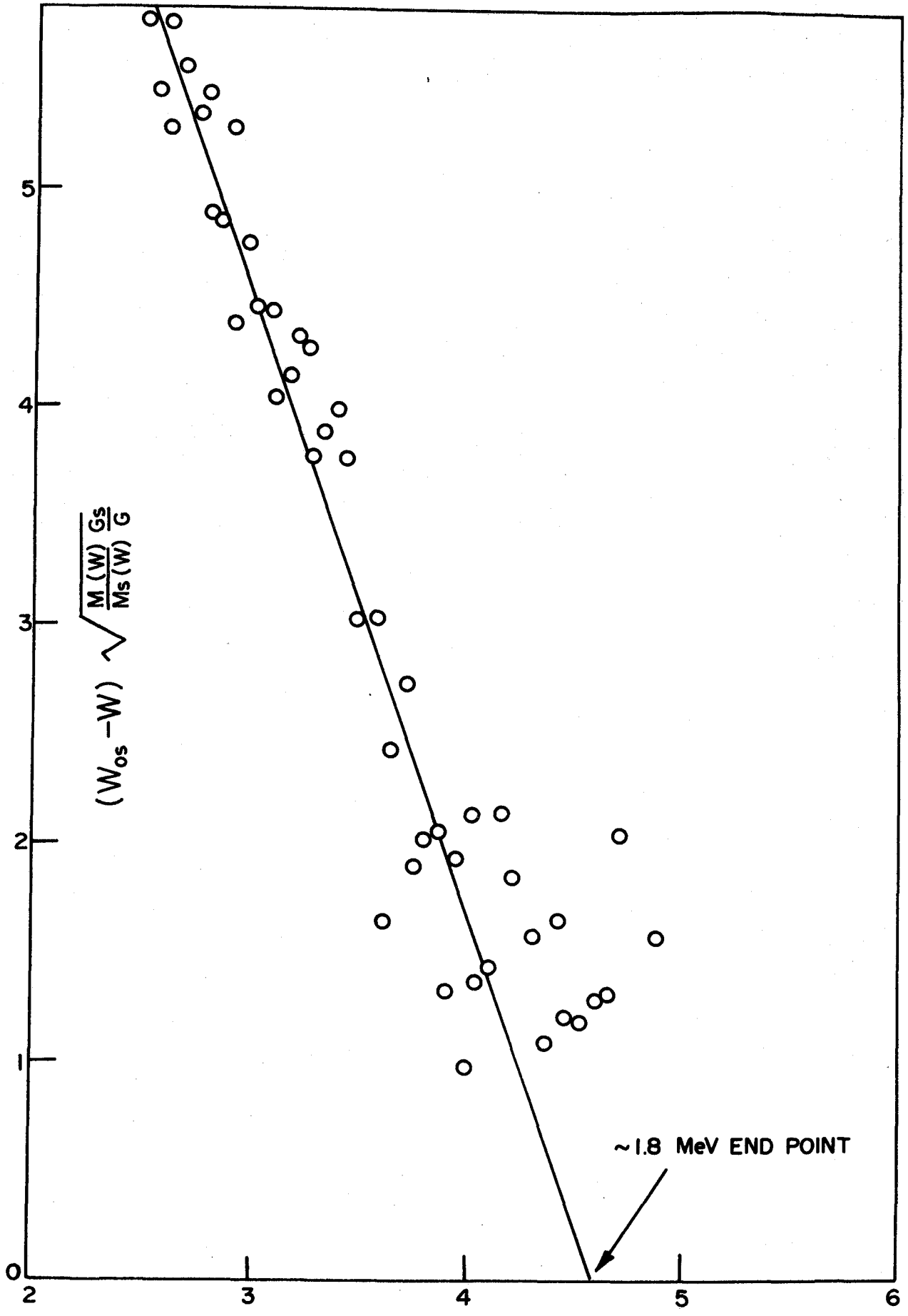

Figure 33 ^{76}As Fermi-Kurie plot for β-rays in coincidence with the 657.4 keV γ-ray

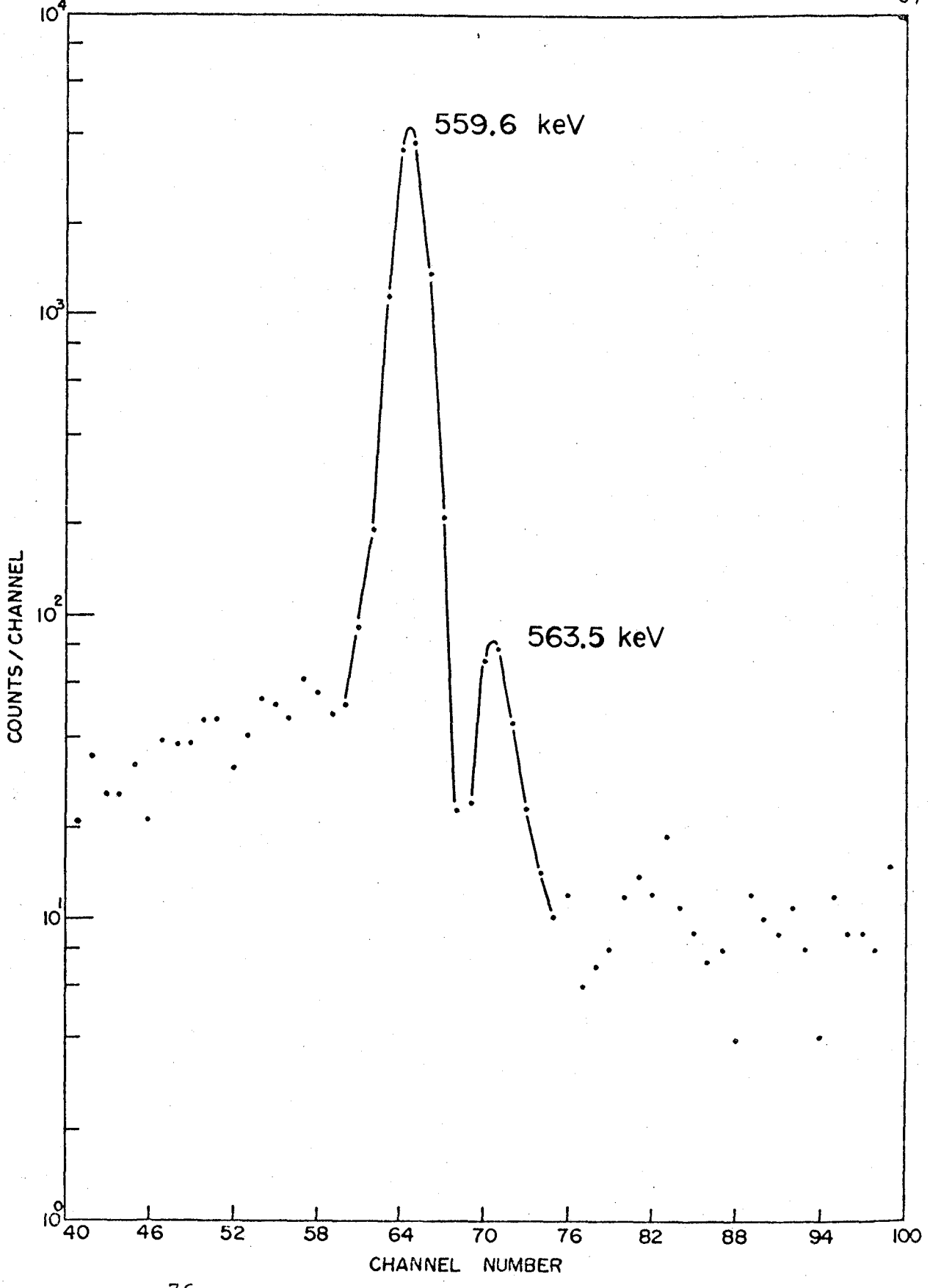

Figure 34 ^{76}As Ge(Li) γ-spectrum in coincidence with β-rays

was shown by β-γ and γ-γ coincidence measurements to result from decay of the 1123.1 keV ^{76}Se level, predicted from (p,p') and (d,d') reaction data[24,93] to have 0^+ character. These results have resolved the long standing dispute regarding the γ-ray peak at 559.6 keV, postulated by many previous authors[4,15] from γ-γ coincidence studies, to be made up of a pair of equal energy γ-rays coincident with one another.

Levels of ^{76}Se at 1690.1, 2127.6 and 2172.6 keV energy, predicted by Dzhelepov et al.[18] from β^+-decay studies of ^{76}Br, are proposed as populated also by ^{76}As β-decay from the γ-γ coincidence data of Figure 27 which indicate that the 1130.5, 1568 and 1613 keV transitions are coincident with the 559.6 keV transition. These data, along with the observation that the 740.0 keV γ-ray is also coincident with the 559.6 keV γ-ray and with energy sum-rule considerations, suggest that the 1690.1 keV level is fed by a 740.0 keV transition from the 2430.5 keV level, assigned a 3^- character by Lin[24] from (d,d') nuclear reaction data.

The 2430.5 keV level is shown in Figure 35 to decay primarily by γ-rays of 1213.5, 1870.5 and 2430.0 keV energy in accordance with the the γ-γ coincidence data in Table 3. The existence of the 1213.5 keV γ-ray is proved by the Ge(Li) spectrum of Figure 25 where this γ-ray is clearly resolved for the first time from the nearby 1217.0 keV γ-ray.

A weak intensity γ-line with energy about 1585 keV was first observed by J. Aten et al.[16] and is observed in the spectrum coincident with the 559.6 keV γ-ray in Figure 27. This γ-line is not included in the ^{76}As decay scheme due to poor statistics and the possibility that it may be the single-escape peak from the 2097.4 keV γ-ray (which is also shown in Figure 27 to be coincident with the 559.6 keV γ-ray).

The weak intensity γ-lines, shown dotted in the decay scheme of Figure 35 due to their large energy and relative intensity uncertainties, at about 727, 807, 1177, 1743 and 2306 keV energy (See bottom of Table 1) all provide weak evidence for a ^{76}Se excited level at about 2866 ± 2 keV. By energy sum-rule considerations, the last three of these γ-lines may result from γ-γ cascades to the 1690.1, 1123.1 and 559.6 keV levels respectively while the first two (which sum to 1534 keV) may result from a γ-γ cascade to the 1332.1 keV level. Further support for a level of 2866 keV energy comes from the (d,d') nuclear reaction data of Lin[24] who predicted a ^{76}Se level at about 2.87 MeV. A

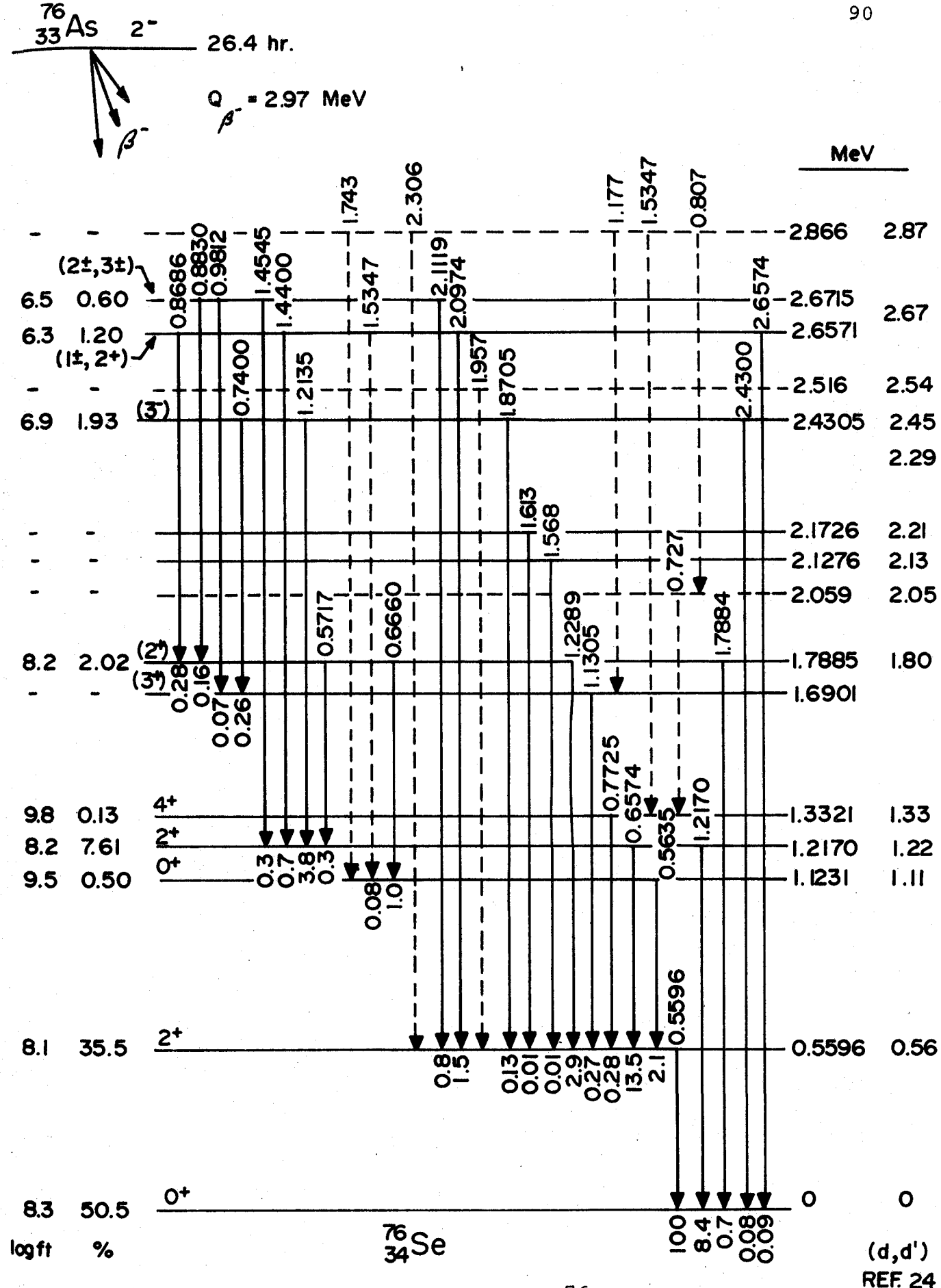

Figure 35 Proposed decay scheme of ^{76}As.

γ-ray of 1534.7 keV energy has been placed in Figure 35 (as resulting from the decay of the 2657.1 keV level to the 1123.1 keV level) from energy sum-rule considerations and the weak γ-γ coincidence data in Table 3. The possibility this latter γ-ray may also result from decay of the 2866 keV level is reflected by showing this transition dotted twice in the ^{76}As decay scheme (Figure 35).

A new γ-ray transition of 981.2 keV energy, previously unreported in the literature, was found to fit into the decay scheme via energy sum-rule considerations between the 2671.5 and 1690.1 keV levels. A transition of 1957 keV energy, first reported by J. Aten et al.[16] and observed as a very weak peak in one of the Ge(Li) γ-spectra taken in this study, is shown in coincidence with the 559.6 keV since the level from which it is then postulated to originate (2516 keV) is close in energy to the 2.54 MeV level found by the nuclear reaction experiments of Lin.[23,24] Other levels predicted by the (d,d') nuclear reaction experiments of Lin[24] are shown in Figure 35 for comparison purposes. Further support for a level at 2516 keV results from the (p,p') nuclear reaction experiments of Darcey et al.[93] which predicted a ^{76}Se level at 2.51 MeV

A decay energy for ^{76}As of 2.97 ± 0.1 MeV, in good agreement with the previously accepted value,[3,25] is deduced from the data of Figures 32 and 33 which indicate the 559.6 and 1217.0 keV levels are coincident with β-ray groups with

end-point energies of 2.4 and 1.8 MeV respectively. The log ft values in Figure 35 were calculated from the relative β-ray intensities populating each excited level (obtained in turn from the observed γ-ray intensities), and the recent estimate by Nagarajan et al.[25] (1969) who used a Siegbahn-Slätis β-ray spectrometer, that 50.5% of the ^{76}As disintegrations lead to the ground state of ^{76}Se. The ^{76}As β-ray intensity to the ground state of ^{76}Se has been measured many times in the past and was not measured again using Si(Li) detectors in the present study due to the superiority of magnetic spectrometers (at high β-ray energies) used previously by earlier investigators.[25,26,27] The log ft values for β-ray transitions to ^{76}Se levels at 2059, 2516 and 2866 keV were not determined due to the lack of statistical accuracy of intensity data for the γ-rays depopulating these levels.

4.2 Decay of ^{78}As

4.2.1 Half Life and Gamma-Ray Spectra

The half life of ^{78}As was determined to be 90.7 ± 0.2 min, in good agreement with the previously accepted value,[1,3] from an analysis of gross β-activity decay using the CLSQ computer program.[38] See Figure 23. Attempts were made to observe the 6-min ^{78}As isomer decaying by a

500 keV transition reported by Nemilov et al.[31] Bombardment times of 2 minutes and chemical separation times of 3 minutes were followed by gross β- and γ- ray counting techniques. No evidence could be found for the existence of this state, a result in accord with the conclusions of Fritze[36] and Fritze and Kiefer.[37]

The γ- spectrum of ^{78}As plus ^{76}As, taken with an 8 cm^3-Ge(Li) detector, is shown on the top half of Figure 36 while the spectrum due only to ^{76}As decay, measured one day later, is shown at the bottom. The ^{78}As decay γ-rays were identified by subtraction of these two spectra. The superiority of high resolution Ge(Li) detectors over NaI(Tl) detectors in γ-ray decay scheme studies is effectively demonstrated by comparing the spectrum on the top of Figure 36 with the corresponding NaI(Tl) spectrum shown in Figure 37. Both of these latter spectra were obtained from identically prepared ^{78}As plus ^{76}As sources. High energy ^{78}As γ-ray peaks appeared clearly in the Ge(Li) spectrum but were almost entirely obscured in the NaI(Tl) spectrum.

To aid the analysis and interpretation of some of the ^{78}As γ-rays appearing in the 8 cm^3-Ge(Li) γ-spectrum measurements, Figures 38 and 39 were constructed showing the variation of the relative area ratios of full energy to double escape peaks[65] and the full width at half maximum (FWHM) as a function of energy respectively. Unresolved

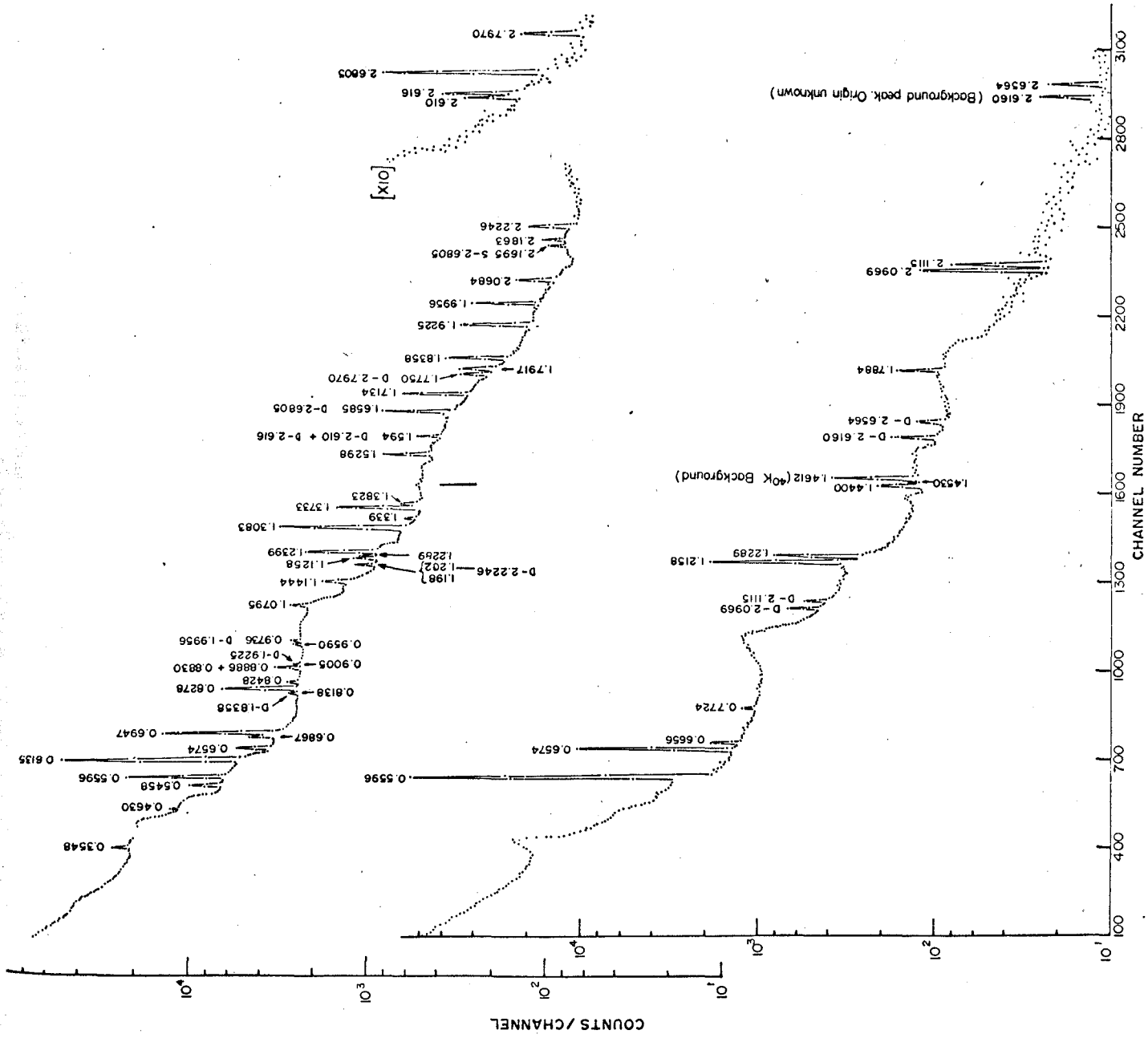

Figure 36 Top half: Single detector Ge(Li) γ-ray spectrum from ^{76}As and ^{78}As decay measured shortly after the end of bombardment.
Bottom half: Single detector Ge(Li) γ-ray spectrum from ^{76}As decay measured one day after the end of bombardment. All energies in MeV

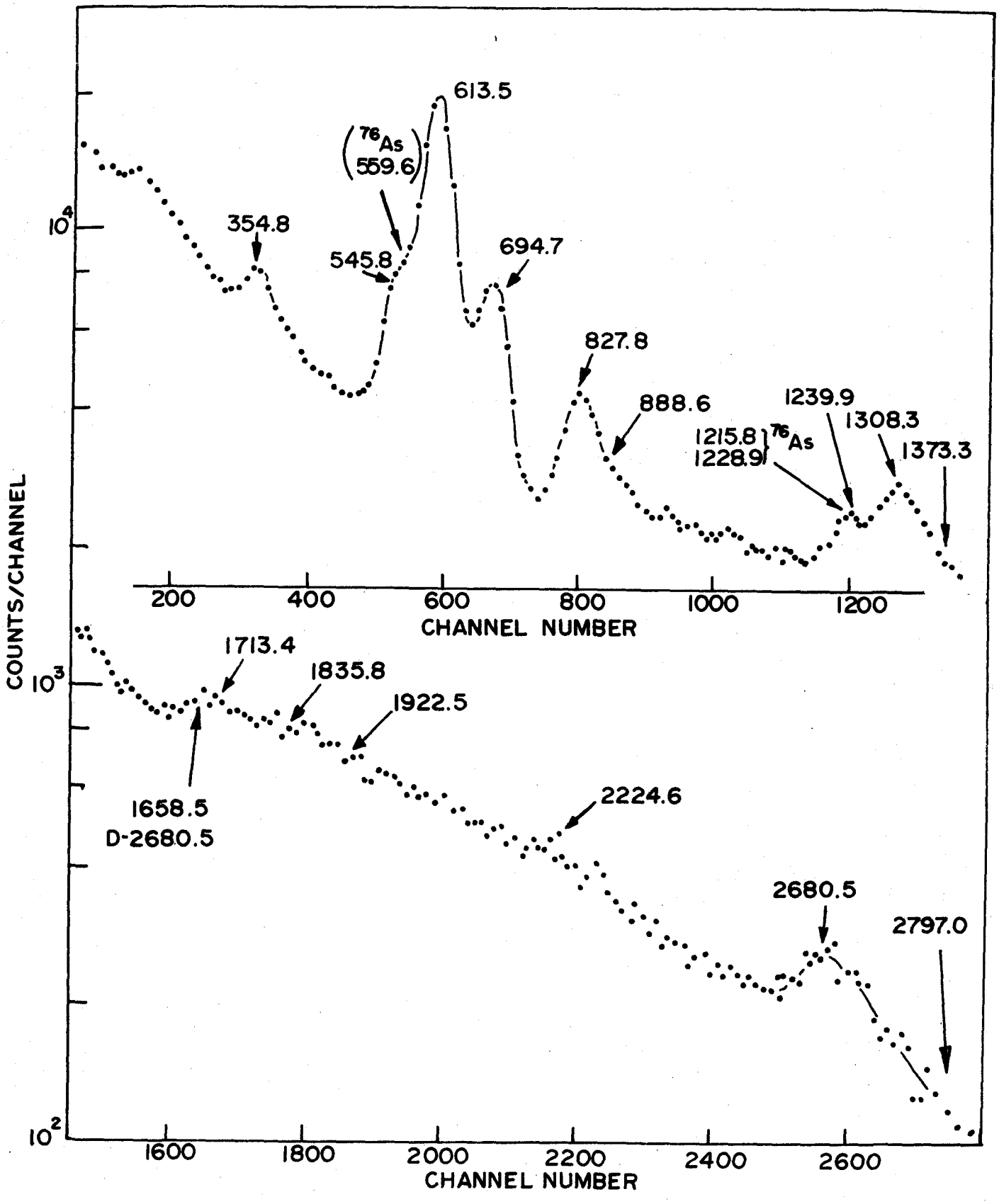

Figure 37 Single detector NaI(Tl) γ-ray spectrum from ^{76}As and ^{78}As decay measured shortly after the end of bombardment

line doublets, identified by anomalously large FWHM values and other visual inspection methods, were graphically resolved using techniques described in sub-section 3.3.2. A typical example of this procedure is shown in Figure 40 for the 686.7 - 694.7 keV pair. The doublets at about 842, 888, 1200 and 2614 keV energy were similarly treated; the 2616.0 keV peak, along with the 1461.0 keV ^{40}K peak, proved to belong to the background while the 2610.0 keV peak appeared only in the early spectrum and was tentatively assigned to ^{78}As.

A low energy γ-ray spectrum of ^{78}As taken with an ORTEC X-ray Ge(Li) detector (0.25 cm^3) revealed no γ-rays between $\simeq$ 13 keV and the lowest energy γ-ray found by the 8 cm^3 Ge(Li) detector (354 keV). Thus the two low-energy γ-rays at 80 keV and 270 keV reported by Nemilov et al.[31] could not be confirmed.

Energies and relative intensities for 32 γ-rays assigned to ^{78}As decay from the results of this work are presented in Table 4. After this work was completed and published,[28] similar values were independently reported by Paradellis and Hontzeas[29] even though most of their ^{78}As samples were prepared by the 14-MeV neutron bombardment of natural SeO_2 with no chemical separation.

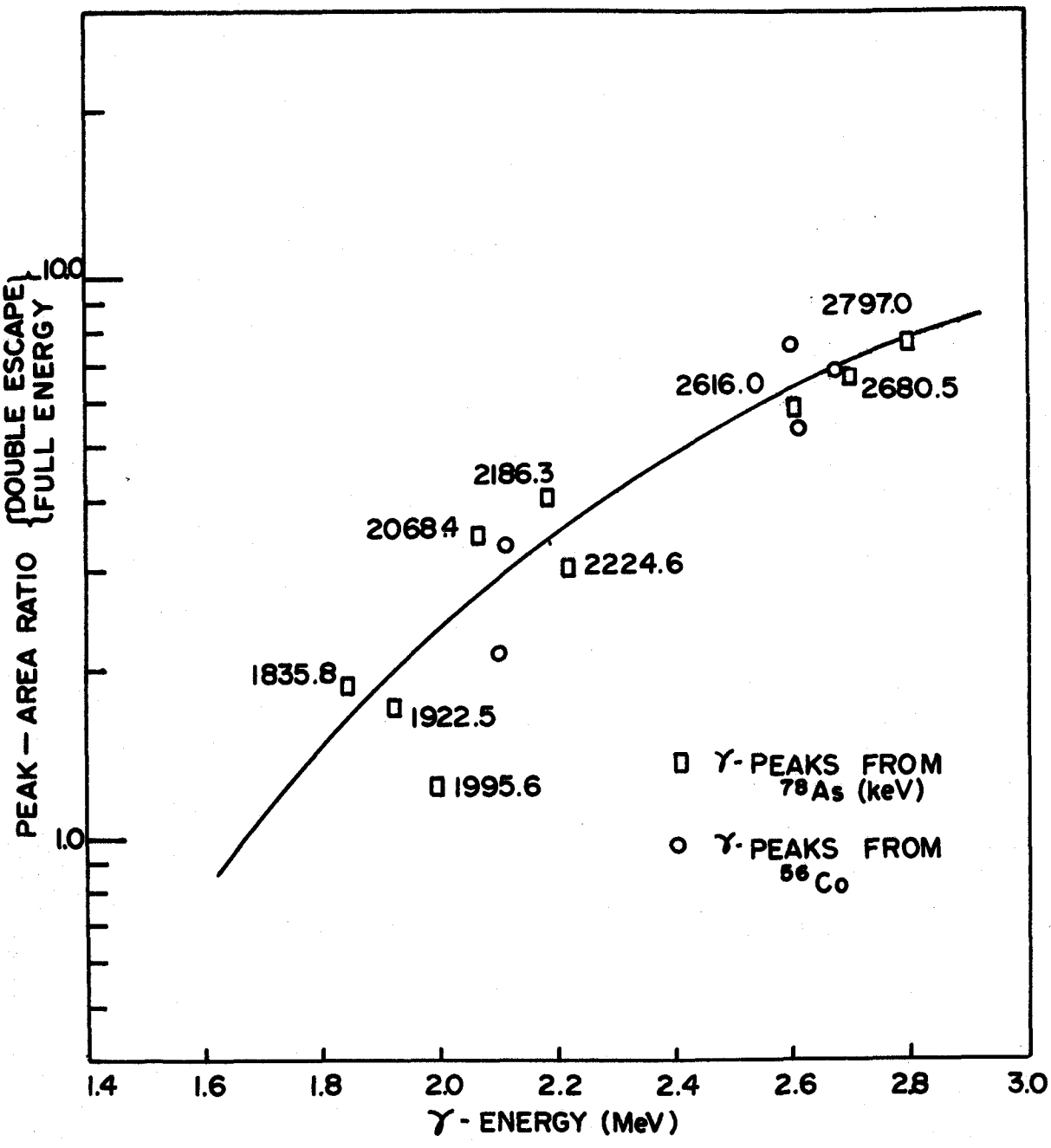

igure 38 Double escape peak data for a 8 cm^3-Ge(Li) detector versus γ-ray energy ; the line passing between the plotted points was drawn as a visual guide.

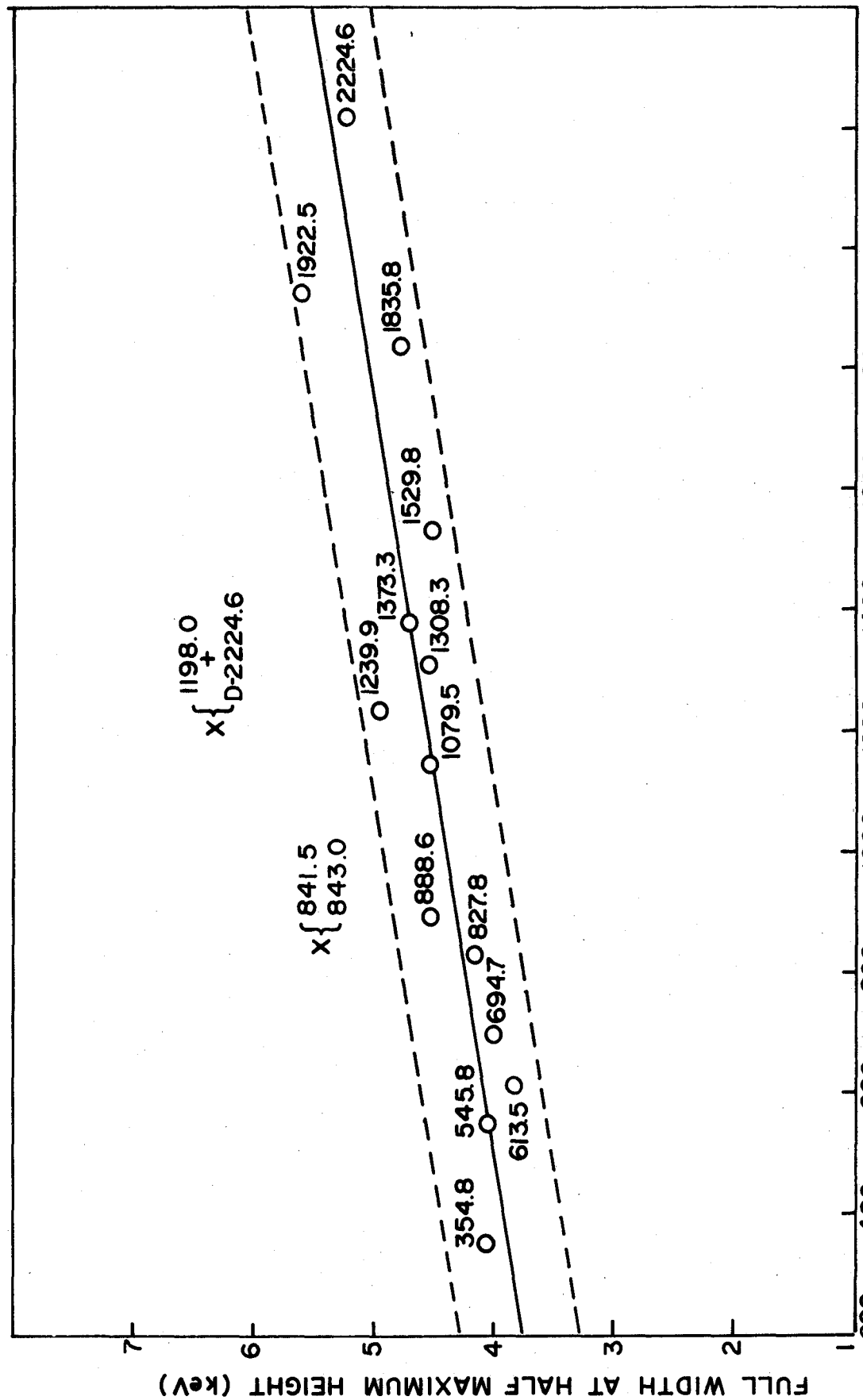

Figure 39 Full width at half maximum height (FWHM) of ^{78}As γ-peaks versus γ-ray energy

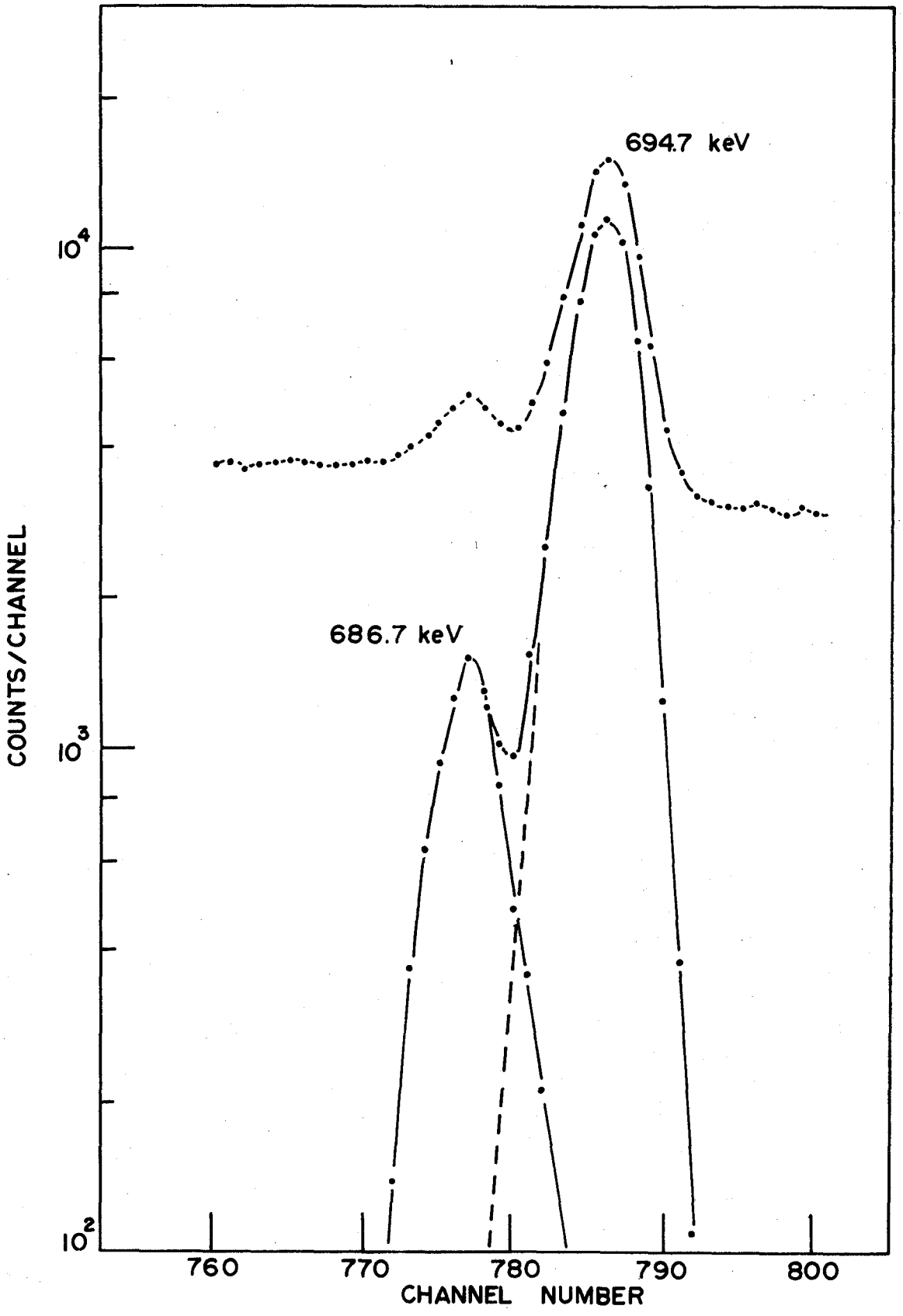

Figure 40 Graphical resolutions of 686.7 and 694.7 keV γ-rays in ^{78}As γ-spectrum obtained with a 8 cm^3 Ge(Li) detector

TABLE 4

ENERGY AND RELATIVE INTENSITY VALUES FOR γ-RAYS FOLLOWING THE DECAY OF ^{78}As

Energy (keV) [a]	Intensity	Energy (keV)	Intensity
354.8 [b]	4.0 ± 0.4	1308.3	26.6 ± 2.4
463.0 ± 1	0.6 ± 0.3	1339.0 ± 1	1.0 ± 0.5
545.8	5.3 ± 0.6	1373.3	10.1 ± 0.9
613.5	100	1382.3	1.4 ± 0.3
686.7	4.0 ± 1.0	1529.8	5.1 ± 0.7
694.7	33.0 ± 1.5	1713.4	3.7 ± 0.4
827.8	16.3 ± 0.7	1791.7	2.0 ± 0.5
841.5 ± 1	0.3 ± 0.2	1835.8	3.0 ± 0.4
843.0 [c]	1.0 ± 0.4	1922.5	3.5 ± 0.3
883.0 ± 1	0.8 ± 0.4	1995.6	2.5 ± 0.7
888.6	5.0 ± 1.0	2068.4	1.1 ± 0.7
959.0 ± 1	1.0 ± 0.5	2186.3 ± 1	1.0 ± 0.5
1079.5	3.5 ± 1.2	2224.6	1.6 ± 0.3
1144.4	3.8 ± 0.5	2610.0 [d]	0.5 ± 0.3
1198.0 ± 1	1.5 ± 0.5	2680.5	3.5 ± 0.2
1239.9	12.9 ± 1.0	2797.0 ± 1	0.4 ± 0.2

Notes

(a) Energy uncertainties ± 0.5 unless otherwise noted. (See sub-section 3.3.2) Intensity uncertainties obtained from six independent spectrum measurements.

(b) Suspected to be a doublet (See sub-section 4.2.4); one with a relative intensity of about 3.7, the other 0.3.

(c) Assigned to two places in the decay scheme; maybe a doublet.

(d) Tentatively assigned to ^{78}As decay.

4.2.2 Gamma-Gamma Coincidence Spectra

Coincidence studies of ^{78}As γ-γ cascades were normally performed with a 7.6 cm by 7.6 cm NaI(Tl) and an 8 cm^3 Ge(Li) detector except in studies of high energy, low intensity γ-rays where two NaI(Tl) detectors had to be used. The coincidence spectra were complicated by the presence of ^{76}As in the samples of ^{78}As. The 613.5 keV peak of ^{78}As, as shown in Figure 37, is close enough to the intense 559.6 keV peak of ^{76}As so that a NaI detector cannot completely resolve the two. The Ge(Li) spectra displayed in Figures 41-45, all corrected for the effects at the selected energy of Compton escape events from higher energy γ-rays (by methods described in sub-section 3.3.2), show ^{78}As γ-rays coincident with photons of 613.5, 694.7, 827.8, 1239.9 and 1308.2 keV respectively. The NaI(Tl) spectra in Figures 46-50 show coincidences with ^{78}As γ-rays of 613.5, 694.7, 827.8, 1239.9 and 1713.4 keV respectively. The NaI(Tl) detector resolution was insufficient to resolve the 1239.9 - 1308.3 keV doublet in Figure 48. The weak 1308.3 keV peak in Figure 47, also shown unresolved from the 1373.3 keV peak, was assumed to arise from a coincidence with the 686.7 keV peak, indicated in the decay scheme of Figure 56. Table 5 summarizes the ^{78}As γ-γ coincidence data obtained in this study.

4.2.3 Beta-Ray and Beta-Gamma Coincidence Spectra

The Fermi-Kurie plot in Figure 52 of the high-energy portion of the ^{78}As β-spectrum in Figure 51, shows the estimated end-point energy for ^{78}As to be 4.27 ± 0.10 MeV. In addition, this plot shows two other possible β-ray groups, one with an end-point energy of ≃ 3.7 MeV and the other

TABLE 5

GAMMA-GAMMA COINCIDENCES IN ^{78}As

Gamma Ray keV	In Coincidence With						
	354.8	545.8	613.5	694.7	827.8	1239.9	1308.2
354.8	-	-	S	-	-	-	-
545.8	-	-	M	M	S	-	S
613.5	S	S	-	S	S	S	-
694.7	-	S	S	-	W	-	-
827.8	-	S	S	W	-	S	W
888.6	-	-	M	-	-	-	-
1079.5	-	-	W	-	-	-	-
1144.4	-	-	W	-	-	-	-
1239.9	-	-	S	-	S	-	-
1308.3	-	S	-	-	S	-	-
1373.3	-	-	S	S	-	-	W
1529.8	-	-	M	M	-	-	-
1713.4	S	-	S	-	-	-	-
1835.8	-	-	-	W	-	-	-
2068.4	-	-	S	-	-	-	-
2186.3	-	-	W	-	-	-	-
2680.5	-	-	W	-	-	-	-

Notes

1. S = strong coincidence

   M = moderately strong coincidence

   W = weak coincidence

2. Dashes (-) indicate no coincidences or no information.

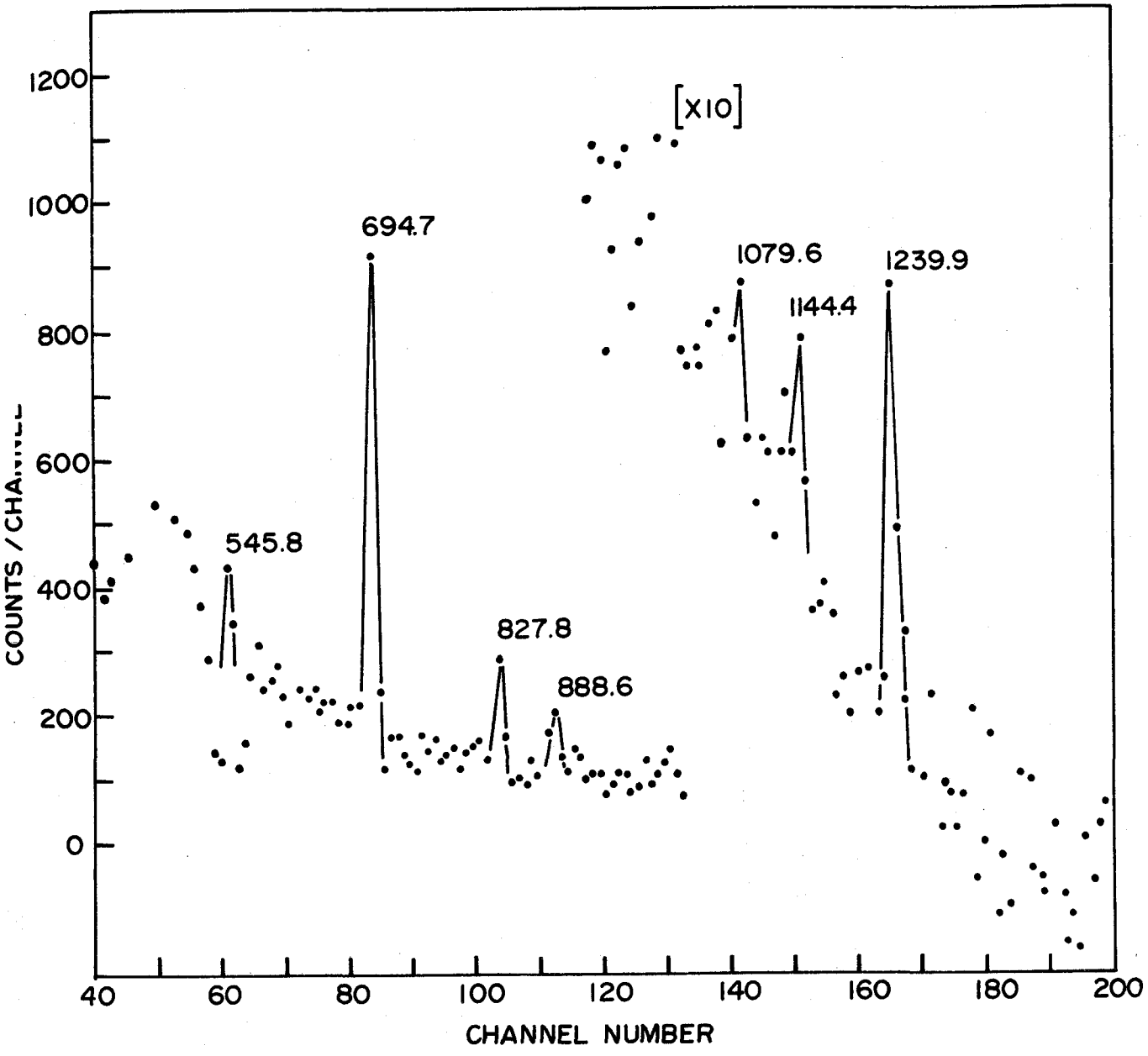

Figure 41 Ge(Li) γ-spectrum from ^{78}As decay in coincidence with 613.5 keV γ-ray

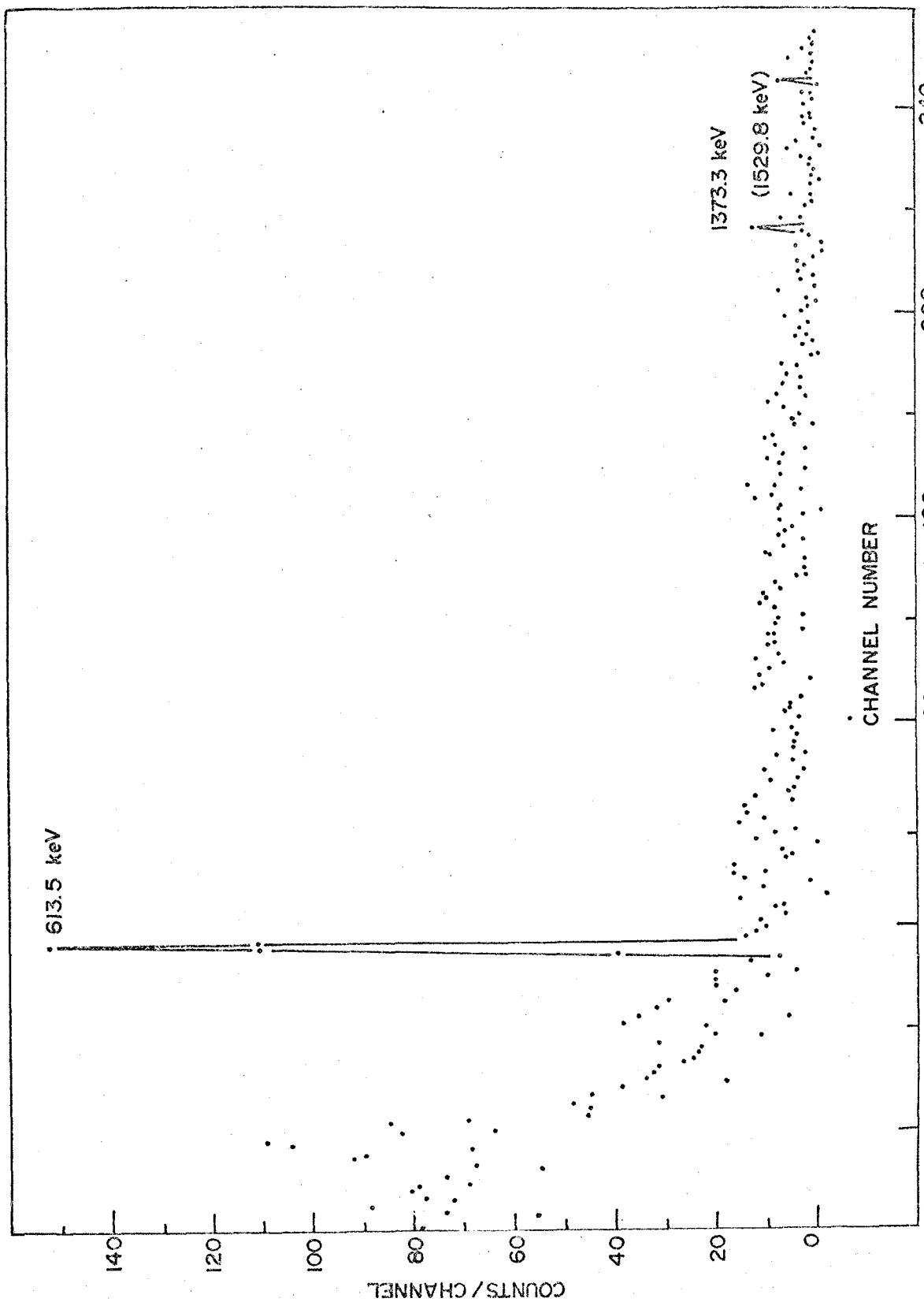

Figure 42 Ge(Li) γ-spectrum from ^{78}As decay in coincidence with 694.7 γ-ray

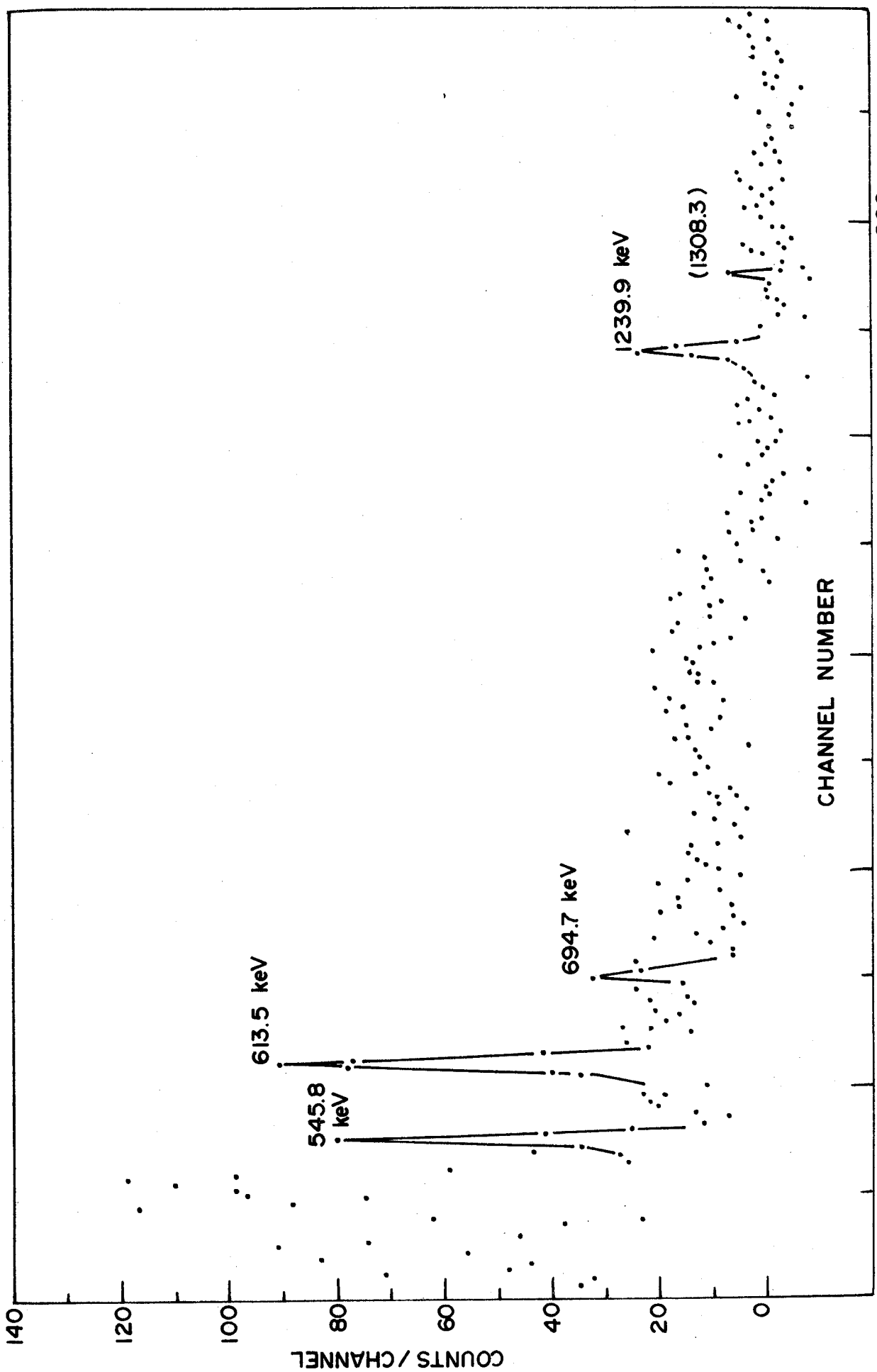

Figure 43 Ge(Li) γ-spectrum from ^{78}As decay in coincidence with 827.8 keV γ-ray

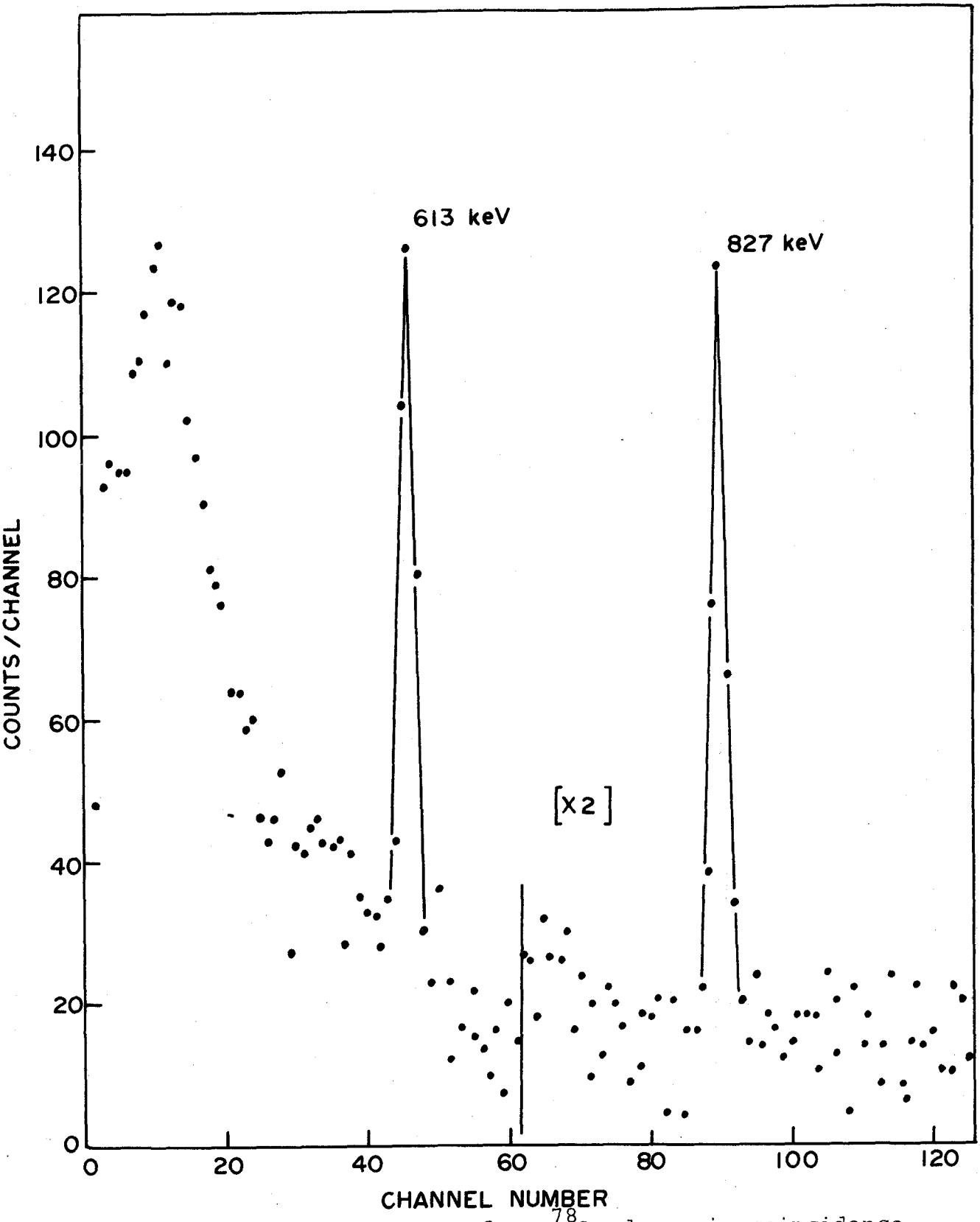

Figure 44 Ge(Li) γ-spectrum from ^{78}As decay in coincidence with 1239.9 keV γ-ray

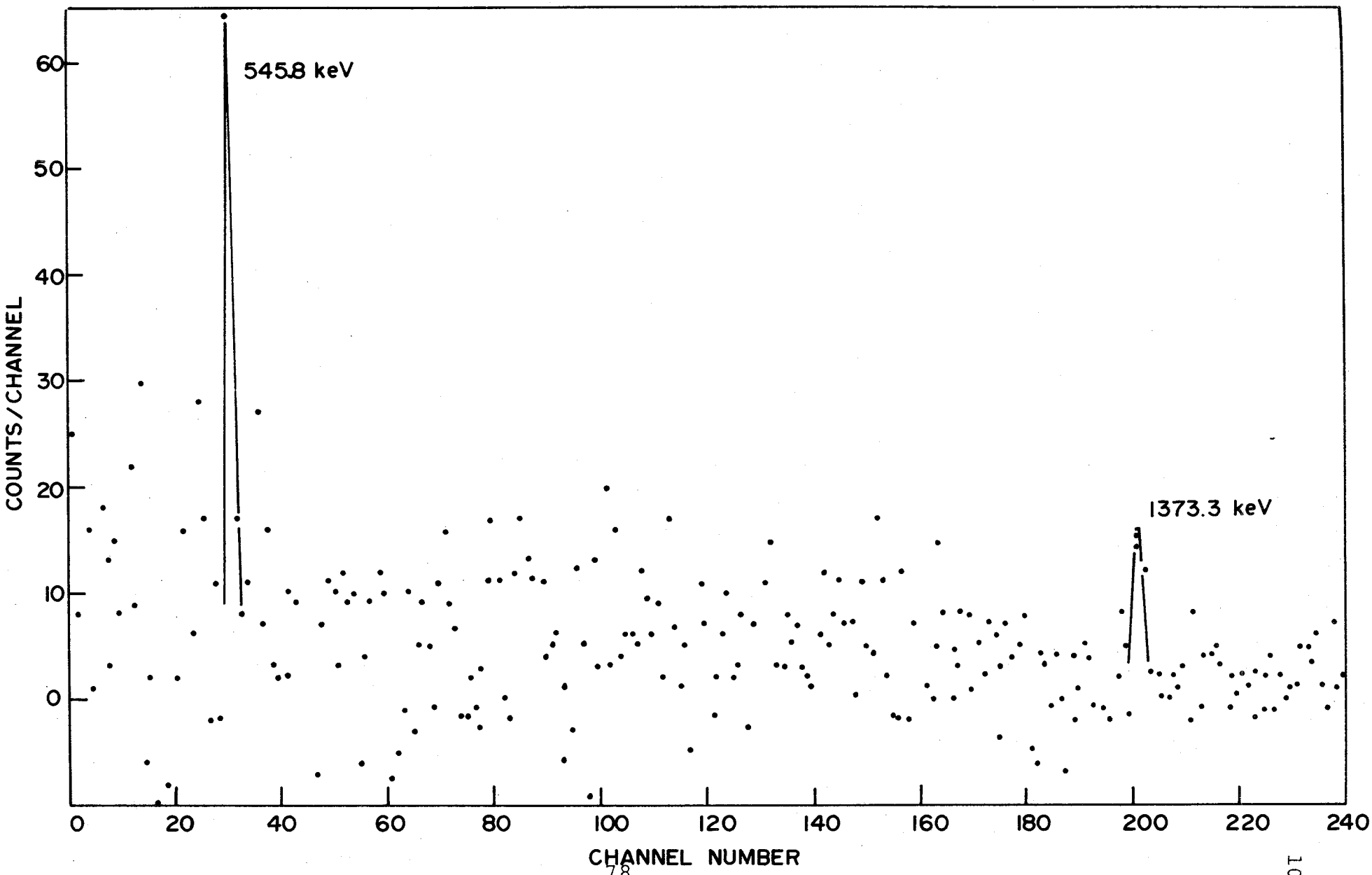

Figure 45 Ge(Li) γ-spectrum from ^{78}As decay in coincidence with 1308.3 keV γ-ray

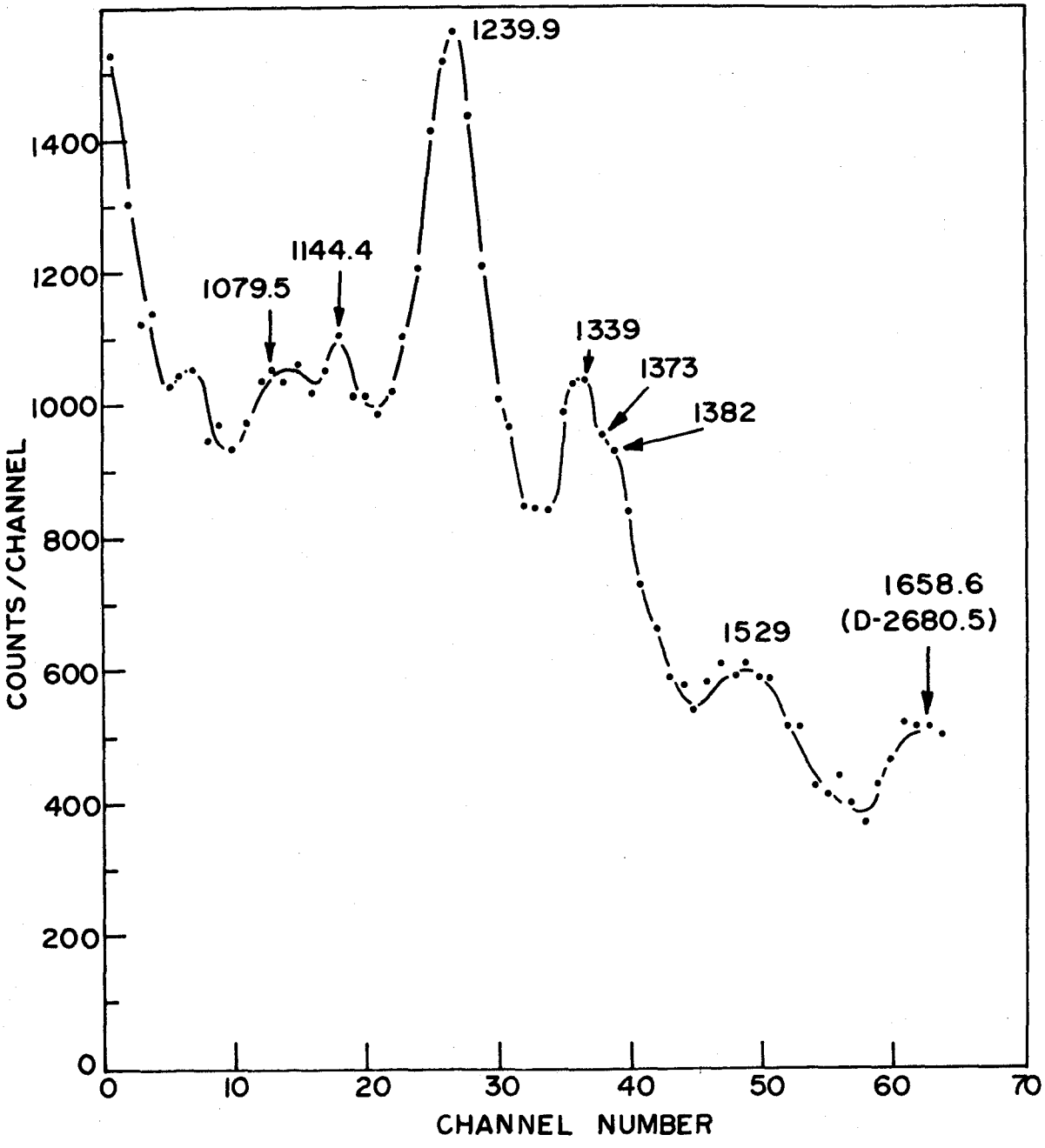

Figure 46 NaI(Tl) γ-spectrum from ^{78}As decay in coincidence with 613.5 keV γ-ray

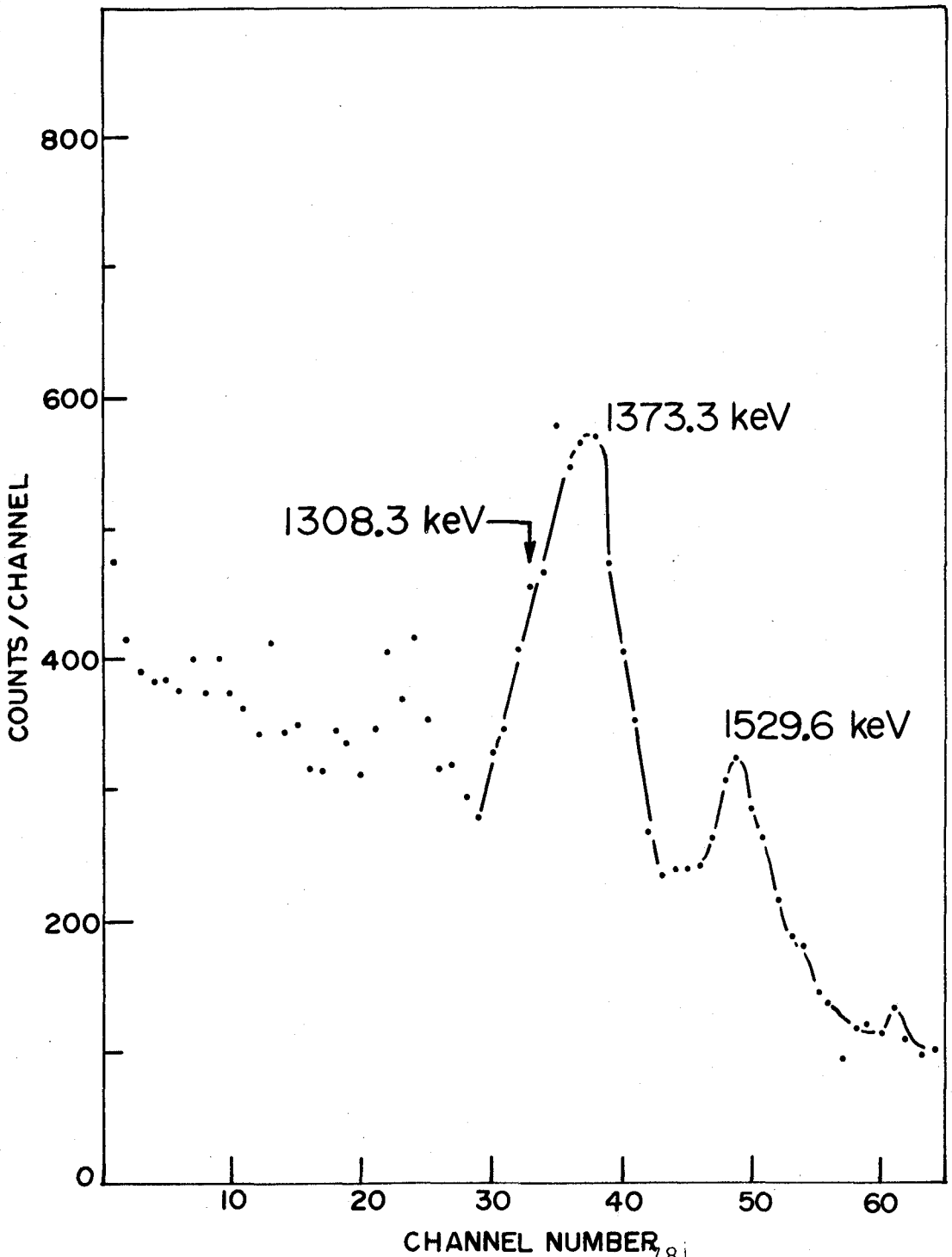

Figure 47 NaI(Tl) γ-spectrum from ^{78}As decay in coincidence with 694.7 keV γ-ray. The weak 1308.3 keV peak is believed to be coincident with the 686.7 keV peak and not the 694.7 keV peak

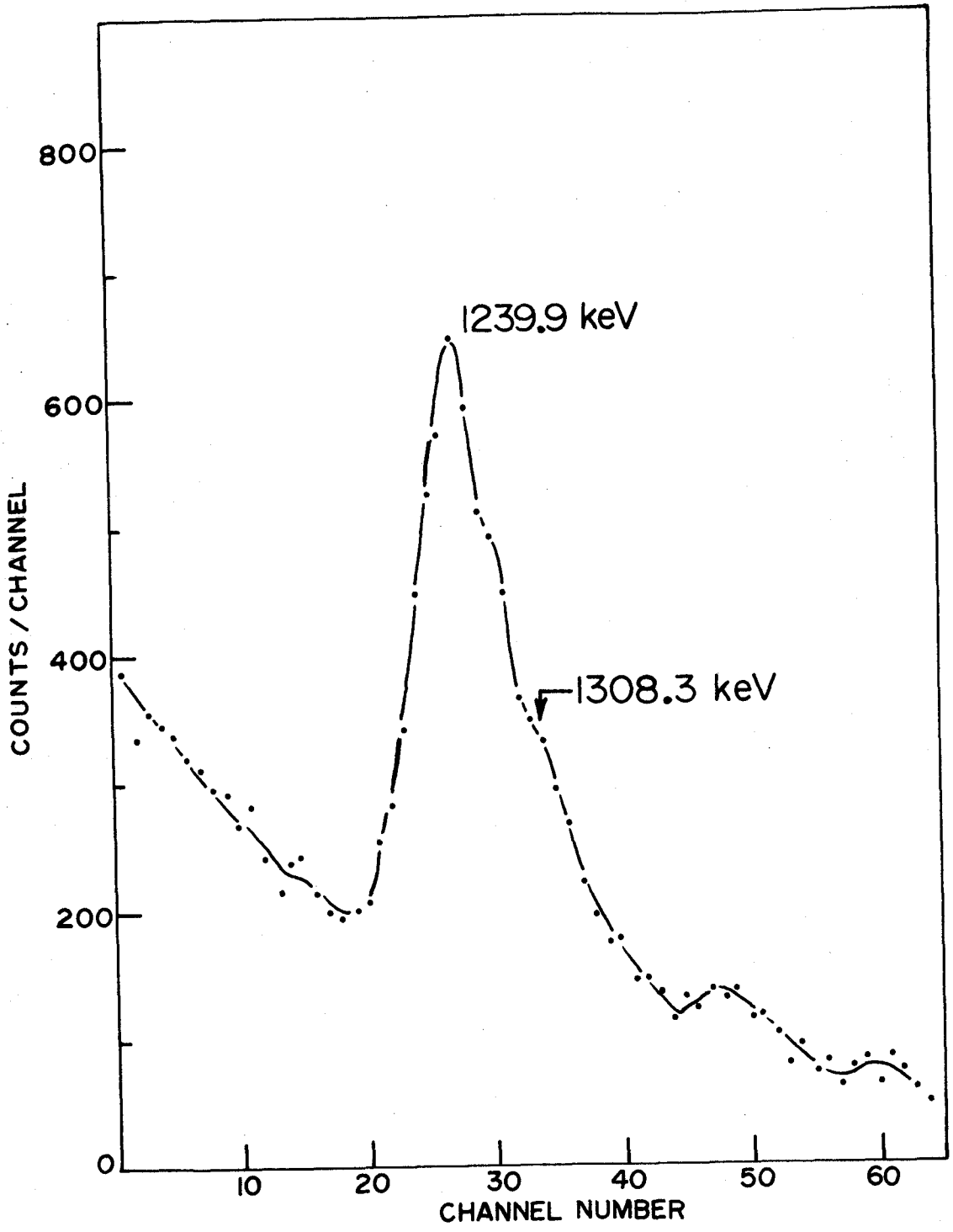

Figure 48 NaI(Tl) γ-spectrum from ^{78}As decay in coincidence with 827.8 keV γ-ray

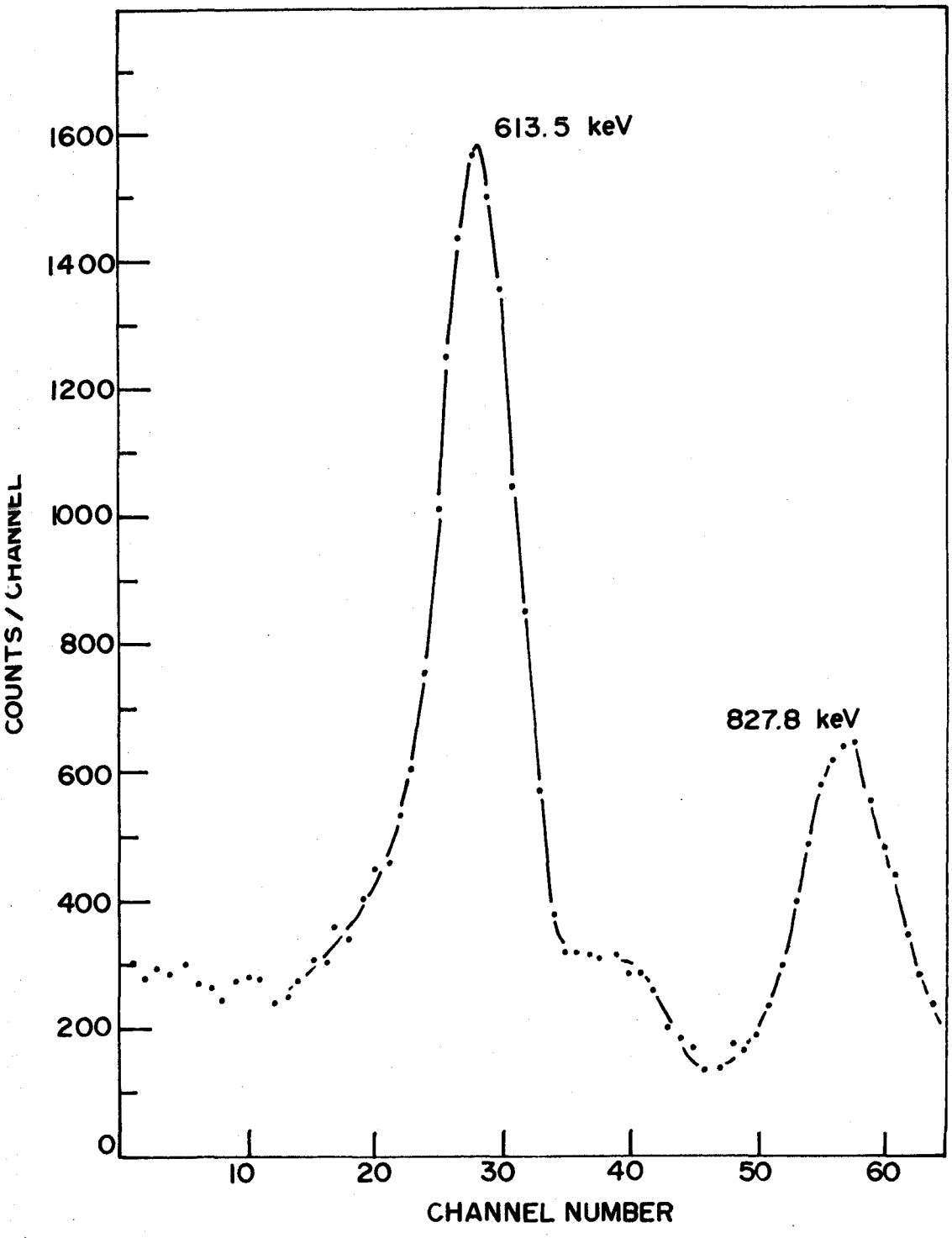

Figure 49 NaI(Tl) γ-spectrum from ^{78}As decay in coincidence with 1239.9 keV γ-ray

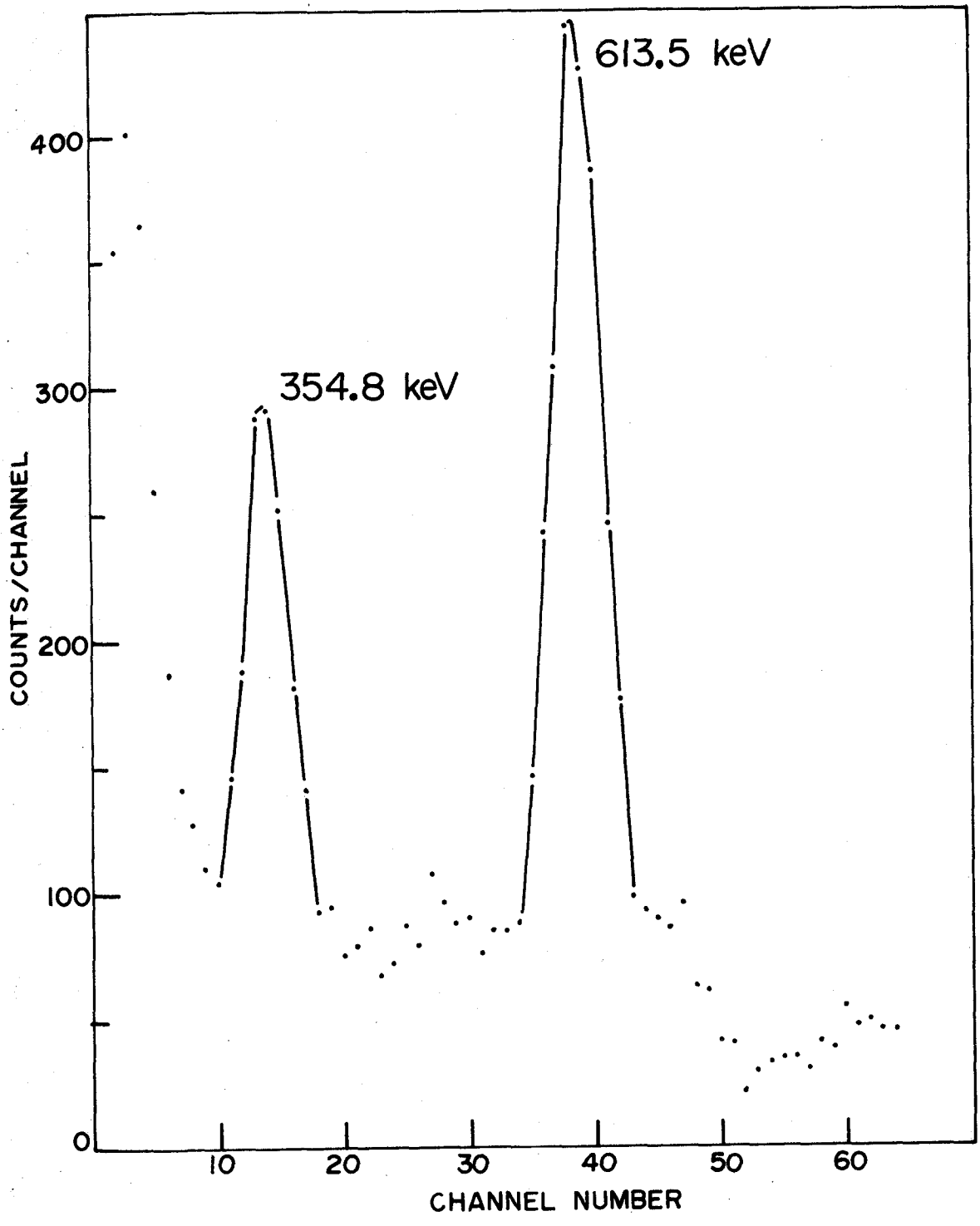

Figure 50 NaI(Tl) γ-spectrum from ^{78}As decay in coincidence with 1713.4 keV γ-ray

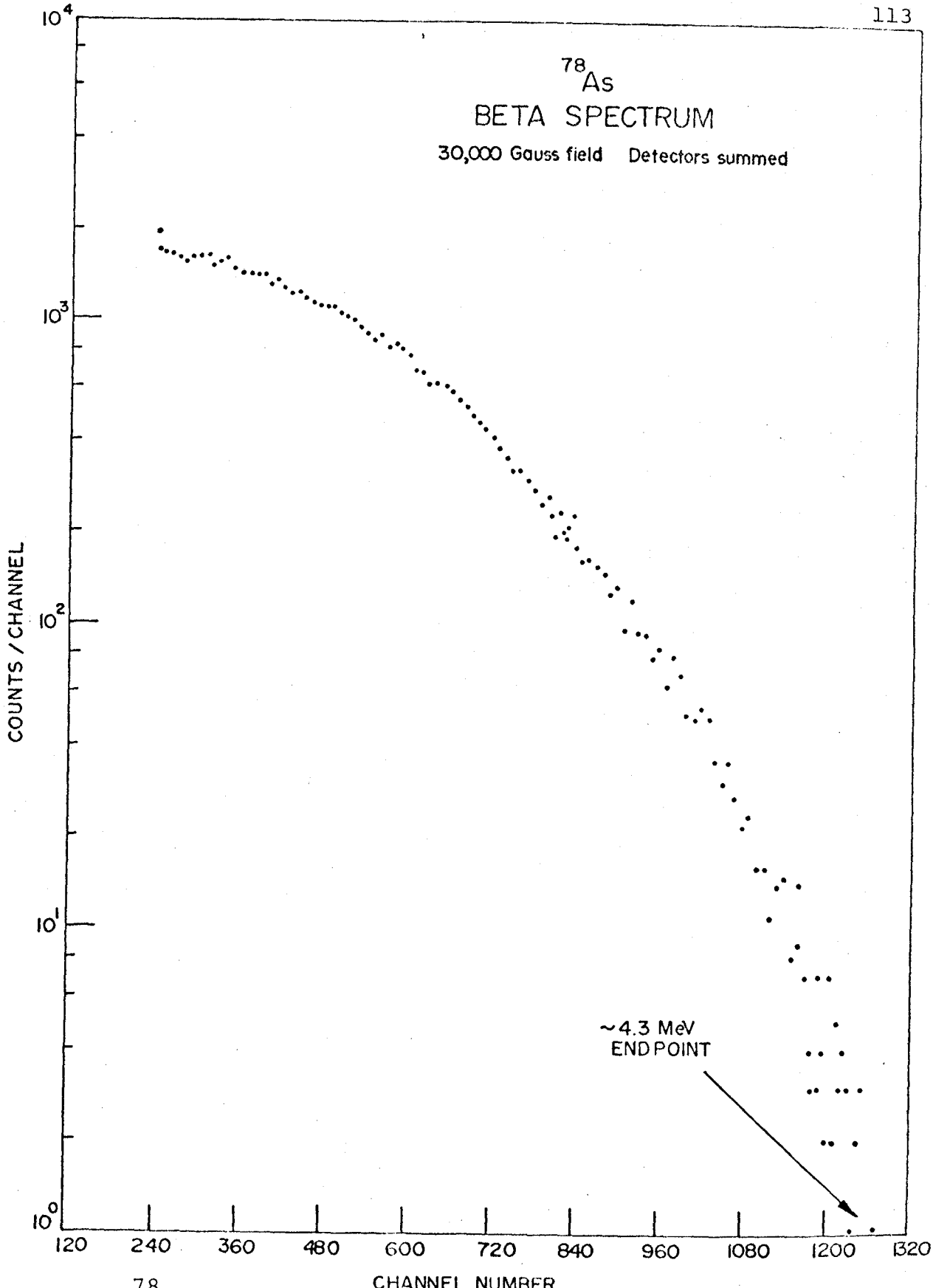

Figure 51 ^{78}As β-spectrum obtained using the superconducting magnet beta spectrometer; magnetic field--30 kilogauss; Si(Li) detector outputs summed

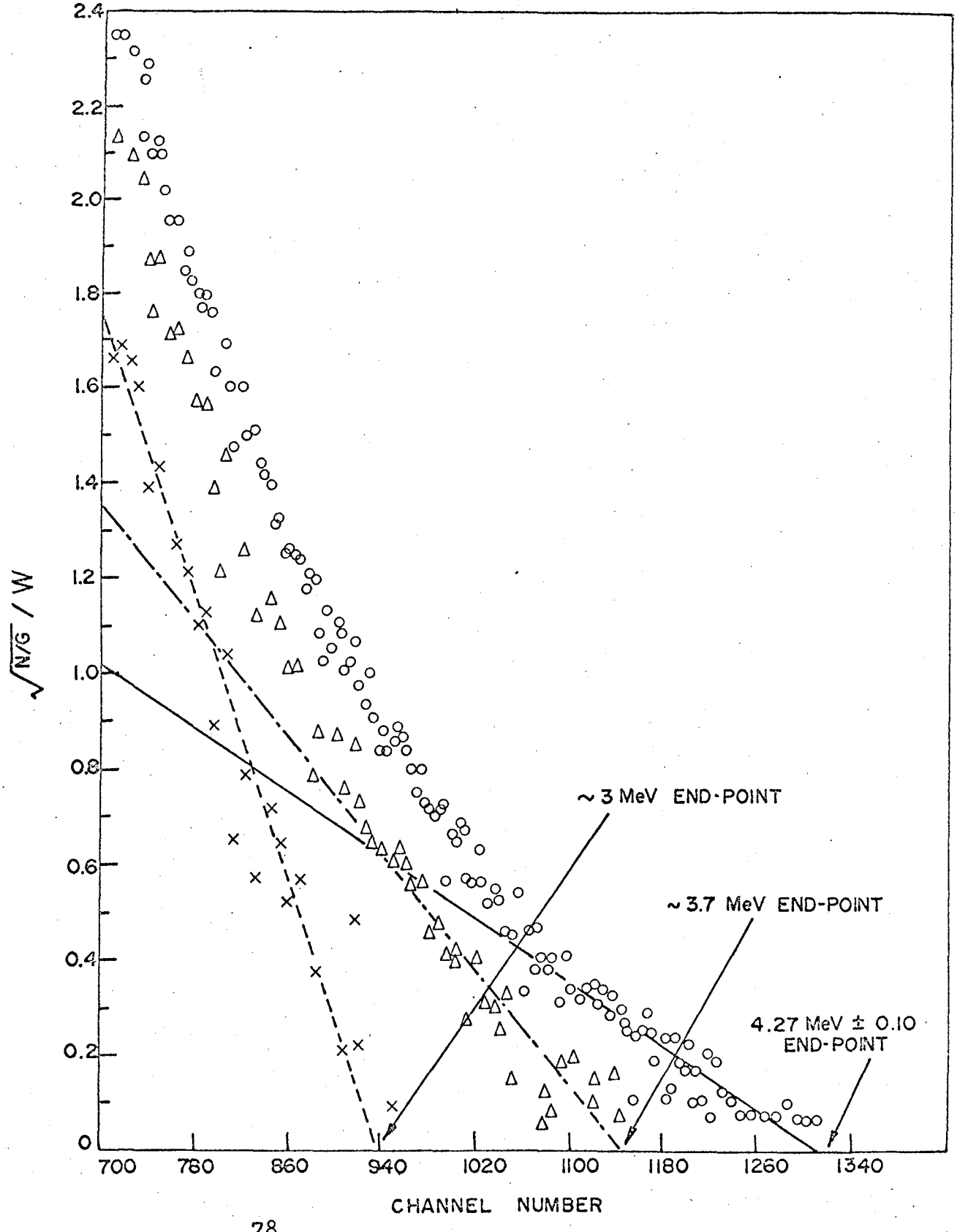

Figure 52 ^{78}As Fermi-Kurie plot of high-energy portion of β-spectrum

≃ 3 MeV. The superconducting magnet beta spectrometer used to obtain these data was operated with both Si(Li) detector outputs summed and with a magnetic field strength of 30 kG.

The Fermi-Kurie plots of the β-spectra of ^{78}As in coincidence with the 694.7, 827.8 and 1308.3 keV γ-rays are shown in Figures 53-55 respectively. Difficulty was encountered in obtaining an end-point energy for the β-spectrum in coincidence with the 613.5 keV γ-ray owing to intensity and distortion problems. The spectrum did appear however, to have a higher end-point energy than any of the β-spectra in coincidence with other γ-rays (as required by the postulated decay scheme) including the spectrum in coincidence with the 694.7 keV γ-ray.

4.2.4 Discussion of Results and Decay scheme

The proposed decay scheme for ^{78}As in Figure 56 has 18 excited levels and places all 32 γ-rays assigned to this isotope. The levels at 613.5, 1308.2, 1502.1, 1853.4, 2681.2 and 2838.0 keV are considered firmly established due to the β-γ and γ-γ coincidence studies described in this work and the results of other investigators.[23,24,32] The remaining levels were based on energy sum-rules, γ-ray relative intensity considerations and the nuclear reaction data due to Lin.[23,24]

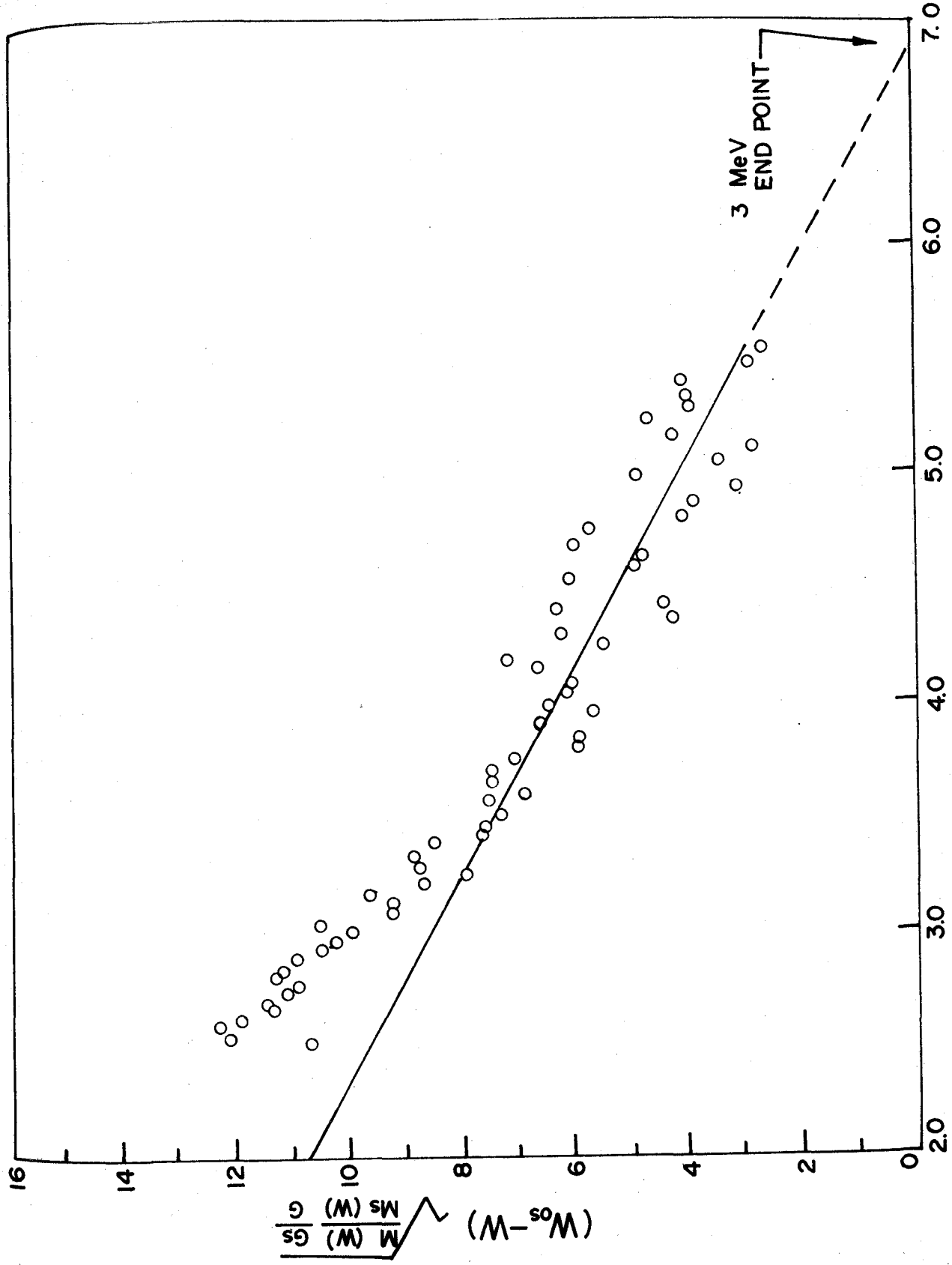

Figure 53 ^{78}As Fermi-Kurie plot for β-rays in coincidence with 694.7 keV γ-ray

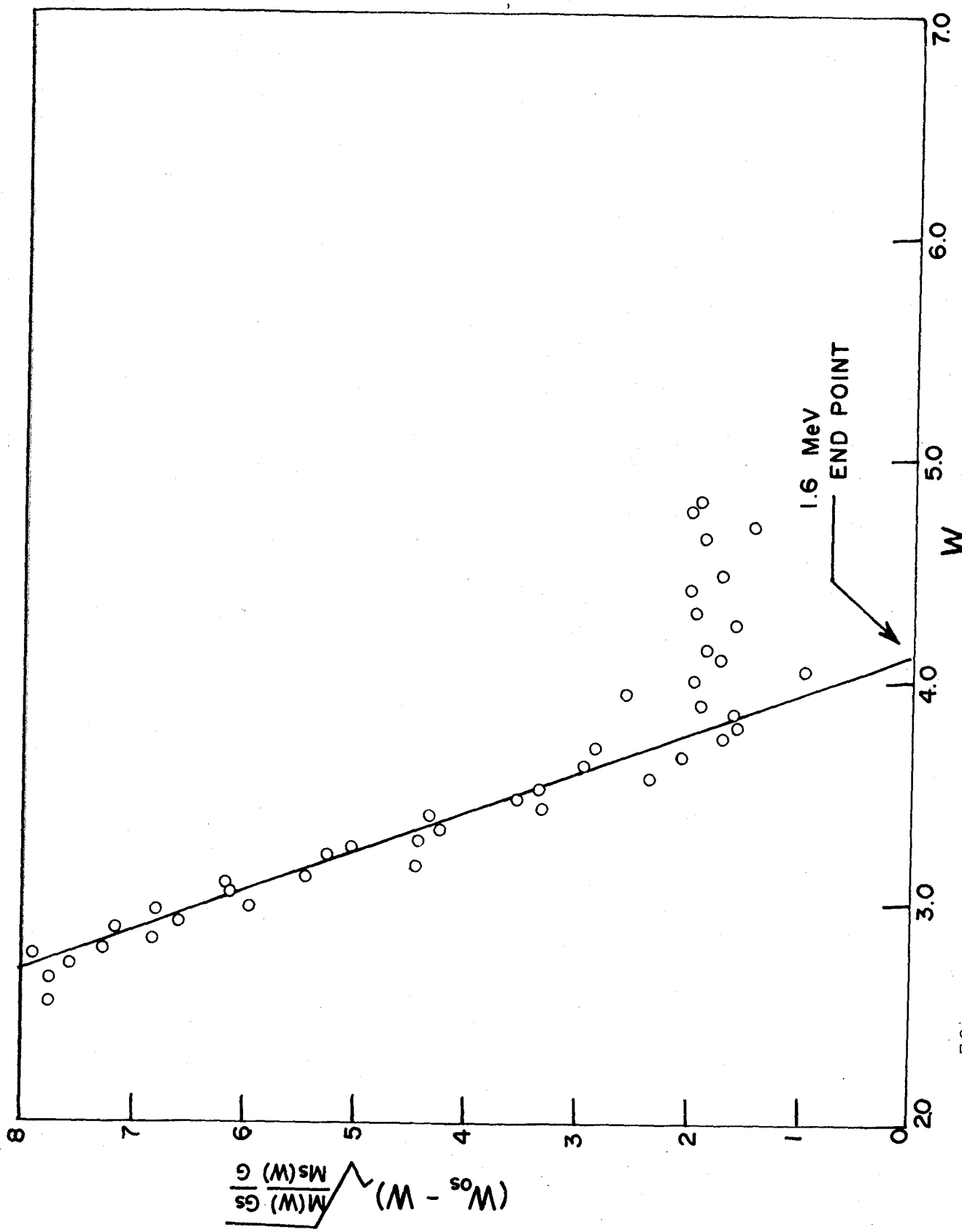

Figure 54 ^{78}As Fermi-Kurie plot for β-rays in coincidence with 827.8 keV γ-ray

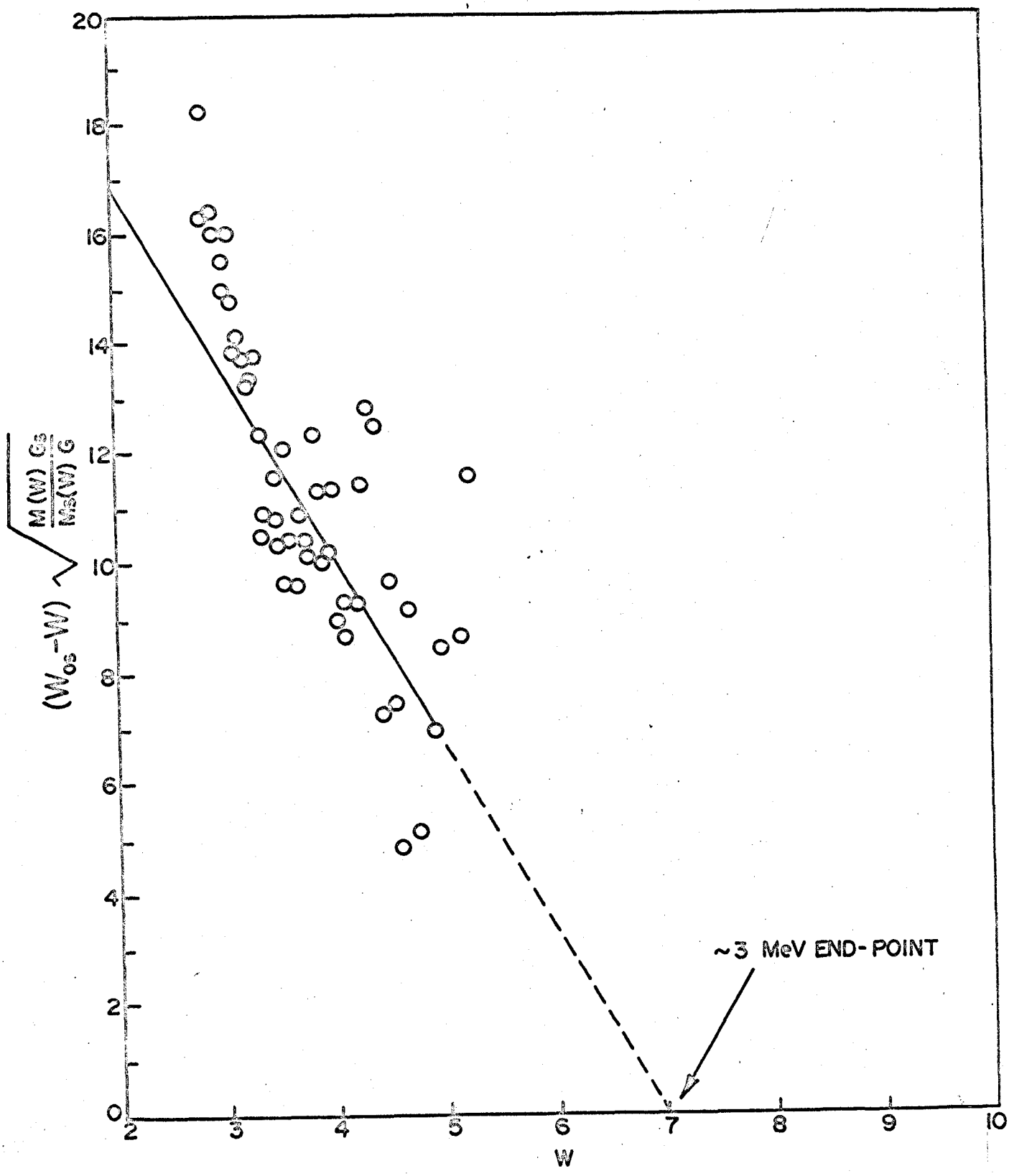

Figure 55 ^{78}As Fermi-Kurie plot for β-rays in coincidence with 1308.3 keV γ-ray

The γ-rays of energy 354.8 and 843.0 keV were found to fit (via the energy sum-rule) into the decay scheme in more than one place. Coincidence studies indicated that the 354.8 keV γ-ray was in coincidence with the 1713.4 keV and 613.5 keV γ-rays. However, since the relative intensity of the 354.8 keV γ-ray was slightly greater than that of the 1713.4 keV γ-ray (which is presumed to follow it) and since an almost exact energy difference of 354.8 keV existed between the 3.1924 and 2.8380 MeV levels, the 354.8 keV peak was assumed to be an unresolved doublet; this would allow two γ-rays of this same energy to be placed in the ^{78}As decay scheme.

There appeared, in all γ-ray single detector spectra, a peak at 842.8 keV with a FWHM consistently greater than was expected for γ-rays of this energy. (See Figure 39). This peak was graphically resolved into components at 841.5 and 843.0 keV of which the first on energy sum-rule grounds could be a γ-transition from the 3294.0 keV level to the 2452.6 keV level. Similarly, a 843.0 keV γ-transition appeared to fit almost exactly in two places in the decay scheme; the position considered less likely is shown dotted.

Coincidence experiments did not prove that the weak 2610.0 and 2797.0 keV γ-rays were in coincidence with the 613.5 keV γ-ray as required by Figure 56. However, these

γ-rays were placed in the scheme as feeding the 613.5 keV level in cascade since the levels from which they were then postulated to originate (see Table 6) were close in energy to levels found by the nuclear reaction experiments of Lin.[23,24] The uncertainty in the positions of these transitions was reflected by showing them dotted in the decay scheme.

The placing (via the γ-γ coincidence data) of the 827.8 keV γ-ray in the decay scheme was important in confirming the 4.27 MeV β-decay energy of ^{78}As determined through the data of Figures 51 and 52. In Figure 49, the peak-areas due to the 613.5 keV and 827.8 keV γ-rays coincident with the 1239.9 keV γ-ray should correspond to equal γ-ray intensities if these three transitions are correctly placed with respect to each other in the proposed decay scheme. The ratio of the intensity of the 613.5 keV peak to the intensity for the 827.8 keV peak in Figure 49 is 1:0.75 after correction for detection efficiency. This ratio is considered to be in agreement with the expected 1:1 ratio in view of the experimental difficulties in the coincidence experiments. From Figure 54, it is seen that the 827.8 keV γ-ray was in strong coincidence with a β-ray group with a maximum end-point energy of 1.6 ± 0.1 MeV. The γ-γ coincidence data place the 827.8 keV γ-ray as originating from the 2.6812 MeV level and hence a total decay energy of 4.28 ± 0.10 MeV is indicated, in good agreement with the conclusion from Figure 52 and the results of other workers.[119] This value is

further supported by the data of Figures 53 and 55 which suggests that the 1.3082 MeV level in ^{78}Se is fed by a β-group with an end-point energy of about 3 MeV. The resolution of the data in Figure 52 into Kurie plots for β-groups with end-point energies of 3.0 and 3.7 MeV is also consistent with intense population of levels in ^{78}Se at 613.5 keV and 1308.2 keV as shown in Figure 56.

The log ft values shown in Figure 56 were calculated from the relative β-ray intensities populating each excited level, (obtained in turn from the observed γ-ray intensities), and the estimate[1,119] that 70% of all ^{78}As disintegrations lead to the ground and first two excited states of ^{78}Se. This latter estimate is consistent with the present β-intensity data and with the observation of Steinberg et al.[119] that 4.1 MeV β-particles arise from 70% of all ^{78}As disintegrations.

The first two excited levels of ^{78}Se at 613.5 and 1308.2 keV are both known to have 2^+ character.[33,39] The energy levels at 1.4965 and 1.5021 MeV possibly correspond to the 0^+, 4^+ unresolved doublet at ≈ 1.51 MeV mentioned by Lin.[23,24] Along with the 2^+ level at 1308.2 keV, these three levels may constitute the triplet two-phonon group predicted by the collective model of Scharff-Goldhaber and Weneser.[55] A level with 3^- octupole vibrational character at 2.55 MeV was proposed by Lin.[23,24] In this work, the spin and parity of the 2.536 MeV level is consistent with a 3^- assignment. This level is now postulated to be fed

by a γ-ray transition of 0.959 MeV from the 3.495 MeV level; the latter could correspond to the 3.50 MeV level with 4^-, 5^- character assigned by Lin.[23,24]

The proposed decay scheme of ^{78}As in Figure 56 indicates a strong preference for most γ-ray transitions to feed the first and second excited levels rather than the ground state. Of the 20 transitions shown feeding these two levels, only the 2.1863, 2.6805, 2.610 and 2.797 MeV γ-rays could be direct γ-transitions to the ground state. The 2.1863 MeV transition could result from a level of the same energy and may correspond to the 2.22 MeV level mentioned by Lin[23,24] and shown in Table 6. This transition was placed in the position shown however, because of energy sum-rule considerations and weak γ-γ coincidence data. (See Table 5). The 2.6805 MeV transition could conceivably originate from decay of the 2.6812 MeV level. It was shown however, as originating from the 3.2940 MeV level because of evidence that it and its double escape peak at 1.6585 MeV are in coincidence with the 613.5 keV transition and because of energy sum-rule considerations.

The ^{78}Se level scheme in Figure 56 is similar in some aspects to the scheme proposed by Maddison[30] who used weak sources, NaI(Tl) detectors and a small Ge(Li) detector but is in very close agreement with the scheme proposed recently by Paradellis and Hontzeas[29] who used strong sources and a large Ge(Li) detector.

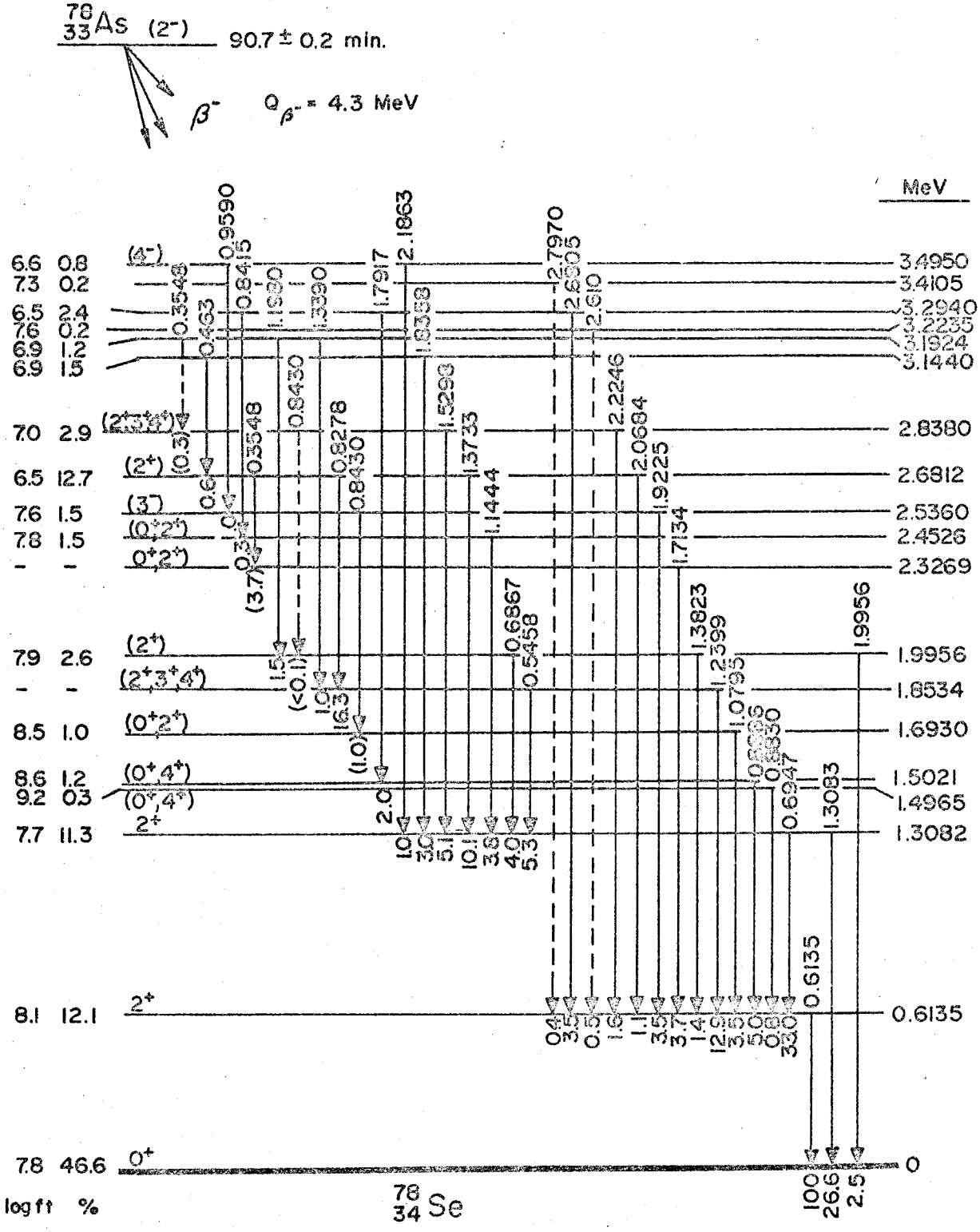

Figure 56 Proposed decay scheme of ^{78}As. All energies in MeV; numbers at arrow heads are intensities relative to the 613.5 keV transition = 100

TABLE 6

LEVEL ENERGIES AND SPIN ASSIGNMENTS OF ^{78}Se

E (MeV)			I^{π}		
Ref. 23 [a]	Ref. 24 [b]	This Work	Ref. 23	Ref. 24 [d]	This Work
0.62	0.62	0.6135	2^+	+	2^+
1.32	1.32	1.3082	2^+	+	2^+
1.51	1.51	1.4965 1.5021	$0^+,4^+$	+	$(0^+,4^+)$ [e]
-	1.76	1.6930	NA [c]	NA	$(0^+,2^+)$
1.88	-	1.8534	$2^+,3^+$	NA	$(2^+,3^+,4^+)$
-	2.03	1.9956	NA	+	(2^+)
-	2.22	-	NA	-	NA
2.36	2.36	2.3269 2.4526	0^+-2^+	NA	$(0^+,2^+)$ [e]
2.56	2.55	2.5360	3^-	-	(3^-)
-	2.73	2.6812	NA	+	(2^+)
-	2.83	2.8380	NA	-	$(2^+,3^+,4^+)$
2.94	2.99	-	$4^-,5^-$	+	NA
3.13	3.17	3.1440 3.1924	0^+-2^+	-	
-	3.27	3.2235 3.2940	NA	NA	
3.33	3.37	3.4105	$0^+-2^+,4^-,5^-$	-	
3.46	3.50	3.4950	$4^-,5^-$	NA	(4^-)
3.55	3.56	-	3^+	-	

Notes

(a) $^{77}Se(d,p)$ reactions.

(b) $^{78}Se(d,d')$ reactions.

(c) NA = not applicable or not available.

(d) Parities only

(e) Applies to both levels

4.3 Decay of ^{80}As

4.3.1 Half Life Measurements

A half life of 16.5 ± 0.3 sec for ^{80}As was determined from an analysis of the decay of 665.8 keV γ-ray events* using the CLSQ computer program.[38] This value is somewhat higher than the previously reported half life of 15.3 ± 0.2 sec for this isotope by Meads et al.[42] due possible in part to the fact the latter authors used a NaI(Tl) detector to select γ-ray events of 665.8 keV energy while this study involved a large volume (23.8 cm^3) Ge(Li) detector. The NaI(Tl) detector would have been incapable of resolving the near-by 654.7 keV γ-ray** of ^{82}As which was determined (via decay of the 654.7 keV γ-ray) in this study to have a half life of 14 ± 2 sec in reasonable agreement with the 15 ± 2 sec assignment due to Mathew et al.[91] and the more recent 13.7 ± 0.8 sec assignment due to Karras et al.[92]

4.3.2 Gamma-Ray Spectra

Selected parts of the spectrum of γ-radiations resulting from the 14-MeV neutron bombardment of natural selenium metal (taken 3 seconds after the end of bombardment with a 23.8 cm^3 Ge(Li) detector), are shown in the upper

---

*Assigned to ^{80}As decay, see Table 7.

**Assigned to ^{82}As decay, see Table 7.

parts of Figures 57-62. Short-lived γ-radiations due to ^{80}As and ^{82}As decay were identified by comparing this spectrum with a corresponding Ge(Li) spectrum taken following a 100 sec delay after the end of each irradiation period and also with a Ge(Li) γ-spectrum (parts of which are shown on the bottom parts of Figures 57-62), beginning 3 minutes after the end of the last bombardment and ending about 2 hours later. Long-lived γ-lines appearing in these latter two spectra were identified as resulting primarily from the decay of 91-min ^{78}As produced in the ^{78}Se(n,p) reaction. A Ge(Li) γ-spectrum of the empty polyethylene capsules (used in the selenium metal irradiations) revealed a prominent γ-line of 1779 keV energy assigned to the ^{28}Si(n,p) ^{28}Al reaction due to traces of silicon impurity in the polyethylene.

Table 7 lists the energies and relative intensities of 23 γ-rays assigned in this study to ^{80}As decay and compares these with the corresponding energies and relative intensities of ^{80}As γ-rays determined by Meads et al.[42] from NaI(Tl) detector measurements. A number of short-lived γ-lines, all with low energies (< 200 keV) from known activities[3] of 17.5-sec ^{77m}Se, 3.9-min ^{79m}Se, 48-sec ^{75m}Ge and 54-sec ^{77m}Ge, were not listed in this table. Three γ-rays of 342.6, 654.7 and 818.1 keV energy listed in Table 7 were assigned to ^{82}As decay based on the work of Karras et al.[92] and Mathew et al.[91] who bombarded selenium samples enriched

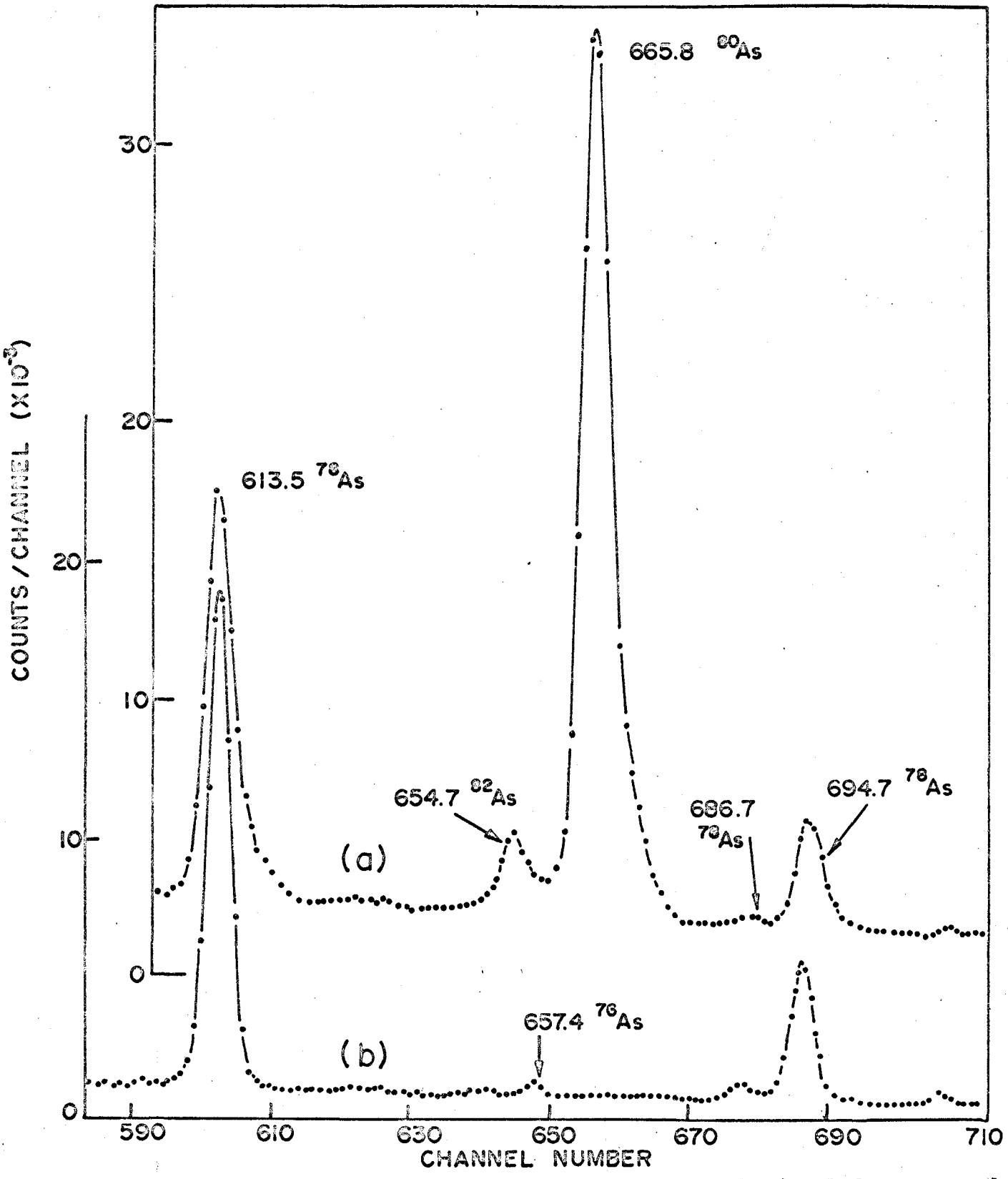

Figure 57 Ge(Li) γ-ray spectra of 14-MeV neutron bombarded natural selenium beginning (a) 3 seconds and (b) 3 minutes after the end of bombardment; 610-700 keV energy region

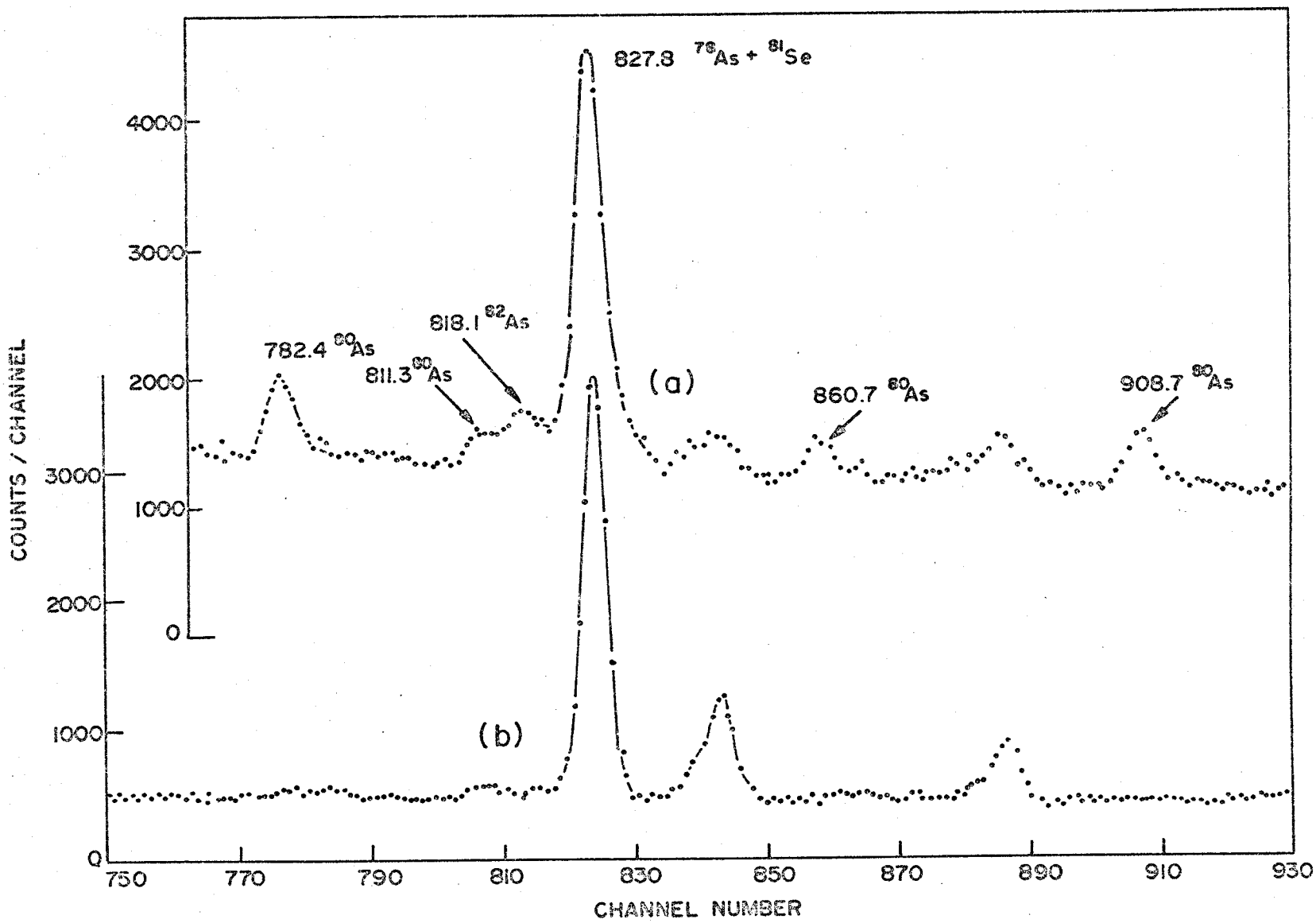

Figure 58 Ge(Li) γ-ray spectra of 14-MeV neutron bombarded natural selenium beginning (a) 3 seconds and (b) 3 minutes after the end of bombardment; 760-950 keV region

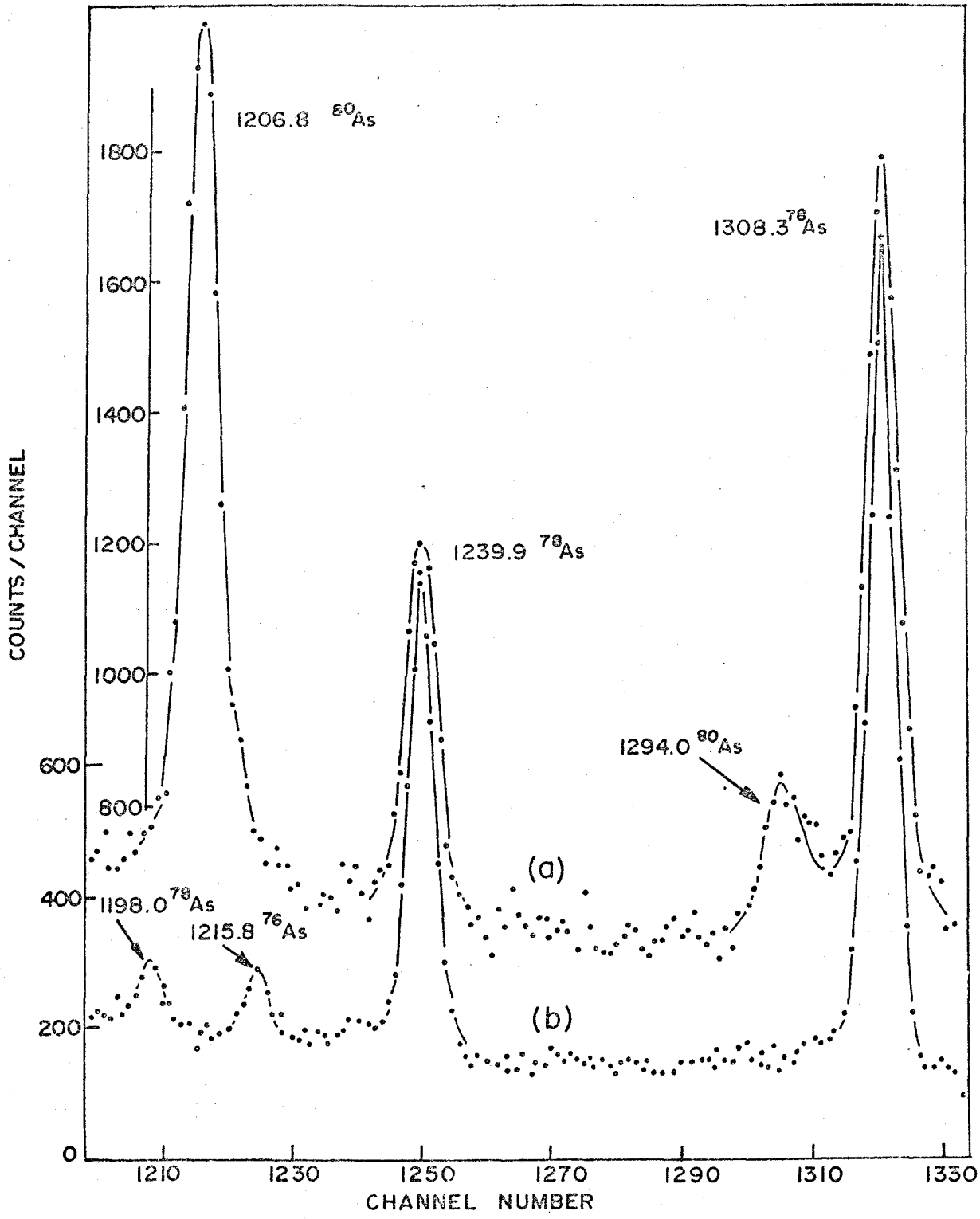

Figure 59 Ge(Li) γ-ray spectra of 14-MeV neutron bombarded natural selenium beginning (a) 3 seconds and (b) 3 minutes after the end of bombardment; 1200-1350 keV energy region

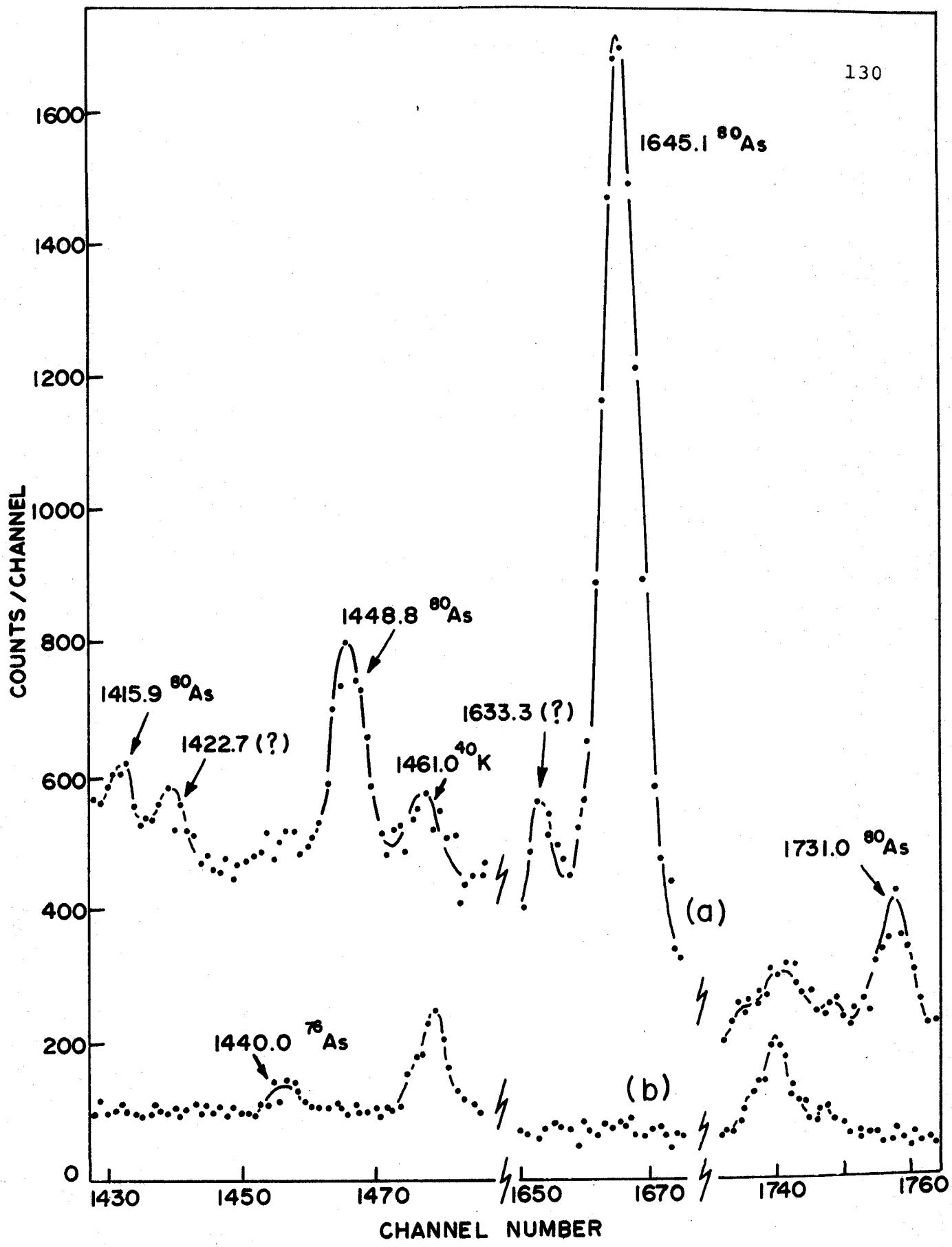

Figure 60 Ge(Li) γ-ray spectra of 14-MeV neutron bombarded natural selenium beginning (a) 3 seconds and (b) 3 minutes after the end of bombardment; 1400-1740 keV energy region

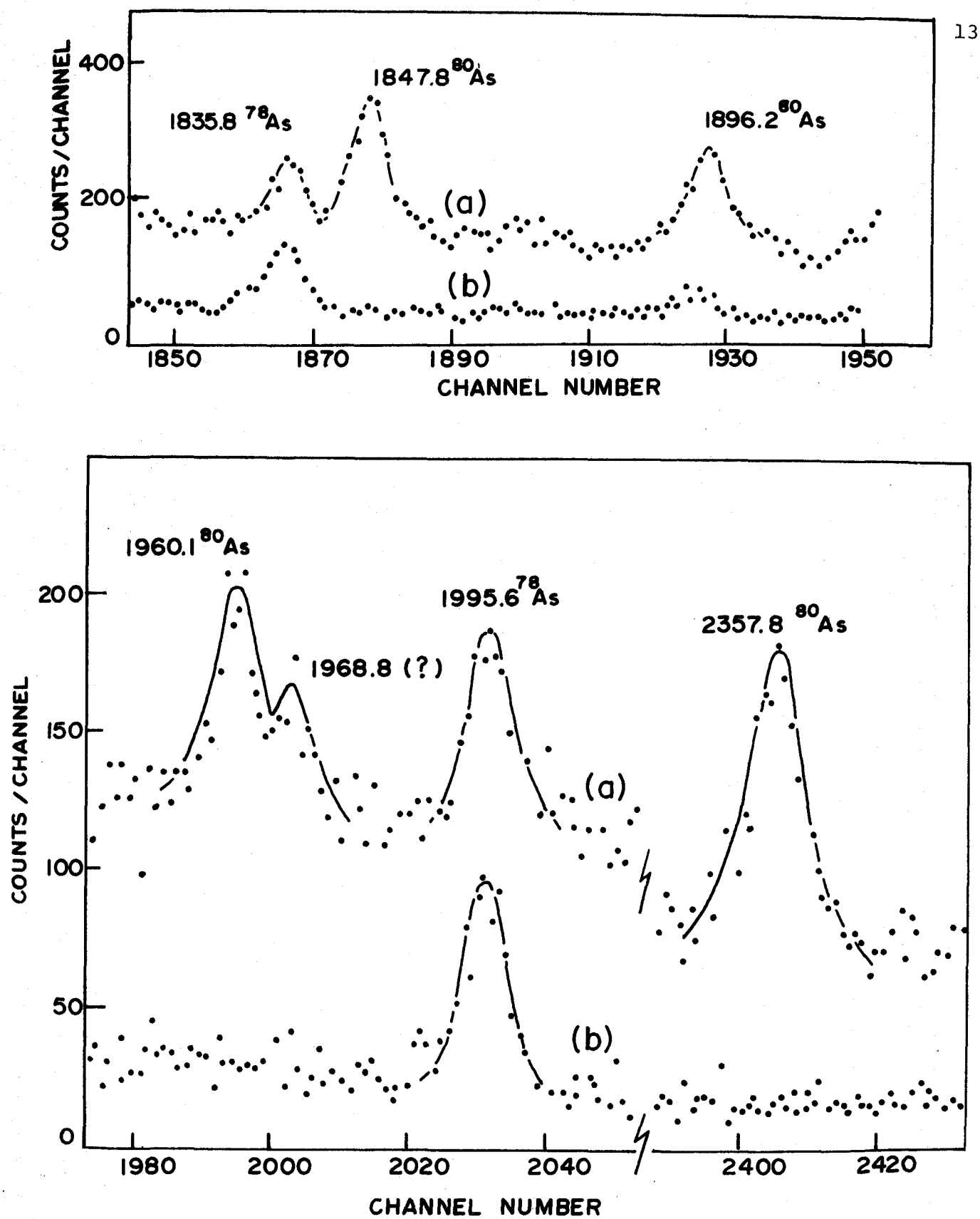

Figure 61 Ge(Li) γ-ray spectra of 14-MeV neutron bombarded natural selenium beginning (a) 3 seconds and (b) 3 minutes after the end of bombardment; top and bottom parts show 1820-1900 keV and 1940-2370 keV regions respectively

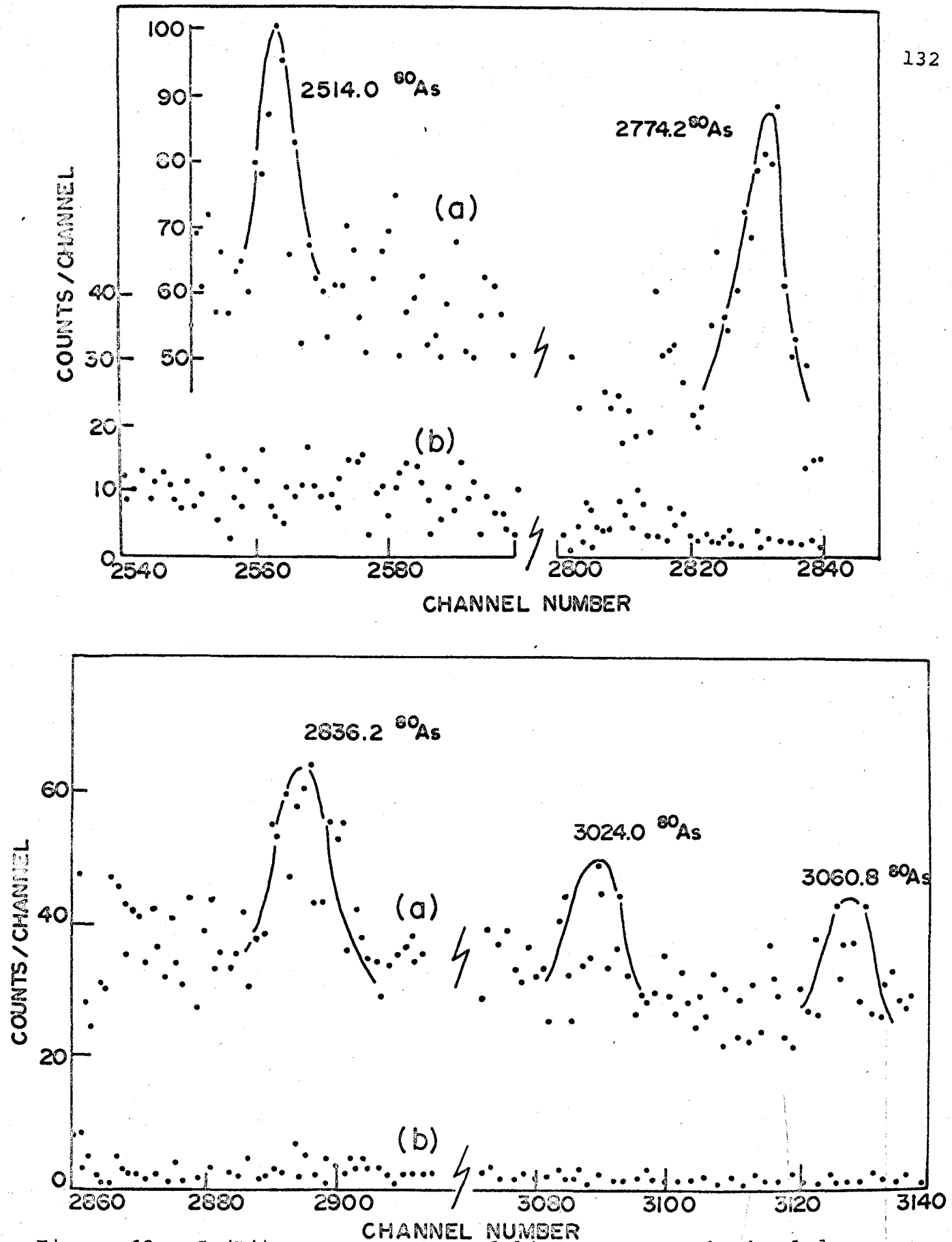

Figure 62 Ge(Li) γ-ray spectra of 14-MeV neutron bombarded natural selenium beginning (a) 3 seconds and (b) 3 minutes after the end of bombardment; top and bottom parts show 2500-2780 keV and 2800-3070 keV energy regions respectively

TABLE 7

SHORT-LIVED γ-RADIATIONS RESULTING FROM THE 14-MeV NEUTRON BOMBARDMENT OF NATURAL SELENIUM METAL [a]

Meads et al.,[42] 1959 [b]		PRESENT WORK		
4"x4" NaI(Tl) Detector		23.8 cm^3 Ge(Li) Detector		
Energy (keV)	Intensity	Energy (keV) [c]	Intensity	Assignment
		229.5	-	^{79}Ge [d]
		321.2	13.0 ± 3	Unknown [h]
		342.6	(19.2 ± 5) [e]	^{82}As [f]
		654.7	(100) [e]	^{82}As [f]
660 ± 10	100	665.8	100	^{80}As
780 ± 10	3	782.4	1.9 ± 0.4	^{80}As
		811.3	1.1 ± 0.4	^{80}As
840 ± 10		818.1	(23.9 ± 6) [e]	^{82}As
		860.7	1.7 ± 0.3	^{80}As
		908.7	1.7 ± 0.3	^{80}As
		1064.7	0.3 ± 0.1	^{80}As
1220 ± 10	9	1206.8	10.0 ± 1.5	^{80}As
		1294.0	2.3 ± 0.5	^{80}As
		1415.9	0.2 ± 0.1	^{80}As
		1422.7	0.1 ± 0.1	Unknown [h]
		1448.8	2.4 ± 0.3	^{80}As
		1633.3	2.8 ± 0.5	Unknown [h]
1640 ± 10	10	1645.1	15.6 ± 1.5	^{80}As
1770 ± 30	4	1731.0	2.2 ± 0.4	^{80}As
		1779.0	-	^{28}Al [g]

R.E. Meads et al.,[42] 1959[(b)]		PRESENT WORK		
Energy (keV)	Intensity	Energy (keV)	Intensity	Assignment
1840 ± 30	1.3	1847.8	2.2 ± 0.4	^{80}As
		1896.2	2.5 ± 0.3	^{80}As
		1960.1	0.9 ± 0.2	^{80}As
		1968.8	0.3 ± 0.2	Unknown[(h)]
		2156.9	0.2 ± 0.1	^{80}As
2350 ± 30	0.9	2357.8	2.1 ± 0.4	^{80}As
		2461.3	0.5 ± 0.3	Unknown[(h)]
		2514.0	0.4 ± 0.2	^{80}As
		2598.1	0.3 ± 0.2	Unknown[(h)]
		2774.2	0.7 ± 0.3	^{80}As
		2836.2	0.6 ± 0.2	^{80}As
		2940.3	0.2 ± 0.1	^{80}As
		3024.0	0.2 ± 0.1	^{80}As
		3060.8	0.1 ± 0.1	^{80}As

Notes

(a) γ-radiations from known short-lived activities of ^{77m}Se, ^{79m}Se, ^{75m}Ge, and ^{77m}Ge etc., with energies less than 229.5 keV are not listed.

(b) γ-rays from 14-MeV neutron bombardment of natural Se and enriched ^{80}Se assigned to ^{80}As decay by Meads et al.[42]

(c) Energy uncertainties ± 0.5 keV unless otherwise specified.

(d) γ-ray of 230 ± 1 keV assigned to decay of 42 ± 2-sec ^{79}Ge by Karras et al.[92]

(e) Relative intensities of these γ-lines are with respect to 654.7 keV ^{82}As γ-ray=100.

(f) Assigned to ^{82}As decay by Karras et al.[92] and by Mathew et al.[91]

(g) Due to silicon impurity in polyethylene capsules used in selenium irradiations.

(h) γ-radiations of unknown origin not assigned to ^{80}As or ^{82}As decay due to insufficient data.

in ^{82}Se with 14-MeV neutrons. Karras et al.[92] also assigned three other γ-rays with energies of 467 ± 2 keV, 1081 ± 3 keV and 1770 ± 3 keV to ^{82}As decay. Short-lived γ-lines with energies around 467 keV and 1770 keV were not seen in the present selenium metal irradiations while a γ-line with an energy of about 1080 keV was observed but appeared to decay with a much longer half life than that of 14-sec ^{82}As. None of the other higher-energy γ-rays listed in Table 7 were assigned to ^{82}As decay due to insufficient data.

4.3.3 Gamma-Gamma Coincidence Spectra

A 23.8 cm^3 Ge(Li) detector was used to obtain a γ-spectrum of ^{80}As decay radiations in coincidence with 665.8 keV γ-ray events selected by a 7.6 cm x 7.6 cm NaI(Tl) detector. As listed in Table 8, γ-ray peaks with energies of 782.4, 1064.7, 1206.8, 1645.1, 1847.8 and 1892.2 keV were found to be coincident with the 665.8 keV γ-ray although the small number of counts in these last two peaks resulted in their being classified as doubtful. A few γ-ray peaks at 613.5, 694.7, 827, 1240 and 1529 keV also appeared in this γ-spectrum but were known[28] to result from the decay of ^{78}As impurity in the ^{80}As samples. The γ-γ coincidence results of Meads et al.,[42] who used two NaI(Tl) detectors, are included in Table 8 for comparison purposes.

4.3.4 Discussion of Results and Decay Scheme

The ^{80}As decay scheme in Figure 63 was assembled using the results of the Ge(Li) single detector and γ-γ coincidence experiments of this study, with the aid of results from the ^{80}Se (d,d') and ^{80}Se (p,p') nuclear reaction experiments of Lin[23,24] and Darcey et al.[93] respectively.

The log ft values shown in Figure 63 for the β-transitions to the various excited states of ^{80}Se were calculated from the relative β-ray intensities populating each excited level (obtained in turn from the observed γ-ray intensities), and the estimate by Meads et al.[42] that 56% of all ^{80}As disintegrations result in 6.0 MeV β-particles feeding the ground state of ^{80}Se. The 1^+ ground state spin-parity assignment of ^{80}As, predicted first by Meads et al.,[42] is based on the measured log ft values of 5.9 and 6.0 corresponding to allowed β-transitions to the ground and first 2^+ excited states of ^{80}Se.

The first 2^+ excited state of ^{80}Se was determined in 1956 by Temmer et al.[111] at 0.65 MeV energy and in 1962 by McGowan et al.[33] at 0.665 ± .007 MeV energy by means of Coulomb excitation experiments using ≃ 6-MeV α-particles. The intense 665.8 keV γ-ray found in this study is therefore considered from energy and relative intensity data to result from γ-decay of the first excited state of ^{80}Se, in good agreement with the above data, the ^{80}Br E.C.-decay

TABLE 8

GAMMA-RAYS APPEARING IN γ-γ SPECTRA IN COINCIDENCE WITH THE 665.8 keV ^{80}As γ-RAY

Meads et al.,[42] (1959) [a]	Present Work [b]
Energy (keV)	Energy (keV) [c]
780	782.4
840	1064.7
1220	1206.8
1640	1645.1
1840	(1847.8) [d]
2350	(1896.2) [d]

Notes

(a) γ-γ coincidence measurements made using two 4 in x 4 in NaI(Tl) detectors.

(b) γ-γ coincidence measurements made using a 23.8 cm^3 Ge(Li) detector and a 3 in x 3 in NaI(Tl) detector.

(c) γ-rays with energies of 613.5, 694.7, 827, 1240, and 1529 keV appearing in this coincidence γ-spectrum were assumed to result from decay of ^{78}As impurity in the ^{80}As samples.

(d) The parentheses reflect the poor statistics associated with these peaks.

data of Katoh et al.[88] and Trehan et al.[90] and the (d,d') nuclear reaction experiments of Lin.[24]

Energy systematics of even-even selenium nuclides (See Figure 1) would predict a triplet of 2-phonon excited levels with I^{π} of 0^+, 2^+ and 4^+ at energies about 2.0 - 2.2 times the first excited state. In the present measurements, the 1448.8 keV γ-ray listed in Table 7 could correspond to decay of the 2^+ member of this 2-phonon triplet with the 782.4 keV γ-ray cascading from this level to the 665.8 keV level. These postulates are in reasonable agreement with the recent E.C.-decay studies of ^{80}Br by Katoh et al.[88] who show a ^{80}Se level with 2^+ character at about 1457 keV decaying by weak γ-transitions of 788 ± 3 keV and 1457 keV. A ^{80}Se level at 1448.8 keV is further supported by the Coulomb excitation data of McGowan et al.,[33] who found a second 2^+ level at about 1455 ± 12 keV, and by the (p,p') and (d,d') nuclear reaction experiments of Darcey et al.[93] and Lin[24] respectively, who found an excited ^{80}Se level at 1.44 MeV.

The 1477.1 keV ^{80}Se level in Figure 63, shown feeding the 665.8 keV level by a 811.3 keV γ-ray transition, does not appear to decay to the 0^+ ground state of ^{80}Se (due to the lack of evidence for a γ-ray of this energy) and could correspond to the 0^+ or 4^+ member of the 2-phonon triplet. A 0^+ assignment for this level would be in agreement with the ^{80}Br E.C.-decay studies of Ramayya et al.[89]

and Katoh et al.[88] who found a 0^+, ^{80}Se level at about 1478 keV. The latter authors also showed the 1478 keV level decaying to the 666 keV level by a 812.7 ± 2.2 keV γ-transition. Beta-decay selection rules,[115] aided by the 1^+ predicted ground state assignment[42] for ^{80}As and the calculated log ft value for the β-transition to the 1477.1 keV level of 7.5, also support the 0^+ rather than the 4^+ assignment for this level. Further support for a ^{80}Se level at 1477.1 keV comes from the (p,p') and (d,d') nuclear reaction experiments of Darcey et al.[93] and Lin[24] respectively who found a 0^+ level at about 1470 keV energy.

A ^{80}Se level of 1731.0 keV energy is proposed from the γ-γ coincidence data of Table 8 which indicates the 665.8 keV level is fed by a 1064.7 keV γ-transition, and the energy-sum of the 1064.7 keV and 665.8 keV γ-rays which is close in energy to that of the 1731.0 keV γ-ray. The 1.69 MeV level found by (p,p')[93] and (d,d')[24] experiments may correspond to the 1731.0 keV level postulated in this study. However, the 4^+ character assigned to the 1.69 MeV level by Darcey et al.[93] and the calculated log ft of 7.0 for the 1.731 MeV level from the present measurements suggests the 1.731 MeV level was not in fact the 1.69 MeV level seen in the nuclear reaction experiments.

A ^{80}Se level of 1872.6 keV is proposed from the γ-γ coincidence results of this work which indicate the 1206.8 keV γ-ray is coincident with the 665.8 keV γ-ray.

This proposal is supported by the γ-γ coincidence results of Meads et al.[42] who found a γ-peak coincident with the 660 keV γ-ray at about 1.22 MeV using NaI(Tl) detectors.

The 1960.1 level shown in Figure 63 which is in line with the (d,d') nuclear reaction data of Lin[24] (who found a level at 1.96 MeV), was proposed from the fact that the energy-sum of the 1294.0 keV and 665.8 keV γ-rays was close in energy to the 1960.1 keV γ-ray.

The remaining levels of ^{80}Se were proposed with the aid of the γ-γ coincidence results in Table 8, energy sum-rule considerations and the (p,p'), (d,d') nuclear reaction data of Darcey et al.[93] and Lin.[24] Table 9 summarizes the level energies and spin assignments of ^{80}Se found in this work and by other investigators.

TABLE 9

LEVEL ENERGIES AND SPIN ASSIGNMENTS OF ^{80}Se

E(MeV)				I^{π}		
Ref. 24(a)	Ref. 93(b)	Ref. 42(c)	This Work	Ref. 24(d)	Ref. 93	This Work
0.66	0.66	0.66	0.6658	+	2^+	2^+
1.44	1.44	1.44	1.4488	-	2^+	2^+
1.48	1.47	1.52	1.4771	+	(0^+)	0^+
1.69	1.69	1.77	1.7310	+	(4^+)	
1.86	1.86	1.88	1.8726	?		
1.96	1.95	-	1.9601	-		
2.15	2.10	-	-	?		
2.32	2.31	2.30	2.3109	+		$(0^+,2^+)$
2.50	2.49	2.50	2.5140	-		
-	-	-	2.5620	NA(e)		$(0^+,2^+)$
2.72	2.71		2.7742	-	3^-	
2.82	2.82	-	2.8362	+		
3.03		3.01	3.0240	?		(2^+)
3.30			-	+		
3.37			3.4227	-		$(0^+,2^+)$
-			3.6061	NA		
3.78			3.7266	-		
4.18				-		

Notes

(a) $^{80}Se(d,d')$ reactions.

(b) $^{80}Se(p,p')$ reactions.

(c) NaI(Tl) detector measurements.

(d) Parities only.

(e) NA = not applicable.

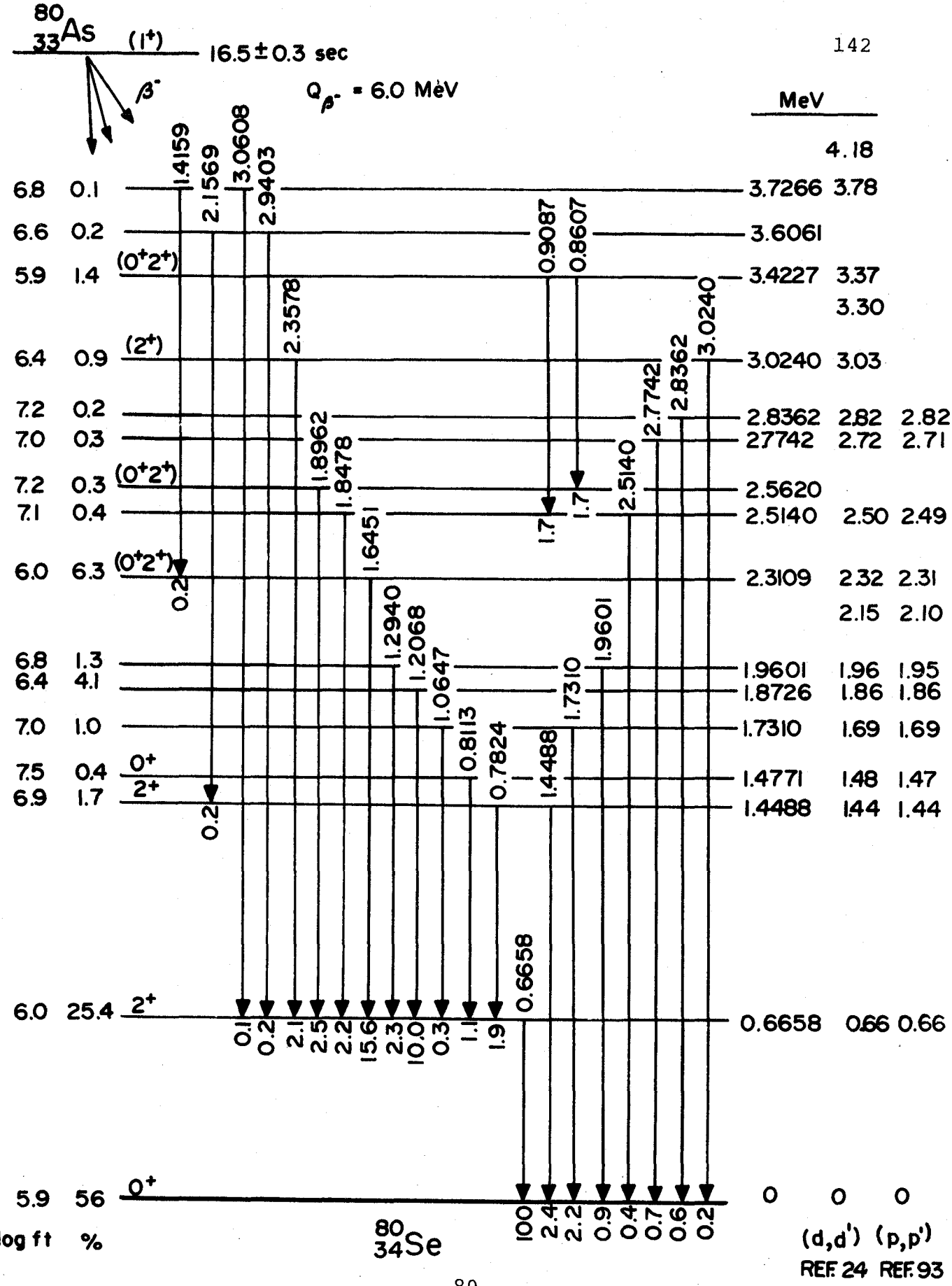

Figure 63 Proposed decay scheme of ^{80}As. All energies in MeV; numbers at arrow heads are intensities relative to the 665.8 keV transition = 100

CHAPTER 5

SUMMARY AND CONCLUSIONS

5.1 Comparison of Results With Other Even-Even Nuclei and Theory

The level schemes of the even-even selenium isotopes with mass numbers 72 through to 82 are shown in Figure 64. The data contained in this figure support the "2^+ rule" pointed out first by Goldhaber[109] which predicts the first excited states of even-even nuclei have predominately spin $I = 2$ and even parity. The distribution of spins and parities for the second excited state also indicates that spin 0, 2 or 4 and even parity is preferred. The fact that most of these nuclei show systematically a triplet of excited states with I^π of 0^+, 2^+ and 4^+ at energies about twice the energy of the first excited 2^+ state suggests these low-lying states may be interpreted in terms of one- and two-phonon quadrupole vibrations about a spherical equilibrium state.[49] Similarly, levels in these nuclei assigned a 3^- character could be classified in terms of one-phonon octupole vibrations.[121] The energies of the first and second excited 2^+ levels shown in Figure 64 vary in a fairly regular manner with neutron number, initially decreasing and then increasing as the shell model $2p_{1/2}$ and $1g_{9/2}$ levels are filled.

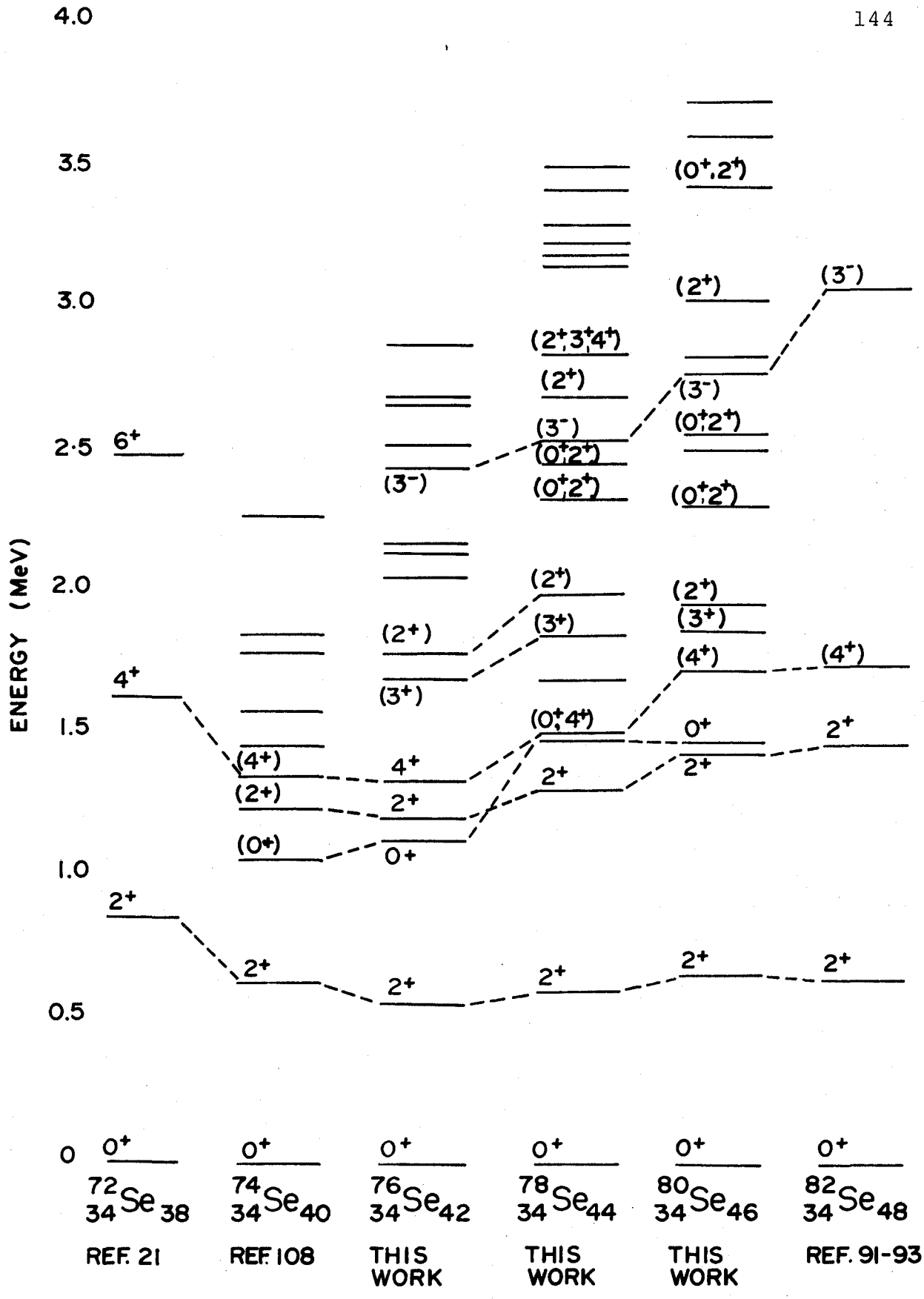

Figure 64 Level schemes of even-even selenium isotopes with mass numbers 72 to 82

Higher than average energies for the first 2^+ and 4^+ levels of ^{72}Se and ^{82}Se along with similar data for other nuclei contained in Figures 65-67 appear to reflect possible sub-shell or closed-shell configurations consisting of 38 and 50 neutrons in agreement with shell model predictions.[50]

The level schemes of ^{76}Se, ^{78}Se, and ^{80}Se determined in this work are compared with those of neighbouring even-even nuclei in Figures 65-67. Inspection of these latter figures plus Figure 64 allow systematic comparisons of the effects of proton and neutron number changes on the level structures of these nuclei. In most cases (as can be seen for example, in the cases of ^{78}Se and ^{80}Kr in Figures 65 and 66), addition of two protons to a nucleus has only a small effect on the energy of the first excited state whereas addition of two neutrons is more pronounced especially in the regions close to the neutron numbers 38 and 50. A theoretical explanation for the observation that the addition of two particles (or holes) to the closed shell of a magic nucleus lowers the first 2^+ level by about one-half has been provided by Malov et al.[110] These authors suggest that this effect may be due to enhanced interactions which favour a transition of one pair of particles to quasiparticle states that react strongly with collective excitations.

The level schemes of ^{76}Se, ^{78}Se and ^{80}Se determined in this study and by other investigators[21,24,93] using

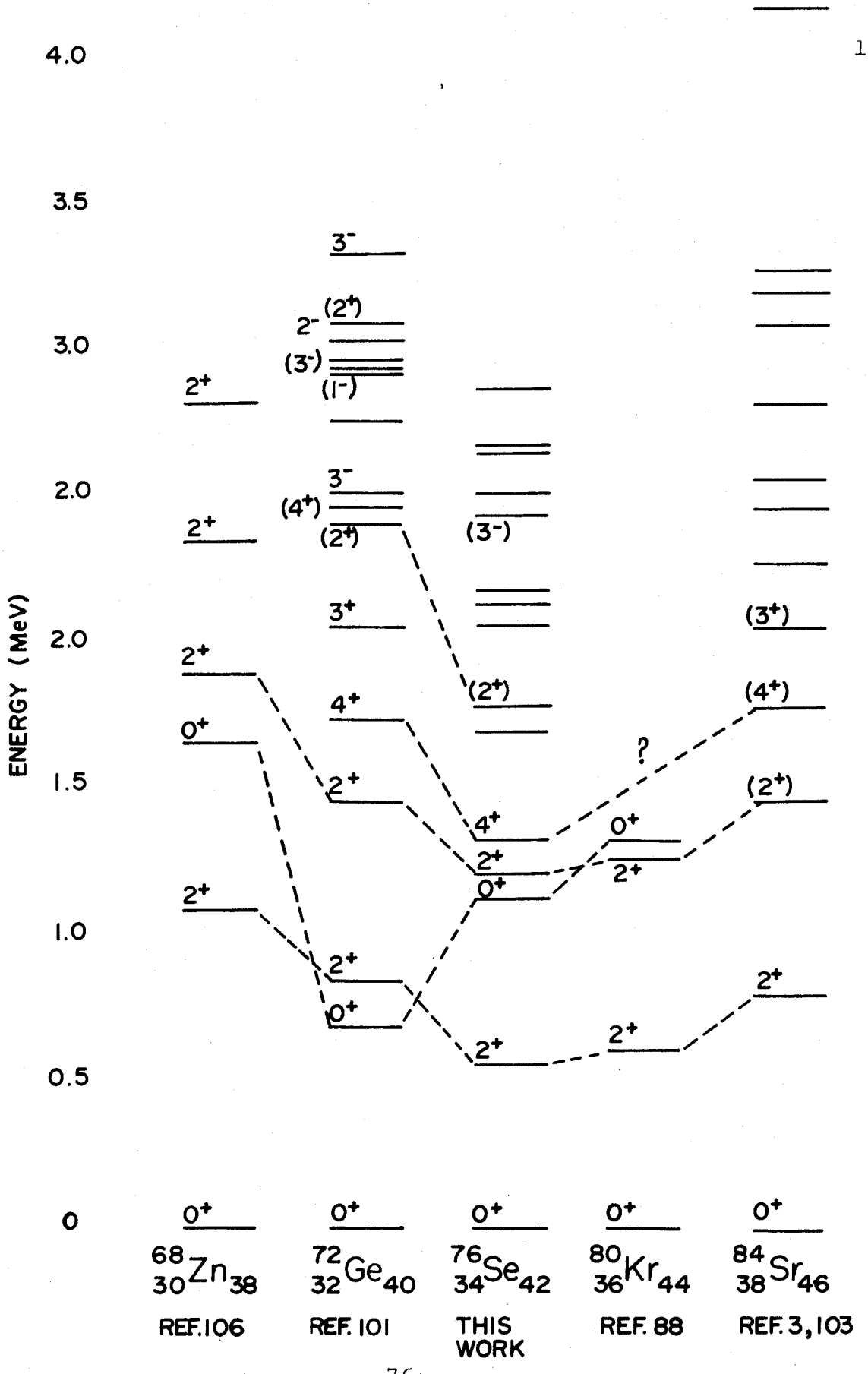

Figure 65 Level schemes of ^{76}Se and neighbouring nuclei

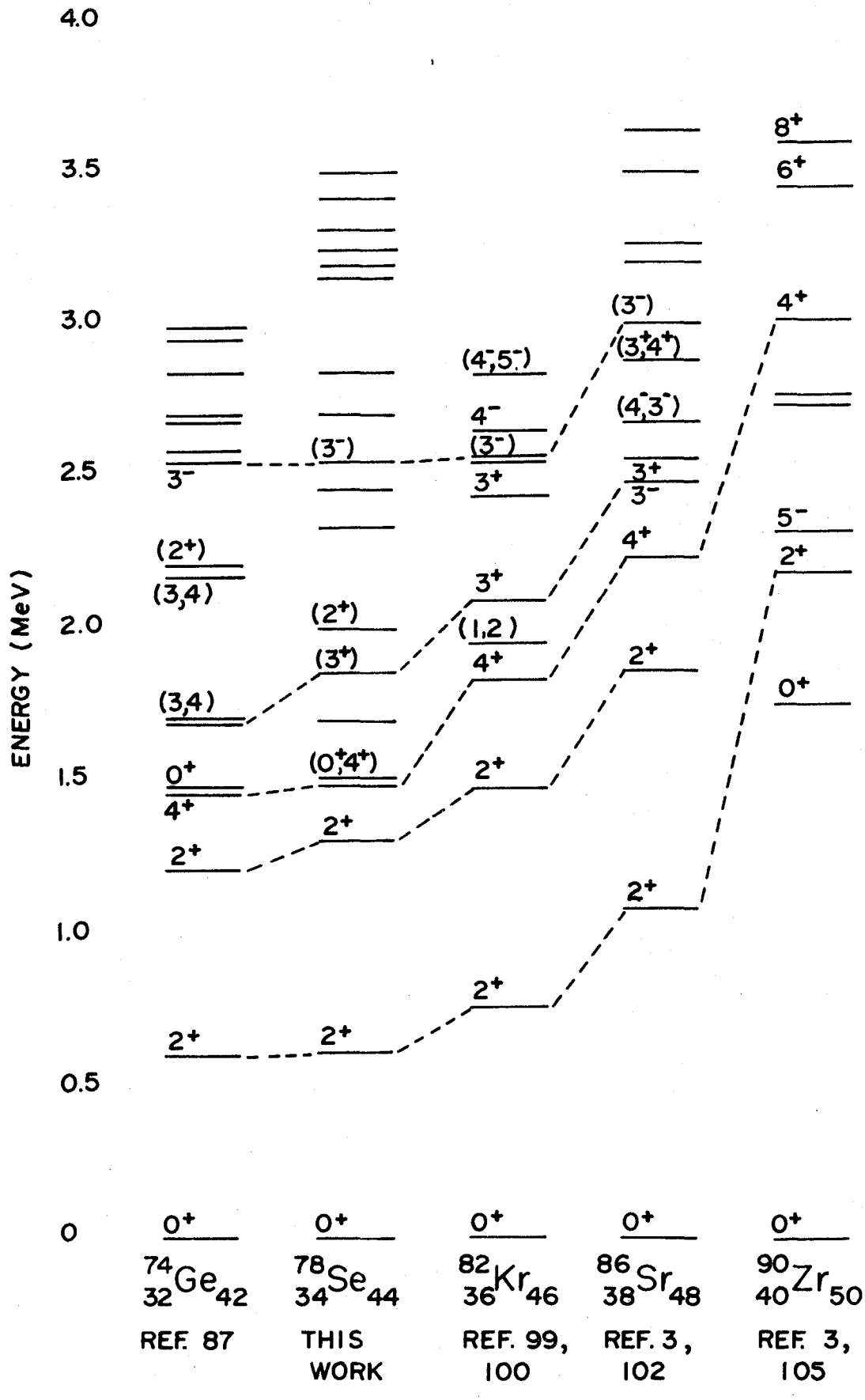

Figure 66 Level schemes of ^{78}Se and neighbouring nuclei

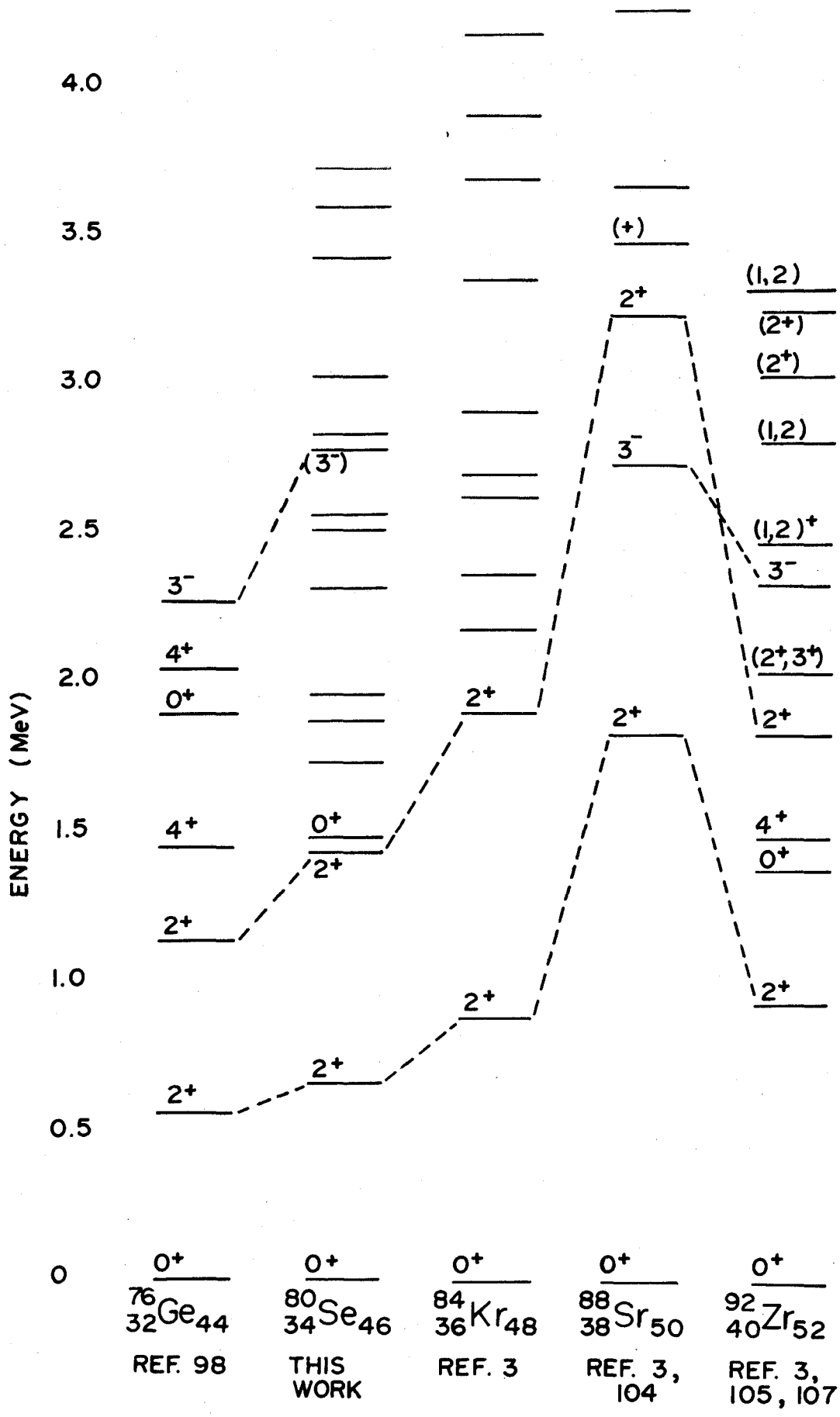

Figure 67 Level schemes of ^{80}Se and neighbouring nuclei

different techniques are compared with predictions of the Davydov and Chaban nuclear model[61] in Figures 68-70. As mentioned earlier (see sub-section 2.3), this model predicts collective quadrupole excited states with even parity for axially asymmetric prolate even-even nuclei as a function of the phenomenological parameters γ and μ. In the case of ^{76}Se, the values $\gamma = 24.3°$ and $\mu = 0.50$ were obtained in the present study by comparing the theoretical and experimental energies of the first two $I = 2^+$ low-lying excited levels and the first $I = 4^+$ level. Similarly, the values $\gamma = 25°$ and $\mu = 0.45$ were obtained for ^{78}Se, and $\gamma = 25°$ and $\mu = 0.40$ for ^{80}Se.

The Davydov and Chaban model predicts low-lying 0^+ and 3^+ levels for ^{76}Se, ^{78}Se and ^{80}Se at energies between 1.6 and 2.7 MeV. The first 0^+ states in these nuclei are found experimentally at lower energies in the 1.1 to 1.5 MeV region while 3^+ levels may possibly exist in ^{76}Se, ^{78}Se and ^{80}Se at 1.690, 1.854 and 1.872 MeV respectively. The 0^+ states predicted by this theory, however, may possibly correspond to levels measured experimentally at higher energies. For example, ^{78}Se levels at 2.326 and 2.452 MeV and ^{80}Se levels at 2.310 and 2.562 MeV are postulated in the present work to have 0^+ or 2^+ character. These levels are energetically in better agreement with the Davydov and Chaban predictions mentioned above. The possibility that the first low-lying 0^+ states in Ge and Se isotopes

may be interpreted as collective states of an oblate-shaped rather than a prolate-shaped rotator has been proposed by Kregar and Mihailovic[123] and by Stewart and Castel.[98] The latter authors used a phenomenological collective model which considers the co-existence of oblate and prolate rotators to predict successfully the low energy level structure of nuclei which are close neighbours to those of selenium, namely ^{70}Ge and ^{72}Ge. The Davydov and Chaban model (for γ values between 0° and 30°) predicts collective states for a prolate-shaped rotator. Therefore, if the above interpretation of the first excited 0^+ states is correct, this model could not be expected to predict the existence of these latter states in the energy region in which they are found experimentally.

Relatively good agreement exists between the Davydov and Chaban theory and some of the high-spin states ($I \geq 6$) found in the (α, $2n\gamma$) nuclear reaction experiments of Lieder and Draper.[21] High-spin collective states are known to be preferentially populated by high energy α-particles which are capable of imparting large angular momentum changes to target nuclei.[21] However, these high-spin states are seldom observed in β- and γ-decay because of strict selection rules[115] which favour small spin changes.

Correlations between the Davydov and Chaban theory and experiment for other high energy, low-spin Se levels

are difficult due to experimental uncertainties in the log ft data which are necessary for the accurate assignment of spin and parity character to these levels. In addition, further complications arise from the fact that some of the Se excited levels above 2-3 MeV possess negative parity[24] which could be due to octupole or individual nucleon excitations not considered in this theory.

5.2 Conclusions

The decay scheme studies of the isotopes investigated in this work through use of high resolution Ge(Li) and Si(Li) detectors have provided new and additional information on the excited states of ^{76}Se, ^{78}Se and ^{80}Se. In the case of ^{78}Se and ^{80}Se, the results represent substantial improvements over previous investigations.

In the present ^{76}As decay studies, Ge(Li) single detector and γ-γ measurements revealed coincident pairs of γ-rays at 559.6 - 563.5 keV and 1213.5 - 1217.0 keV and thereby confirmed ^{76}Se levels at 559.6, 1123.1 and 2430.5 keV. Similar measurements on other weak intensity γ-rays provided evidence for possible ^{76}Se levels at 1690.1, 2059, 2127.6, 2516 and 2866 keV as well as confirming other well-known levels predicted by previous workers.

The ^{78}As β- and γ-ray measurements allowed proposal of a decay scheme for ^{78}Se containing 32 γ-transitions and

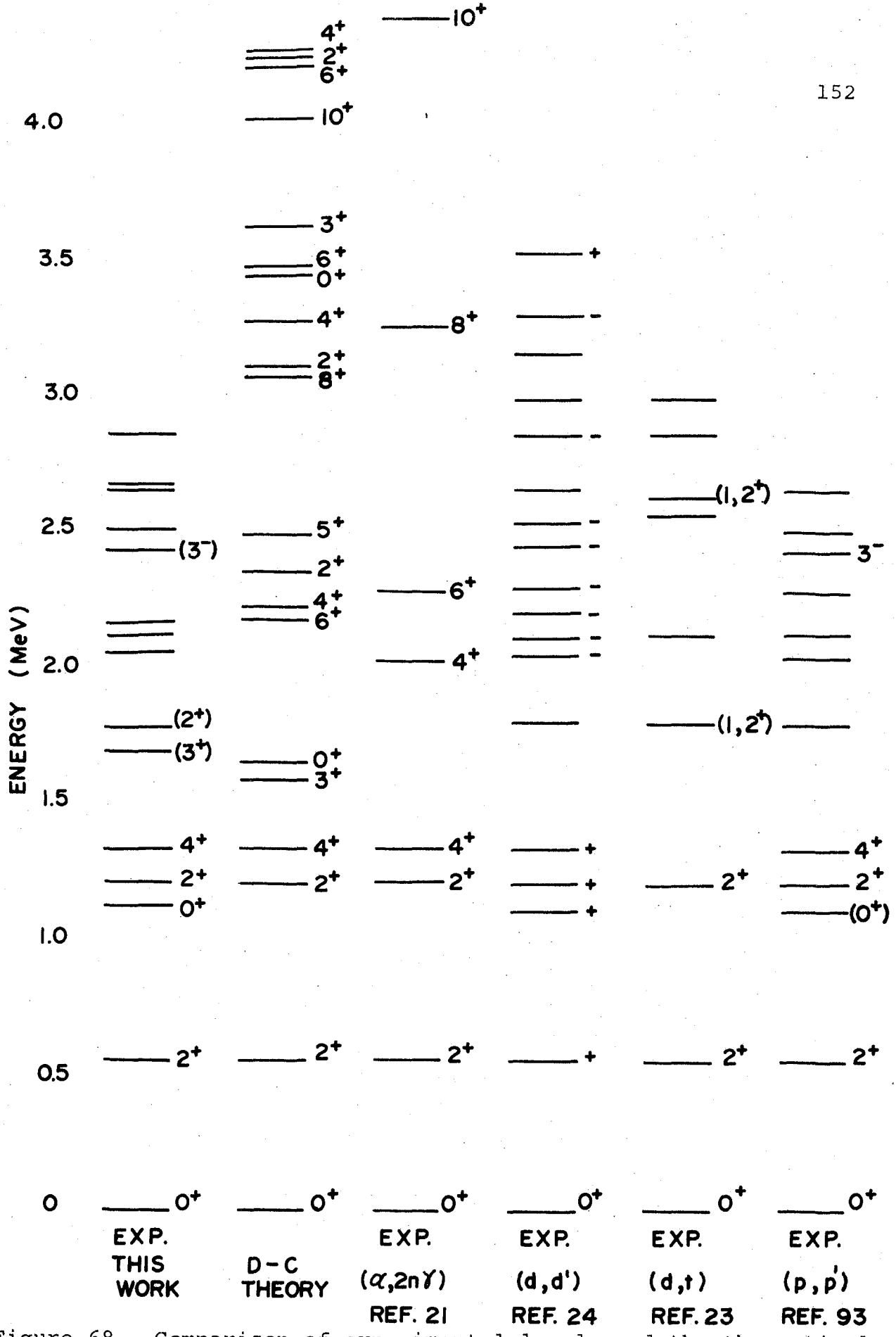

Figure 68 Comparison of experimental levels and the theoretical predictions of the Davydov and Chaban model for ^{76}Se

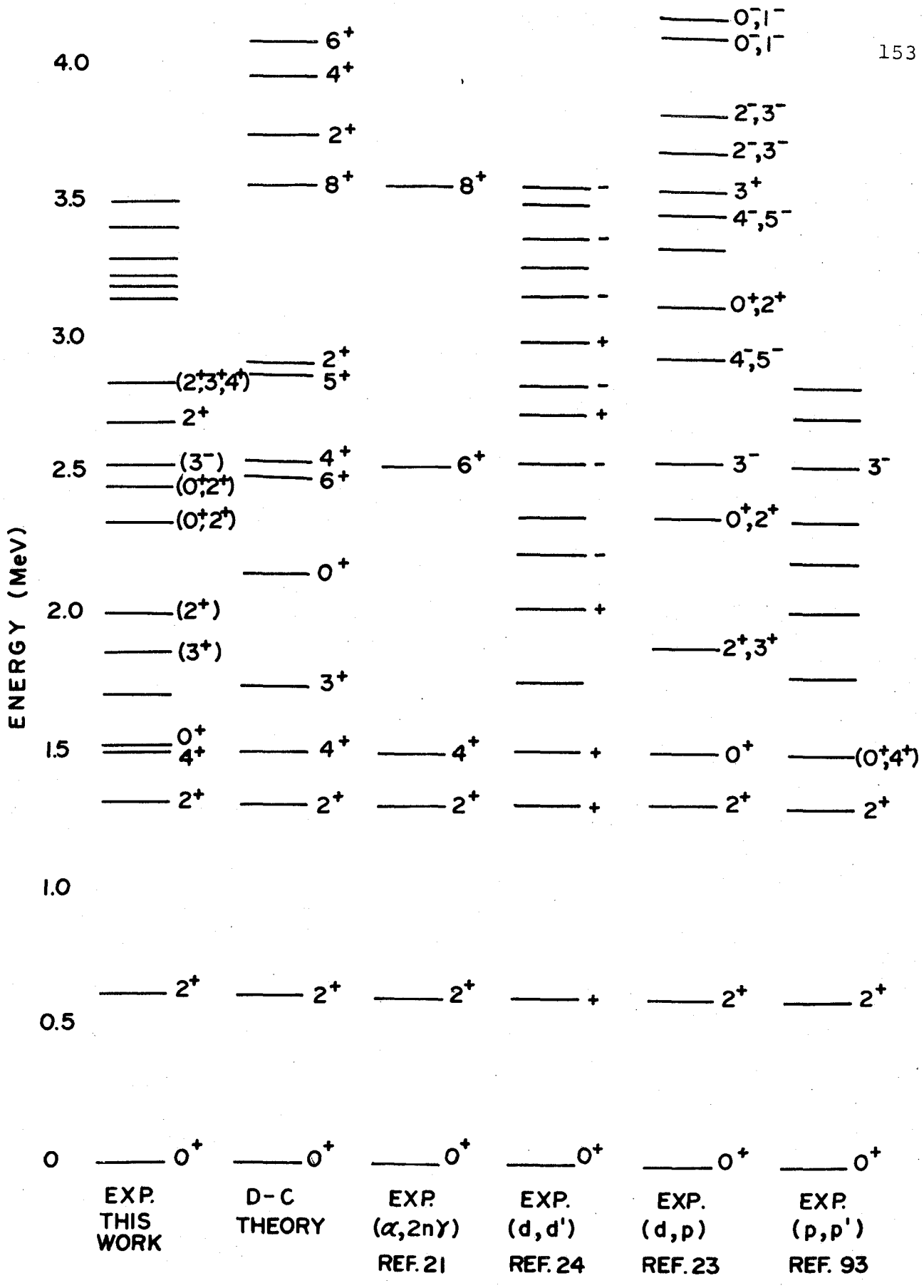

Figure 69 Comparison of experimental levels and the theoretical predictions of the Davydov and Chaban model for ^{78}Se

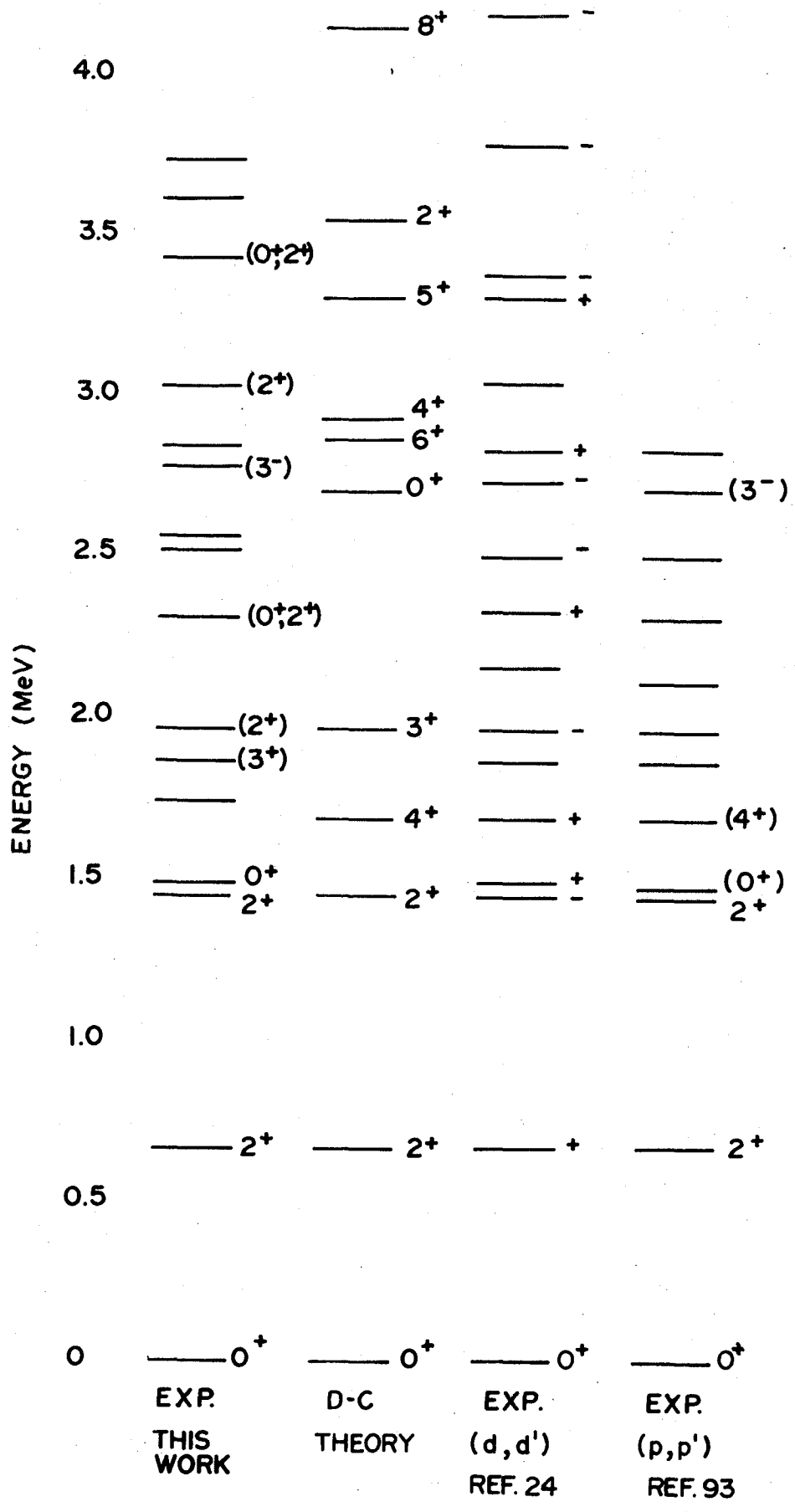

Figure 70 Comparison of experimental levels and the theoretical predictions of the Davydov and Chaban model for ^{80}Se

18 excited levels. The half-life of ^{78}As was determined to be 90.7 ± 0.2 min. No evidence was obtained for a 6-min ^{78}As isomeric state reported by previous investigators.[31]

The Ge(Li) single detector and γ-γ measurements on ^{80}As decay resulted in a decay scheme for ^{80}Se which included 23 γ-transitions and 15 excited levels. The half-life of ^{80}As was determined to be 16.5 ± 0.3 sec, slightly higher than the previously reported value.[42]

Analyses of the ^{80}As Ge(Li) γ-spectra obtained in the present studies also revealed the presence of γ-lines at 342.6, 654.7 and 818.3 keV. These γ-rays were assigned to ^{82}As decay on the basis of ^{82}Se (n,p) experiments performed by other workers[91,92] using selenium samples enriched in ^{82}Se. The half life of ^{82}As was measured in this study to be 14 ± 2 sec by following the decay of 654.7 keV γ-ray events.

Applied to the ^{76}Se, ^{78}Se and ^{80}Se isotopes, the Davydov and Chaban model reproduced with good agreement between theory and experiment, the energies of low-lying states often described as one-phonon and two-phonon quadrupole vibrational states.[49,53] Reasonable agreement was obtained with some of the other levels although complete agreement was not expected at these higher energies where additional degrees of freedom, such as octupole and hexadecapole vibrations or individual nucleon excitations, may occur.

REFERENCES

1. Nuclear Data Sheets, compiled by K. Way et al., (Printing and Publishing Office, National Academy of Sciences - National Research Council, Washington 25, D.C., 1962).

2. K. Way, Nuclear Data, B1(4) 1966, B1(6) 1966, Academic Press, Inc., New York, N.Y.

3. Lederer, C.M., Hollander, J.M., and Perlman, I., Table of Isotopes, 6th Ed., (John Wiley & Sons, New York, 1967).

4. Girgis, R.K., Ricci, R.A., and Van Lieshout, R., Nuclear Physics 13 (1959) 461.

5. Kurbatov, J.D., Murray, B.B., and Sakai, M., Phys. Rev. 98 (1955) 674.

6. Delyagin, N.N., and Sorokin, A.A., JETP (Sov. Phys.) 11 (1960) 799.

7. Miller, L.C., and Curtiss, L.F., Phys. Rev. 70 (1946) 983.

8. Funk, E.G., and Wiedenbeck, M.L., Phys. Rev. 109 (1958) 922.

9. Fischbeck, H.J., and Newsome, R.W., Phys. Rev. 129 (1963) 2231.

10. Pipkin, F.M., Bradley, G.E., and Simpson, R.E., Nucl. Phys. 27 (1961) 353.

11. Macklin, R.L., Lazar, N.H., and Lyon, W.S., Phys. Rev. 107 (1957) 504.

12. Bäckström, G., Arkiv För Fysik, 11 (1956) 357.

13. Scobie, J., Nucl. Phys. 3 (1957) 465.

14. Vitman, V.D., Voinova, N.A., and Dzhelepov, B.S., Invest. Akad. Nauk. S.S.S.R., Ser. Fyz., 28 (1964) 222; Bull. Acad. Sc. U.S.S.R., Phys. Ser, 28 (1965) 139.

15. Murray, J., McMath, T.A., Cameron, J.A., Can. J. Phys. 45 (1967) 1821.

16. Aten, J., Marsol, C., Forrest, H., C.R. Acad. Sc. Paris, Serie C, 265 (1967) 465.

17. White, D.H., Saunders, B.G., Bull. Amer. Phys. Soc., 10 (1965) 13; Nuclear Data B1, No. 6 (1966) 111.

18. Dzhelepov, B.S., Dmitriev, A.G., and Zhukovskii, N.N., Izv. Akad. Nauk . SSSR, Ser. Fyz. 33 (1969) 14.

19. Ivanenko, V.V., Bugorkov, S.S., Petrzhak, K.A., and Sorokina, A.N., Sov. J. of Nucl. Phys. 4 (1967) 837.

20. Bäckström, G., and Marklund, I., Arkiv För Fysik. 17 (1960) 393.

21. Lieder, R.M., and Draper, J.E., Phys. Rev. C. 2 (1970) 531.

22. Girgis, R.K., Ricci, R.A., and Van Lieshout, R., Nucl. Phys. 13 (1959) 473.

23. Lin, E.K., Phys. Rev. 139B (1965) 340.

24. Lin, E.K., Nucl. Phys. 73 (1965) 613.

25. Nagarajan, T., Ravindranath, M., Uenkata Reddy, K., Nucl. Phys. A137 (1967) 467.

26. Tomlinson, E.P., and Ridgway, S.L., Phys. Rev. 88 (1952) 170.

27. Hubert, P., Ann. of Phys. 8 (1953) 662.

28. McMillan, D.K., and Pate, B.D., Nucl. Phys. A140 (1970) 529.

29. Paradellis, T., and Hontzeas, S., Nucl. Phys. A142 (1970) 204.

30. Maddison, D.W., Washington State University, Pullman, Washington, U.S.A., Ph.D. thesis, 1968.

31. Nemilov, A., Pisarevskii, A.N. and Soshin, L.D., ZhETF (USSR) 35 (1958) 801; JETP (Sov. Phys.) 8 (1959) 555.

32. Van Lieshout, R., private communication to N.D.S. (1958), published in Lederer, C.M., Hollander, J.M., and Perlman, I., Table of Isotopes, 6th Ed. (Wiley, New York, 1967) p. 212.

33. McGowan, F.K., and Stelson, P.H., Phys. Rev. 126 (1962) 257.

34. Bygrave, W., Nucl. Phys. 53 (1964) 385.

35. Andreyev, D.S., Grinberg, A.P., Erokhina, K.I., and Lemberg, I.K., Nucl. Phys. 19 (1960) 400.

36. Fritze, K., Nucl. Phys. 64 (1965) 303.

37. Fritze, K., and Kiefer, W., Radiochim Acta 4 (1965) 166.

38. Cumming, J.B., NAS-NS Publication number 3107 (1962) p. 25.

39. Stelson, PLH., and McGowan, F.K., Nucl. Phys. 32 (1962) 652.

40. Marlow, K.W., Bull. Am. Phys. Soc., 11, (1966) 66.

41. Adams, F., and Dams, R., J. Radioanal. Chem. 3 (1969) 106.

42. Meads, R.E., and McIldowie, J.E.G., Proc. Phys. Soc (London) 74 (1959) 693.

43. Scharff-Goldhaber, G., and McKeown, M., Phys. Rev. 92 (1953) 356.

44. Hamilton, J.H., and Carter, H.K., Phys. Rev. 186 (1969) 186.

45. Del Marmol. P., and Van Tigchelt, H., Radiochim. Acta 12 (1969) 57.

46. Zoller, W.H., and Walters, W.B., Phys. Rev. 185 (1969) 1541.

47. Tomlinson, L., and Hurdus, M.H., Radiochim. Acta 12 (1969) 182.

48. Donnelly, D.P., Reidy, J.J., and Wiedenbeck, M.L., Nucl. Phys. A112 (1968) 145.

49. Mottelson, B.R., Rev. Mod. Phys. 29 (1957) 186.

50. Mayer, M.G., and Jensen, J.H.D., Elementary Theory of Nuclear Structure, John Wiley and Sons, Inc., New York, N.Y. (1955).

51. Mayer, M.G., Jensen, J.H.D., Kurath, D., Bohr, A., and mottelson, B.R., Alpha-, Beta-, and Gamma-Ray Spectroscopy, ed. by Siegbahn, K., (North-Holland Publishing Company, Amsterdam, 1964), Chapters IX and X.

52. Rose, M.E., Beta-, and Gamma-Ray Spectroscopy, ed. by Siegbahn, K., (North-Holland Publishing Company, Amsterdam, 1955), Chapter IX.

53. Eichler, E., Rev. Mod. Phys. 36 (1964) 809.

54. Scharff-Goldhaber, G., Phys. Rev. 90 (1953) 587.

55. Scharff-Goldhaber, G., and Weneser, J., Phys. Rev. 98 (1955) 212.

56. Langer, L.M., Rev. Sci. Instr. 20 (1949) 216.

57. Day, P.P., Klema, E.D., and Mallman, C.A., ANL-6220, Physics and Mathematics, (TID-4500, 15th Ed.), AEC Research and Development Report, November 1960.

58. Davydov, A.S., and Filippov, G.F., Nucl. Phys. 8 (1958) 237.

59. Davydov, A.S., and Rostovsky, V.S., Nucl. Phys. 12 (1958) 58.

60. Davydov, A.S., Rabotnov, N.S., and Chaban, A.A., Nucl. Phys. 17 (1960) 169.

61. Davydov, A.S., and Chaban, A.A., Nucl. Phys. 20 (1960) 499.

62. Williams, S.A., and Davidson, J.P., Can. J. of Phys. 40 (1962) 1423.

63. Klema, E.D., Mallman, C.A., and Day, P., Nucl. Phys. 25 (1961) 266.

64. Varshni, V.P., and Bose, S., Nucl. Phys. A144 (1970) 645.

65. Sher, A.H., Simon Fraser University, Burnaby, B.C., Ph.D. thesis, 1967.

66. Taylor, D., The Measurement of Radio Isotopes, John Wiley and Sons, Inc., New York, N.Y., (1959).

67. Van Patter, D.M., Nucl. Phys. 14 (1959) 42.

68. Shera, E.B., Bedesem, M.P., and Casper, K.J., Rev. Sci. Instr. 38 (1967) 1110.

69. Burginyon, G.A., and Greenberg, J.S., Nucl. Instr. Methods 41 (1966) 109.

70. Andersen, V., and Christensen, C.J., Nucl. Instr. Methods 61 (1968) 77.

71. Andersen, V., Nucl. Instr. Methods 65 (1968) 225.

72. Hulbert, J.A., J. Sci. Instrum. 43 (1966) 771.

73. Muszynski, S., and Mark, S.K., Nucl. Phys. A142 (1970) 459.

74. Imanishi, N., and Nishi, T., Nucl. Phys. A154 (1970) 321.

75. Rogers, V.C., Anal. Chem. 42 (1970) 807.

76. Charoenkwan, P., Nucl. Instr. Methods 34 (1965) 93.

77. Beraud, R., Berkes, I., Daniere, J., Escudie, B., Levy, M., Marest, G., and Rougny, R., Nucl. Instr. Methods 60 (1968) 219.

78. Tomlinson, L., and Hurdus, M.H., J. Inorg. Nucl. Chem. 30 (1968) 1125.

79. Rogers, D., and Heron, A.E., Analyst 71 (1946) 414.

80. Hyde, E.K., Perlman, I., and Seaborg, G.T., The Nuclear Properties of the Heavy Elements, Prentice-Hall, Inc., Englewood Cliffs, N.J. (1964).

81. Lopac, V., Nucl. Phys. A155 (1970) 513.

82. Steinberg, E.P., and Engelkemeir, D.W., National Nuclear Energy Series, Manhattan Project Technical Section, Division IV, Vol. 9, (1950), 566.

83. Nilsson, S.G., Dan. Mat. Fys. Med., 29, No. 16 (1955).

84. Sakai, M., Nucl. Phys. A104 (1967) 301.

85. Kvavle, E., and Pappas, A.C., Nucl. Phys. 74 (1965) 27.

86. KuKoc, A.H., King, J.D., and Taylor, H.W., Nucl. Phys. A115 (1968) 625.

87. Magruder, A.P. and Smither, R.K., Phys. Rev. 183 (1969) 927.

88. Katoh, T., Morii, T., Inoue, H., Yoshizawa, Y., Gotah, H., and Sakai, E., J. Phys. Soc. Japan. 26 (1969), 1071.

89. Ramayya, A.V., Hamilton, J.H., Van Nooijen, B., and Johnson, N.R., Phys. Rev. 157 (1967) 1015.

90. Trehan, P.N., and Van Patter, D.M., Phys. Rev. 126 (1962) 266.

91. Mathew, P.T., and McCallum, G.J., Phys. Letters 28B (1968) 106.

92. Karras, M., Ward, T.E., and Ihochi, H., Nucl. Phys. A147 (1970) 120.

93. Darcey, W., Pullen, D.J., and Tanner, N.W., Direct Interactions and Nuclear Reaction Mechanisms, ed. by Clementel, E., and Villi, C., Gordon and Breach, Science Publishers, New York, (1963).

94. Bohr, A., Mat. Fys. Medd. Dan. Vid. Selsk., 28 (1952) No. 14.

95. Bohr, A., and Mottelson, B., Mat. Fys. Medd. Dan. Vid. Selsk. 27 (1953) No. 16.

96. Day, P.P., and Mallman, C.A., ANL-6184, Physics and Mathematics, (TID-4500, 15th Ed.), AEC Research and Development Report, August 1960.

97. Davydov, A.S. and Orcharenko, V.I., Sov. J. of Nucl. Phys. 3 (1966) 740.

98. Stewart, K.W.C., and Castel, B., Lettere Al Nuovo Cimento, 4 (1970) 589.

99. Meredith, G.R., and Meyer, R.A., Nucl. Phys. A142 (1970) 513.

100. Liukkonen, E., Hattula, J., and Anttila, A., Nucl. Phys. A138 (1969) 163.

101. Camp, D.C., Nucl. Phys. A121 (1968) 561.

102. Arit, et al., Izv. Akad. Nauk. SSSR. Ser. Fiz. 33 (1969) 1594.

103. Zaitseva, et al., Izv. Akad. Nauk. SSSR. Ser. Fiz. 33 (1969) 1283.

104. Lycklama, H., Archer, N.P.,and Kennett, K.I., Can. J. Phys. 47 (1969) 393.

105. Berman, B.L., and Baglan, R.J., I. Inorg. Nucl. Chem. 31 (1969) 9.

106. Vaughan, K., Sher, A.H., and Pate, B.D., Nucl. Phys. A132 (1969) 561.

107. Talbert, W.L., Wohn, F.K., Hsn, H.H., and Hsue, S.T., Nucl. Phys. A146 (1970) 149.

108. Belyaw, B.N., Gudov, V.I., Guozdev, B.A., and Krizhanskii, L.M., Izv. Akad. Nauk. SSSR, Ser. Fiz. 32 (1968) 137.

109. Goldhaber, M., and Sunyar, A.W., Phys. Rev. 83 (1951) 906.

110. Malov, V.V. and Troitskii, M.A., Sov. J. of Nucl. Phys. 11 (1970) 42.

111. Temmer, G.M., and Heydenburg, N.P., Phys. Rev. 104 (1956) 967.

112. Siegbahn, K., Alpha-, Beta-, and Gamma-Ray Spectroscopy, (North-Holland Publishing Company, Amsterdam, 1964), Chapter III.

113. Bahn, Jr., E.L., Washington University, St. Louis, Missouri, Ph.D. thesis, 1962.

114. Alburger, D.E., and Sunyar, A.W., Phys. Rev. 99 (1955) 695.

115. Friedlander, G., Kennedy, J.W., and Miller, J.M. Nuclear and Radiochemistry, 2nd Ed.n, John Wiley & Sons, Inc., New York, 1964.

116. Barford, N.C., Experimental Measurements: Precision, Error and Truth, Addison-Wesley Publishing Company, Inc., London, 1967.

117. Verrall, R.I., Hardy, J.C., and Bell, R.E., Nucl. Instr. Meth. 42 (1966) 258.

118. Moszkowskii, S.A., Phys. Rev. 82 (1951) 35.

119. Steinberg, E.P., and Engelkemeir, D.W., National Nuclear Energy Series, Manhattan Project Technical Section, Division IV, Vol. 9, (1950) 566.

120. Mellor, J.W., A Comprehensive Treatise on Inorganic and Theoretical Chemistry, John Wiley & Sons, Inc., New York, N.Y., Vol. IX, Chapter LI.

121. Lane, A.M., and Pendlebury, E.D., Nucl Phys. 15 (1960) 39.

122. Grigoriev, E.P., and Avotina, M.P., Nucl. Phys. 19 (1960) 248.

123. Kregar, M., and Milhailovic, M.V., Nucl. Phys. A93 (1967) 402.

A P P E N D I X

GRAYPLOT Fortran Computer Program

FORTRAN PROGRAM "GRAYPLOT"

The Fortran IV computer program GRAYPLOT, was used extensively in the early stages of the present work to plot and perform calculations on γ-spectra obtained with Ge(Li) detectors; the program was run on the IBM-360/40 computer at Simon Fraser University. The GRAYPLOT program in the version shown here contains full energy γ-peak efficiency data only for a 8 cm^3-Ge(Li) detector. Hence, these data must be changed if other detectors are used and if γ-ray relative intensity calculations are desired to be done.

A typical data deck consisted of:

CARD

1: COMMENT CARD, contains any information of interest to the program user;

2-Y: γ-SPECTRUM DATA CARDS, contain COUNTS (versus channel number data) in a 4X, 10F6.0 format with $2 < Y \leq 321$, six 9's were placed in the last number slot of the last of these cards to stop the read-in procedure;

Y+1: ENERGY CALIBRATION CARD, contains the values of the A, B and C parameters from the equation $E = Ax^2 + Bx + C$, in a 3E11.7 format, could be left blank if γ-ray intensity calculations were not desired.

```
      C     GRAYPLOT3 VERSION7 APRIL22/68  DKMCMILLAN
      C     DATA FORMAT MUST BE 4X,10F6.0
0001        DIMENSION COUNT(3201),COMNT(20),O(3201),SUMT(3201),S(3201)
0002        COMMONA,B,C,COUNT,SS,IX,IX1,A2,A4,A6,A8,A10,A12,A14,X2,X4,X6,X8,X1
           10,X12,X14,O,E2,E4,E6,E8,E10,E12,E14
0003     65432 READ(5,100) COMNT
0004     100   FORMAT(20A4)
0005        J=10
0006        JJ=1
0007        DO 1  I=1,320
0008        READ (5,2) (COUNT(K),K=JJ,J)
0009     2     FORMAT(4X,10F6.0)
0010        IF(COUNT(J).GE.999998) GO TO 3
0011        JJ=JJ+10
0012        J=J+10
0013     1  CONTINUE
0014     3     NC=J-1
0015        LITE=1
0016        DO 9 I=2,NC
0017     9     COUNT(I-1)=COUNT(I)
0018        READ(5,5)A,B,C
0019     5     FORMAT(3E11.7)
0020        IX=1
0021        IX1=60
0022     17    SS= COUNT(IX)
0023        IX=IX+1
0024        DO 11 I=IX,IX1
0025        X=COUNT(I)
0026        IF(X-SS) 12,11,11
0027     12     SS=X
0028     11     CONTINUE
0029        IX=IX-1
0030        Y=COUNT(IX)
0031        IX=IX+1
0032        DO 13 I=IX,IX1
0033        X=COUNT(I)
0034        IF(X-Y) 13,13,15
0035     15     Y=X
0036     13     CONTINUE
0037        IF(Y) 7777,7777,7778
0038     7777  Y=10.0
0039     7778  CONTINUE
0040         IF(Y-SS)666,666,667
0041     656    Y=SS+10.0
0042     667     CONTINUE
0043        WRITE(6,102) COMNT
0044     102     FORMAT(1HO,20A4)
0045        WRITE(6,8) Y,SS
0046     8     FORMAT(1HO,' SCALE CHANGE   MAXIMUM NUMBER# @,F10.1,'   MINIMUM   NU
           1MBER# @,F10.1 ,  //)
0047        IX=IX-1
0048        WRITE(6,491)
```

```
0049      491   FORMAT(25H    CN    COUNTS   ENERGY , /)
0050            CALL PLOT(Y)
0051            GO TO( 90,99),LITE
0052      90    IX=IX1-20
0053            IX1=IX1+160
0054            IF(IX1-NC) 17,98,97
0055         97 IX1=NC
0056      98    LITE=2
0057            GO TO 17
0058      99    IX=NC/2
0059            IX1=IX+10
0060            LITE=1
0061      299   SUMO=0.0
0062            DO 202 J=IX,IX1
0063      202   SUMO=SUMO+ COUNT(J)
0064            IF(SUMO-30.0) 205,205,206
0065      206   GO TO (220,210),LITE
0066      205   NC=IX
0067            GO TO 210
0068      220   IX=IX+10
0069            IX1=IX1+ 10
0070            IF(IX1-NC)207,208,209
0071       209  IX1=NC
0072      208   LITE=2
0073      207   GO TO 299
0074      210   NC=IX
0075            DO 200 J=1,NC
0076            O(J)=COUNT(J)
0077            IF(O(J)-0.1) 201,201,500
0078      201   O(J)= 1.0
0079      500   S(J)=SQRT(O(J))
0080      200   CONTINUE
0081            NC=NC-8
0082            DO 4 J=8,NC
0083      4     SUMT(J)=(O(J)-O(J-4))/S(J-4)  + (O(J)-O(J+4))/S(J+4)  +
               1 (O(J)-O(J-2))/S(J-2) + (O(J)-O(J+2))/S(J+2) +
               2 (O(J)-O(J-3))/S(J-3) + (O(J)-O(J+3))/S(J+3)
               3+(O(J)-O(J-1))/S(J-1) + (O(J)-O(J+1))/S(J+1)
0084            WRITE(6,111)
0085      111   FORMAT(1H1, '  PEAK IDENTIFICATION ROUTINE - CALCULATION OF PEAK
               1AREAS,INTENSITIES,AND ENERGIES @, //)
0086            WRITE(6,102) COMNT
0087            WRITE(6,101)
0088      101   FORMAT(1HO,  ' CHAN NO    COUNTS  ENERGY          A14             A12
               1          A10             A8             A6             A4
               2  A2@ ,/)
0089            WRITE(6,103)
0090      103   FORMAT( ' DE IS DETECTOR EFFICIENCY USED     I14             I12
               1       I10             I8             I6             I4             I2
               2@, /)
0091            WRITE(6,104)
0092      104   FORMAT( ' PEAK CHANNEL NUMBERS                X14             X12
```

```
                1       X10             X8              X6              X4              X2
               2@, /)
0093            WRITE(6,105)
0094      105   FORMAT( ' PEAK ENERGIES                                 E14             E12
                1       E10             E8              E6              E4              E2
               2@, ///)
0095            LIT=1
0096            NP=0
0097            K=7
0098      280   K=K+1
0099            IF(K-NC) 281,281,211
0100      281   IF(SUMT(K)-20.0) 280,282,282
0101      282   MP=0
0102            MS=K
0103      283   K=K+1
0104            MP=MP+1
0105            IF(K-NC)284,284,285
0106      285   NP=NP+1
0107            LIT=2
0108            N=K-1
0109            GO TO 909
0110      284   IF(SUMT(K)-20.0) 286,283,283
0111      286   OMAX=O(MS)
0112            MPP= MS+MP -1
0113            DO 287 JL=MS,MPP
0114            X=O(JL)
0115            IF(X-OMAX)287,288,288
0116      288   OMAX=X
0117            MAXC=JL
0118      287   CONTINUE
0119            K=MPP
0120            N=MAXC
0121      909   X=N
0122            E=(A*X + B)*X + C
0123            CALL AREA(N)
0124      922   CONTINUE
                C       COMPUTE DETECTOR EFFICIENCY,I2,I4,I6,I8,I10,I12,I14
0125            IF(E-0.1) 5555,5555,5556
0126      5555  DE=0.0
0127            XI2=0.0
0128            XI4=0.0
0129            XI6=0.0
0130            XI8=0.0
0131            XI10=0.0
0132            XI12=0.0
0133            XI14=0.0
0134            E511=0.0
0135            E1022=0.0
0136            GO TO 903
0137      5556  IF(E-50.0)1000,1001,1002
0138      1000  DE= 98.0
0139            GO TO 1006
```

```
0140        1001  DE=96.0
0141              GO TO 1006
0142        1002  IF(E-69.0) 1003,1004,1005
0143        1003  DE=95.0
0144              GO TO 1006
0145        1004  DE=91.0
0146              GO TO 1006
0147        1005  EL= ALOG10(E)
0148              DATA C1,C2,C3,C4,C5,C6  /0.13502557E-01,-0.76127827E-01,0.17433661
                 1,-0.11826248E+01,0.31062498E+01,-0.24766427  /
0149              DX=((((C1*EL + C2)*EL + C3)*EL + C4)*EL + C5)*EL + C6
0150              IF(DX) 1007,1008,1009
0151        1007  DX=-DX
0152              DE=(1.0)/(10.0**(DX))
0153              GO TO 1006
0154        1008  DE=1.0
0155              GO TO 1006
0156        1009  DE=(10.0**(DX))
0157        1006  CONTINUE
0158              XI2=A2*100.0/DE
0159              XI4=A4*100./DE
0160              XI6=A6*100./DE
0161              XI8=A8*100./DE
0162              XI10=A10*100./DE
0163              XI12=A12*100./DE
0164              XI14=A14*100./DE
0165              E511=E+511.0
0166              E1022=E+1022.0
0167        903   WRITE(6,905)N,O(N),E,A14,A12,A10,A8,A6,A4,A2
0168        905   FORMAT(1H0,I7,F10.1,F9.2,7F14.2 )
0169        904   WRITE(6,216)DE,XI14,XI12,XI10,XI8,XI6,XI4,XI2
0170        216   FORMAT( ' HD1 DE @,F10.5,F23.2,6F14.2)
0171              WRITE(6,217)E511,X14,X12,     X10,X8,X6,X4,X2
0172        217   FORMAT( '      ENERGY & 511@,F9.2,7E14.2 )
0173              WRITE(6,399)E1022,E14,E12,E10,E8,E6,E4,E2
0174        399   FORMAT( '      ENERGY & 1022@,F9.2,7F14.2 )
0175              GO TO (218,3334),LIT
0176         218   NP=NP+1
0177        3333  GO TO 280
0178        211   CONTINUE
0179        3334  WRITE(6,219)NC,NP
0180        219   FORMAT(//,' NO OF CHANNELS UP TO@,I8,' WHICH HAVE A SUMT GREATER
                 1THAN 20.0 IS # @,I8,//)
0181               WRITE(6,102) COMNT
0182               WRITE(6,999)
0183        999   FORMAT(1H0,84H **********DKM**********DKM**********DKM**********
                 1**********DKM**********DKM**********DKM**********DKM**********  )
0184               GO TO 65432
0185               END
```

```
0001                SUBROUTINE PLOT(Y)
0002                DIMENSION COUNT(3201),CHART(101)
0003                COMMONA,B,C,COUNT,SS,IX,IX1,A2,A4,A6,A8,A10,A12,A14,X2,X4,X6,X8,X1
                   10,X12,X14,0,E2,E4,E6,E8,E10,E12,E14
0004                  DATA BLANK,DOT,STAR  /1H   ,1H. ,1H*  /
0005                CHART(1)=DOT
0006                DO 1 I=2,101
0007          1     CHART(I)= BLANK
0008                DO 2 I=IX,IX1
0009                X=I
0010                E=(A*X+B)*X+C
0011                J=((COUNT(I)-SS)/(Y-SS))*100. + .5
0012                IF(J.LE.0) GO TO 3
0013                CHART(J)=STAR
0014                WRITE(6,4)I,COUNT(I),E,CHART
0015          4      FORMAT(I6,F10.1,E10.2,5X,101A1)
0016                CHART(J)=BLANK
0017                CHART(1)=DOT
0018                GO TO 2
0019          3     CHART(1)=STAR
0020                 WRITE(6,4)I,COUNT(I),E,CHART
0021                CHART(1)=DOT
0022          2      CONTINUE
0023                 RETURN
0024                 END
```

```
0001                SUBROUTINE AREA(N)
0002                DIMENSION COUNT(3201),O(3201)
0003                COMMONA,B,C,COUNT,SS,IX,IX1,A2,A4,A6,A8,A10,A12,A14,X2,X4,X6,X8,X1
                   10,X12,X14,O,E2,E4,E6,E8,E10,E12,E14
0004                SUM4=0.0
0005                SUM6=0.0
0006                 SUM8=0.0
0007                SUM10=0.0
0008                SUM12=0.0
0009                SUM14=0.0
0010                N1=N-7
0011                N2=N-6
0012                N3=N-5
0013                N4=N-4
0014                N5=N-3
0015                N6=N-2
0016                N7=N-1
0017                N8=N
0018                N9=N+1
0019                N10=N+2
0020                 N11=N+3
0021                N12=N+4
0022                N13=N+5
0023                N14=N+6
0024                N15=N+7
                C   COMPUTE A2
0025                 XM2=(O(N7)-O(N9))/2.0
0026                A2=O(N8)-O(N7) +XM2
                C   COMPUTE A4
0027                 XM4=(O(N6)-O(N10))/4.0
0028                DO 802 JK=N7,N9
0029           802  SUM4=SUM4 + O(JK)
0030                A4=SUM4-3.0*O(N6) + 6.0*XM4
                C   COMPUTE A6
0031                XM6=(O(N5) - O(N11))/6.0
0032                DO 803 JK=N6,N10
0033           803   SUM6=SUM6 + O(JK)
0034                A6=SUM6 -5.0*O(N5) + 15.0*XM6
                C   COMPUTE A8
0035                XM8=(O(N4) - O(N12))/8.0
0036                DO 804 JK=N5,N11
0037           804  SUM8=SUM8 + O(JK)
0038                A8=SUM8-7.0*O(N4) + 28.0*XM8
                C   COMPUTEA10
0039                XM10=(O(N3) - O(N13))/10.0
0040                DO 805  JK=N4,N12
0041           805  SUM10=SUM10 + O(JK)
0042                A10=SUM10-9.0*O(N3) + 45.0*XM10
                C   COMPUTE A12
0043                XM12=(O(N2)-O(N14))/12.0
0044                DO 806 JK=N3,N13
0045           806   SUM12=SUM12 + O(JK)
```

```
0046                A12=SUM12 -11.0*O(N2) + 66.0*XM12
                C   COMPUTE A14
0047                XM14=(O(N1) - O(N15))/14.0
0048                 DO 807 JK=N2,N14
0049            807 SUM14=SUM14 + O(JK)
0050                A14=SUM14 -13.0*O(N1) + 91.0*XM14
                C   COMPUTEX2,X4,X6,X8,X10,X12,X14
0051                X2=N8
0052                ORD7=O(N7) -O(N6)  + XM4
0053                ORD8=O(N8) -O(N6) + 2.0*XM4
0054                ORD9=O(N9)-O(N6) + 3.0*XM4
0055                SUM44=ORD7+ORD8+ORD9
0056                X4  =(ORD7*N7 + ORD8*N8 + ORD9*N9)/SUM44
0057                ORD6=O(N6)-O(N5) + XM6
0058                ORD7 =O(N7) - O(N5) + 2.0*XM6
0059                ORD8 =O(N8) - O(N5) + 3.0*XM6
0060                ORD9= O(N9) - O(N5) + 4.0*XM6
0061                ORD10=O(N10)-O(N5) + 5.0*XM6
0062                SUM66=ORD6+ORD7+ORD8+ORD9+ORD10
0063                X6=(ORD6*N6 + ORD7*N7 + ORD8*N8 + ORD9*N9 + ORD10*N10)/SUM66
0064                ORD5=O(N5)-O(N4) +   XM8
0065                ORD6=O(N6)-O(N4) + 2.0*XM8
0066                ORD7=O(N7)-O(N4) + 3.0*XM8
0067                ORD8=O(N8)-O(N4) + 4.0*XM8
0068                ORD9=O(N9)-O(N4) + 5.0*XM8
0069                ORD10=O(N10)-O(N4) + 5.0*XM8
0070                ORD11=O(N11)-O(N4) + 7.0*XM8
0071                SUM88=ORD5+ORD6+ORD7+ORD8+ORD9+ORD10+ORD11
0072                X8=(ORD5*N5 + ORD6*N6 + ORD7*N7 + ORD8*N8 + ORD9*N9 + ORD11*N11
                   1  + ORD10*N10 )/SUM88
0073                ORD4=O(N4) -O(N3)  +    XM10
0074                ORD5=O(N5)-O(N3)  + 2.0*XM10
0075                ORD6=O(N6) -O(N3)  + 3.0*XM10
0076                ORD7=O(N7)-O(N3)+ 4.0*XM10
0077                ORD8=O(N8)  -O(N3)  + 5.0*XM10
0078                ORD9=O(N9) -O(N3)  + 6.0*XM10
0079                ORD10=O(N10)-O(N3)  + 7.0*XM10
0080                ORD11=O(N11)-O(N3)        + 8.0*XM10
0081                ORD12=O(N12)-O(N3)  + 9.0*XM10
0082                SUM100=ORD4+ORD5+ORD6+ORD7+ORD8+ORD9+ORD11+ORD12 +ORD10
0083                X10=(ORD4*N4 + ORD5*N5 + ORD6*N6 + ORD7*N7 + ORD8*N8 + ORD9*N9 +
                   1 ORD10*N10 + ORD11*N11 + ORD12*N12 )/SUM100
0084                ORD3=O(N3)-O(N2)+XM12
0085                ORD4=O(N4)-O(N2)+2.0*XM12
0086                ORD5=O(N5)-O(N2)+3.0*XM12
0087                ORD6=O(N6)-O(N2)+ 4.0*XM12
0088                ORD7=O(N7)-O(N2)+5.0*XM12
0089                ORD8=O(N8)-O(N2)+6.0*XM12
0090                ORD9=O(N9)-O(N2)+ 7.0*XM12
0091                ORD10=O(N10)-O(N2)+8.0*XM12
0092                ORD11=O(N11)-O(N2)+ 9.0*XM12
0093                ORD12=O(N12)-O(N2) + 10.0*XM12
```

```
0094                ORD13=O           (N13)-O(N2)+11.0*XM12
0095                SUM122=ORD3+ORD4+ORD5+ORD6+ORD7+ORD8+ORD9+ORD10+ORD11+ORD12+ORD13
0096                X12=(ORD3*N3+ORD4*N4+ORD5*N5+ORD6*N6+ORD7*N7+ORD8*N8+ORD9*N9+
                   1  ORD10*N10+ ORD11*N11+ORD12*N12+          ORD13*N13 )/SUM122
0097                ORD2=O(N2)-O(N1)+   XM14
0098                ORD3=O(N3)-O(N1)+2.0*XM14
0099                ORD4=O(N4)-O(N1)+3.0*XM14
0100                ORD5=O(N5)-O(N1)+4.0*XM14
0101                ORD6=O(N6)-O(N1)+ 5.0*XM14
0102                ORD7=O(N7)-O(N1)+6.0*XM14
0103                ORD8=O(N8)-O(N1)+7.0*XM14
0104                ORD9=O(N9)-O(N1)+8.0*XM14
0105                ORD10=O(N10)-O(N1)+9.0*XM14
0106                ORD11=O(N11)-O(N1)+10.0*XM14
0107                ORD12=O(N12)-O(N1)+ 11.0*XM14
0108                ORD13=O(N13)-O(N1)+12.0*XM14
0109                ORD14=O(N14)-O(N1)+13.0*XM14
0110                SUM144=ORD2+ORD3+ORD4+ORD5+ORD6+ORD7+ORD8+ORD9+ORD10+ORD11+ORD12+
                   1  ORD13+ORD14
0111                X14=(ORD2*N2+ORD3*N3+ORD4*N4+ORD5*N5+ORD6*N6+ORD7*N7+ORD8*N8+
                   1ORD9*N9+ORD10*N10+ORD11*N11+ORD12*N12+ORD13*N13+ORD14*N14)/SUM144
                C   COMPUTE E2,E4,E6,E8,E10,E12,E14
0112                E2=(A*X2 +B)*X2 +C
0113                E4=(A*X4 + B) *X4 + C
0114                E6=(A*X6 +B)*X6 + C
0115                E8=(A*X8 + B)*X8 + C
0116                E10=(A*X10 + B)*X10 + C
0117                 E12=(A*X12 + B)*X12 + C
0118                E14=(A*X14+B)*X14+C
0119                 RETURN
0120                 END
```